Masterarbeit

Belly-fairing design space exploration for a forward swept natural laminar flow aircraft

Javier Ruberte Bailo
Matrikelnummer 4429461

Technische Universität Carolo-Wilhelmina zu Braunschweig

Deutsches Zentrum für Luft- und Raumfahrt e.V.
Institut für Aerodynamik und Strömungstechnik

Erstprüfer: Prof. Dr.-Ing. Cord-Christian Rossow
Zweitprüfer: Prof. Dr.-Ing. Rolf Radespiel
Betreuer: Dr.-Ing. Arne Seitz

12. Oktober 2020

Acknowledgements

To my parents, Arturo Ruberte Sancho and Maria Pilar Bailo Cebollada, who constantly supported me through my academic life and made all academic achievements possible.

To my supervisor, Arne Seitz, who invested many time and effort in the mentoring of this work.

To all the other DLR Scientist who helped out in this work, Stefan Melber, Thomas Streit, Arno Ronzheimer and Phillip Bekemeyer.

To all of you, Thank you

Zusammenfassung

Einer der wichtigsten Faktoren bei der Konstruktion transsonischer Flugzeuge ist die aerodynamische Integration. Eine schlechte Integration kann die Verbesserungen der einzelnen Komponenten schmälern, während eine gute Integration eine bessere Leistung als die einzelnen Komponenten allein erzielen kann. Ein Teil der Flügel-Rumpf-Integration ist das Belly-Fairing, die üblicherweise verwendet wird, um eine gewünschte Verbindung zwischen dem Flügel und dem Rumpf zu erzeugen. Die Kontrolle der Verbindung ist entscheidend, da sie einen großen Einfluss auf die Stoßposition und damit auf die Leistung im inneren Bereich des Flügels hat.

Obwohl es Alternativen zu dieser Praxis gibt, wird sie allgemein verwendet, da die Hinzufügung eines dritten Körpers zum Flügel-Rumpf-Übergang eine flexiblere Konstruktion sowohl des Flügels als auch des Rumpfes ermöglicht. Abgesehen von der aerodynamischen Funktion dient das Belly-Fairing zur Aufnahme des eingefahrenen Fahrwerks.

Natürliche Laminar-Flow-Konfigurationen (NLF) für Mittelstrecken-Transportflugzeuge versprechen große Effizienzvorteile im Vergleich zu traditionellen superkritischen Konfigurationen. Der große Unterschied zu traditionellen Konfigurationen erfordert jedoch eine neue, von Grund auf für diese Art von Konfiguration entworfene Bauchverkleidung.

In der folgenden Arbeit werden die Grundlinien für vorwärtsgepfeilte NLF-Konfigurationen untersucht. Es wurden einige verschiedene Geometrien gefunden, die eine vielversprechende Leistung mit einer Gleitzahl nahe 23 aufweisen. Die nächsten Schritte zur weiteren Verbesserung der Leistung der Konfiguration wurden ebenfalls diskutiert. Schließlich wurde die turbulente Leistung für die leistungsstärksten Geometrien untersucht und es wurde festgestellt, dass der Leistungsvorteil zwischen laminarer und turbulenter Strömung in diesen Konfigurationen zwischen 2.53 und 3.14 Einheiten der Gleitzahl liegt.

Abstract

One of the most important factor in transonic aircraft design is integration. A bad integration can diminish the improvements of individual components while a good integration can achieve better performance than the individual components by themselves. Part of the wing-fuselage integration is the belly fairing, which is is commonly used to generate a desired junction between the wing and the fuselage. The control of the junction is critical because it has a major impact on the shock position and therefore on the performance in the inner region of the wing.

Although there are alternatives to this practice, it is commonly used as the addition of a third body to the wing-fuselage junction allows a more flexible design in both the wing and the fuselage. Apart from the aerodynamic function, the belly fairing is used for housing landing gear when retracted.

Natural laminar flow configurations (NLF) in middle range transport aircraft promise big efficiency advantages compared to traditional supercritical configurations. However the big difference with traditional configurations demands a new belly fairing designed from the ground up for this kind of configuration.

In the following work the baselines for a belly fairing for forward swept NLF configuration are explored. A few different geometries have been found with a promising performance of a gliding ratio close to 23. The next steps for further improving the performance of the configuration have also been discussed. Finally, the turbulent performance it has been explored for the best performing geometries and has been found that the performance advantage between laminar and turbulent flow in those configurations is between 2.53 and 3.14 glide ratio units.

Eidesstattliche Erklärung

Hiermit erkläre ich, Javier Ruberte Bailo, geb. am 03.12.1990 an Eides Statt, dass ich die vorliegende Masterarbeit selbständig und nur unter Zuhilfenahme der angegebenen Literatur angefertigt habe.

Braunschweig, 12. Oktober 2020

**Deutsches Zentrum
DLR für Luft- und Raumfahrt** e.V.
in der Helmholtz-Gemeinschaft

Masterarbeit

am Institut für Aerodynamik und Strömungstechnik
Abteilung Transportflugzeuge

mit dem Thema

Belly-Fairing Design Space Exploration for a Forward Swept Natural Laminar Flow Aircraft

(Exploration des Entwurfsraumes für ein Belly-Fairing an einem Flugzeug mit vorwärts gepfeiltem Flügel und natürlicher Laminarhaltung)

für

B.Sc. Javier Ruberte Bailo, Matr.-Nr. 4429461

Background and Motivation

Laminarization of boundary layers on wings, tail units and engine nacelles has without doubt the greatest potential for improving the aerodynamic performance of commercial aircraft. For this reason, the internal project TuLam (Toughen-up Laminar Technology) was conducted out at the German Aerospace Center (DLR) between 2014 and 2017. The project pursued the two technology paths "Hybrid Laminar Flow Control" (HLFC) and Natural Laminar Flow (NLF). In the NLF path a short and medium range aircraft with Forward Swept Wing (FSW) and the design requirements of an A320-200, the reference aircraft, was designed, Seitz et al. [1]. This design is the starting point of the present master thesis.

The detailed aerodynamic design for wing sections in the vicinity of the wing-fuselage junction (dimensionless half span 0.1< < 0.3) was carried out 3d inversely using the calculation method FLOWer/Takanashi. Fuselage and belly fairing of the configuration were taken from the previous project LamAiR, Kruse et al. [2].

However, the analysis of the final design with the high-fidelity RANS method Tau showed deviations from the FLOWer results, especially regarding the isobars and the position of the compression shock on the upper side of the inner wing. Contrary to what was intended in the design, the isobars show a decreasing sweep angle when approaching the fuselage, which results in an increased wave drag. The reasons for this are probably:

1. The design calculations were done on a comparatively rough computational grid.
2. The boundary layer on fuselage and belly fairing were not modelled (i.e. here an Euler boundary condition was applied) so that their displacement effect could not be considered.

It has been known since the early 1980s that by adjusting the belly fairing the detrimental effects of the center effect on the supersonic flow field of the wing can be reduced. At that time, with the transition from the A300 to the A310, a wing featuring supercritical airfoil sections and an adapted belly fairing was designed for the first time for an Airbus aircraft. But although this technology has been used for more than four decades, only a few publications on this important design aspect of modern transport aircraft can be found.

Task definition

Therefore, the task of this master thesis is to investigate how the transonic flow field on the upper side of the inner wing can be influenced by systematically changing the geometry of the belly fairing, especially with respect to minimizing the wave drag and maximizing the glide ratio in cruise flight. The geometry variations are to be generated by an existing, parameterized CAD model of the belly fairings using the CATIA program, the aerodynamic analysis is to be performed using the high-fidelity RANS method Tau on a grid generated with the Solar software. The results of the work are to be documented in such a way that they can be used as a basis for the derivation of automated optimization processes for belly fairings on arbitrary configurations.

Working steps

To process the task, the following steps must be carried out:

1. Familiarization with the task and use of the programs CATIA, Solar (for grid generation) and TAU.
2. Adaptation / extension of an existing post-processor for the aerodynamic evaluation of the belly fairing geometry variations.
3. Evaluation of the reference aircraft from the TuLam project at its design point.
4. Definition of the parameter space to be investigated. As mentioned above, an already existing parametric CAD model shall be used for the belly fairing of the TuLam configuration.
5. Performing the geometry variations with subsequent aerodynamic analysis at the cruise flight design point of the TuLam configuration.
6. Evaluation of the calculation results after each step and subsequent opening / limitation of the parameter space in agreement with the supervisor.
7. Development of recommendations for the aerodynamic design or the optimization of belly fairings based on the results obtained.

Report

The work carried out and results must be described and discussed in a clearly structured report.

Literature

[1]   A. Seitz, A. Hübner, K. Risse: *The DLR TuLam project: design of a short and medium range transport aircraft with forward swept NLF wing*. CEAS Aeronautical Journal (2019), https://doi.org/10.1007/s13272-019-00421-1

[2]   M. Kruse, T. Wunderlich, L. Heinrich: *A Conceptual Study of a Transonic NLF Transport Air craft with Forward Swept Wings*. AIAA Conference Paper 2012-3208 (2012), https://doi.org/10.2514/6.2012-3208

[3]   J. D. Anderson: *Modern Compressible Flow: With Historical Perspective*. McGraw-Hill Education – Europe (1990) , ISBN 0071006656

[4]   C.-C. Rossow, K. Wolf, P. Horst: Handbuch der Luftfahrzeugtechnik. Carl Hanser Verlag, München (2014)

Betreuer:
Dr.-Ing. Arne Seitz
DLR-Institut für Aerodynamik und
Strömungstechnik
Lilienthalplatz 7
38108 Braunschweig
Tel.: +49 (0) 531 295 2888

Bearbeitungszeitraum: **6 Monate**
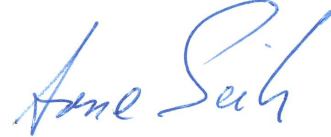
Aufgabe ausgegeben am: ~~02.03.2020~~ 25.02.2020

Abgabedatum: ~~02.09.2020~~ 25.08.2020

geändert am 02.03.2020 aufgrund Mitteilung der Fakultät für Maschinenbau, Fr. Eilers

(Prof. Dr.-Ing. C.-C. Rossow)
Erstprüfer

**Deutsches Zentrum
für Luft- und Raumfahrt e.V.**
Institut für Aerodynamik
und Strömungstechnik
Lilienthalplatz 7
38108 Braunschweig

(Dr.-Ing. Arne Seitz)
Betreuer

Nomenclature

Latin nomenclature

a	Speed of sound
C_D	Drag coefficient
C_L	Lift coefficient
$C_{L,\,MAX}$	Maximum Lift coefficient
C_P	Pressure coefficient
C_{DW}	Wave drag coefficient
$E = C_L/C_D$	Glide Ratio
Ma	Mach number
p	pressure
R	allgemeine Gaskonstante
Re	Reynolds number
T	Temperatur
x	Coordinate parallel to the fuselage mid axis
y	Coordinate parallel to the wingspan
z	Coordinate parallel to the gravitational force

Greek nomenclature

η_{BF}	Belly fairing cross-section position relative to the wing root chord length
η_W	Wing profile position relative to the Wingspan

Abkürzungsverzeichnis

ALT	Attachment Line Transition
ATRA	Advanced Technology Research Aircraft
CFD	Computational Fluid Dynamics
CF	Cross Flow
CFL	Courant-Friedrichs-Lewy
CFRP	Carbon Fibre Reinforced Plastics

CS	Cross-section
DeSiReH	Design, Simulation and Flight Reynolds Number testing for advanced High Lift Solutions
DLR	Deutsches Zentrum für Luft- und Raumfahrt
FL 350	Flight level 350
HLFC	Hybrid Laminar Flow Control (Combination of LFC and NLF)
LamAir	Laminar Aircraft Research
LFC	Laminar Flow Control
LST	Lineare Stability Theory
NLF	Natural Laminar Flow
RA	Reference Angle
RANS	Reynolds-Averaged Navier-Stokes
RG1	Reference Geometry 1 (LamAir Adapted)
RG2	Reference Geometry 2 (TuLam)
SG	Starting Geometry
TG1	Test Geometry 1
TG2	Test Geometry 2 (Streamlined)
TS	Tollmien-Schlichting
TuLam	Toughen up Laminar Technology
YR	Y Ratio

Contents

1. Introduction

Fuel efficiency has been always a big goal for aircraft research. Furthermore these days that climate change and carbon dioxide reduction are a hot topic, many efforts are being focused in developing novel, more efficient technologies. One of the answers towards more efficient aircraft are natural laminar flow (NLF) wings, which achieve laminar flow only with passive methods. Because of the big performance increase that a NLF wing can achieve, up to 12% block fuel reduction as Seitz et al. [19] claims, NLF wings may be a huge step towards more efficient aircraft. Already in the 80s there was research in laminar aircraft, such as Redeker et al. [14], nevertheless NLF wings have many requirements which made them for a long time either very difficult and therefore costly to manufacture or gave them disadvantages in other ways. Some of the requirements are high quality, low roughness surfaces, no steps between panels, low leading edge sweep, etc. With technology development in fields like composite materials and many research projects like Seitz et al. [18], Seitz et al. [19], Redeker et al. [14] and others, it has been reached the point in which the requirements no longer outweighs the gains, and therefore laminar wings are closer to being built in transport aircraft.
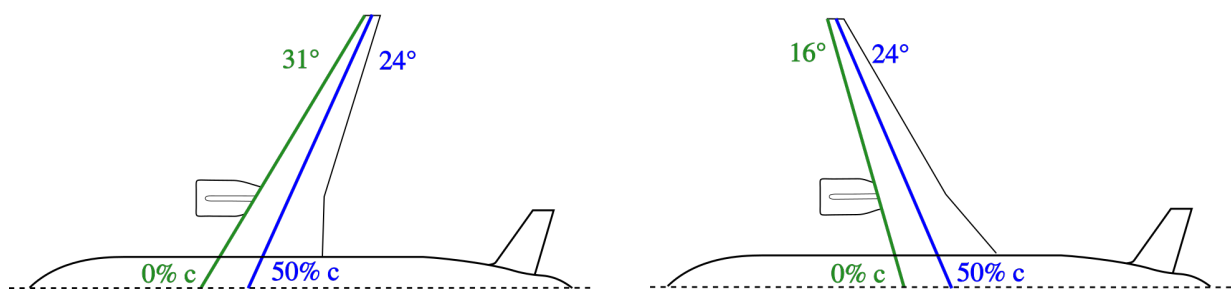

Figure 1-1 Sketch of a forward swept wing and a backwards swept wing, both configurations have a 24° sweep at 50% of the chord, however the backwars swept wing needs a greater leading edge sweep. Sketch based on Seitz et al. [19]

Some design choices in transonic aircraft design have become very popular because of the associated advantages. Two of them are wing sweep and wing taper. Wing sweep is important to reduce the compressibility losses and wing taper reduces induced drag and leads to lightweight wings with small and light wing tips and big and resistant wing roots with little added coplexity. Nevertheless when put together, a careful design must be done. Due to the isobar distribution along the wingspan the local sweep changes along the chord. A representation can be found in Fig. 1-1 where it can be seen that for the case with forward sweep the local sweep increases along the chord. On the other hand, for backward swept wings, the local sweep decreases along the chord. This property is the founding stone of forward swept wings. Due to the local sweep increase along the chord, a low sweep leading edge can be achieved while there is still a moderate sweep in the re-compression region of the wing. The reason why a low leading edge sweep is important for NLF wings is the so called cross-flow transition (CF) and the attachment line transition (ALT). When the leading edge has a high sweep, cross-flow instabilities take place, which will lead to transition at a given Reynolds number if the angles are too high. Redeker et al. [14] found that for the con-

ditions analysed already with a leading edge sweep angle of 21° the laminar surface was greatly reduced. When this limitation is applied to modern short and medium range transport aircraft with the high flying speeds i.e Airbus A320 with a cruise speed of Ma 0.78 [11], can be quickly realized that forward swept wings are the only way towards NLF wings. Higher leading edge sweep angles lead to high CF instabilities, which can be controlled with laminar flow control (LFC) but lead to an increased system complexity and higher weight penalties.
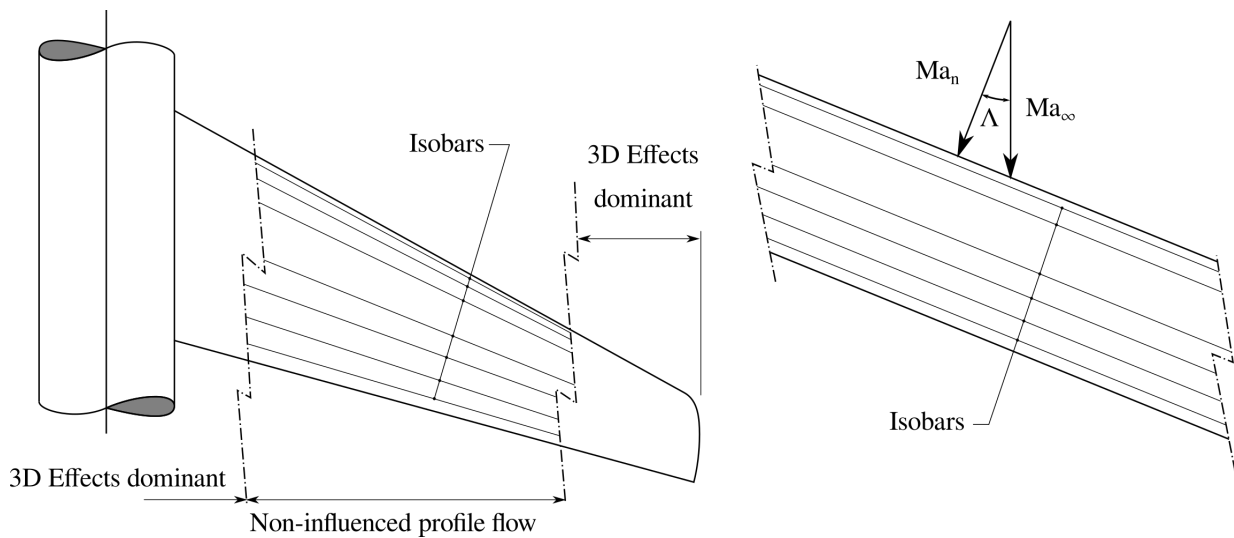
Figure 1-2 Sketch of a infinite swept wing with isobar pressure distribution, and the region in a installed wing where the infinite swept wing results can be used as an aproximation. Sketch based on Torebeek [23]

So far the properties of swept wings have been described from a 2.75d perspective, in which sweep and taper are considered. That is to say, the pressure distributions are constant along the wingspan and the isobars coincide with constant chordlines. Nevertheless when the wing is integrated in a fuselage, 3d effects take place. As Fig. 1-2 represents, at the wing root and the wing tip 3d effects take place, and only in the rest of the wing the 2.75d approximation can be used. This is a long known issue, usually known as middle plane effect. In the region close to the fuselage the isobars no longer follow the the conic distribution typical from the 2.75d, but instead tend to run perpendicular to the fuselage surface.
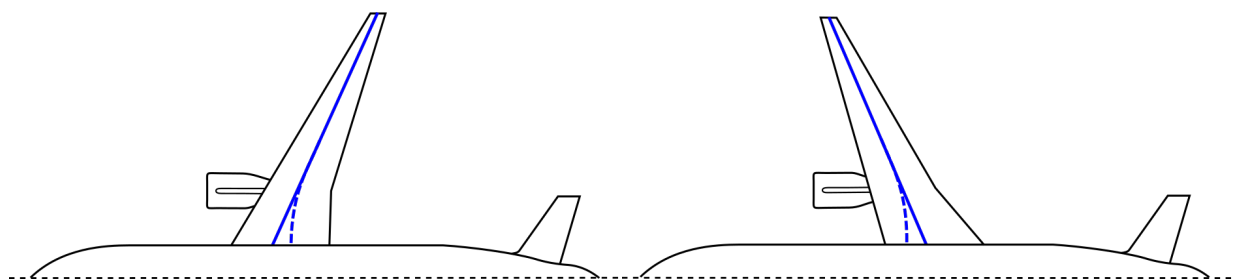
Figure 1-3 Sketch of a forward swept wing and a backwards sept wing, the continuous line represents in both cases the shock in a isobar distribution along the wingspan, the dashed line represent the real shock position with the fuselage influence.

As Streit and Hoffrogge [21] found out, at the wing root, this effect leads to more gradual accelerations in backward swept wings and to sharper accelerations in forward swept wings compared to the same profile outside of the affected zone. Another consequence of the 3d effects is the de-sweeping of the shockwave in transonic wings, which leads to an increase in the wave drag and a reduction in the lift, which has to be compensated with an increased angle of attack.
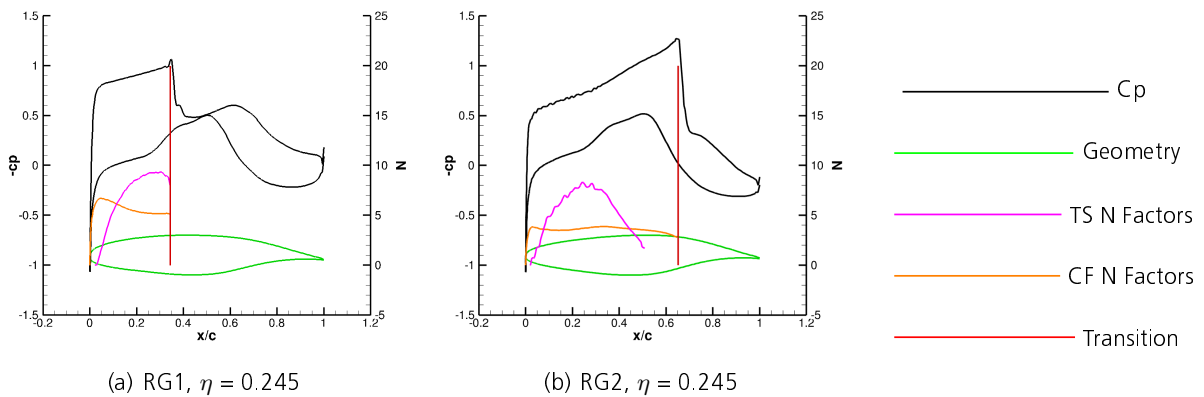

(a) RG1, $\eta = 0.245$ (b) RG2, $\eta = 0.245$

Figure 1-4 Effects of the shock position in lift distribution, the C_P distribution has been taken at the same position for two different belly fairing geometries at constant lift

A representation of the shockwave desweeping can be observed in Fig. 1-3. This phenomena leads to a big influence in the pressure distribution, represented in Fig. 1-4. For the same wing at the same span and constant lift coefficient two different belly fairings lead to completly different results. Streit and Hoffrogge [21] tried with help of the inverse design approach to bring the shock wave to the isobar position by varying only the wing profiles but found out that the support of additional geometry was necessary. A common approach to regain the optimal isobar distribution is the usage of a belly fairing, which consists in a third body in the wing-fuselage junction. Its main function is to support the 3d developed airfoils to achieve the desired pressure distribution. In Fig. 1-5 a representation of a belly fairing can be observed. While belly fairings have been used for a long time in transport aircraft, the high number of degrees of freedom makes the design of a belly fairing a complex task. Furthermore, the limited literature available about belly fairing design and the lack of baselines regarding forward swept wing belly fairings make the design a difficult task.
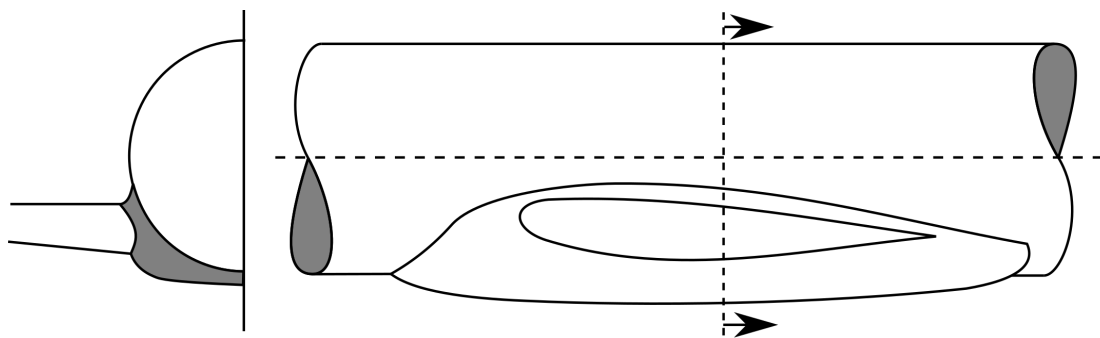

Figure 1-5 Sketch of a belly fairing. Sketch based on Torenbeek [23]

This work starts from the configuration designed during the DLR TuLam project, which consists of a forward swept NLF wing transport aircraft. The development will take place with help of a parametric belly fairing and the RANS solver TAU. The goal of this work is to found the baselines for further development. In order to do so, a systematic variation of the geometric parameters of the belly fairing will be performed and aerodynamically analysed. The simulations will be performed at the design point of the wing-belly-fuselage combination of Ma = 0.78, FL350 and C_L = 0.52. For the results analysis the most important performance metrics are the glide ratio E, drag coeffcient C_D and wave drag coefficient C_{DW}. The wing and the fuselage originate from the TuLam project [19] and will be kept constant during the whole work.

The following report on the work conducted is structured as follows: Chapter 2 will discuss the literature review and the theoretic background of the work. Chapter 3 will be take a view about the previous work and the starting point of this work. Chapter 4 will explain the methodology, the geometry generation, the grid generation, the simulation strategy and the results post-processing. In chapter 5 the results will be shown. In chapter 6 the conclusions will be discussed and the proposed future work will be shown.

2. Literature review

In this chapter the necessary information regarding sampling strategies for design space explorations will be discussed. Later, a review of wave drag definition and its influence will be performed.

2.1. Sampling strategies

When performing a parameter study, there are different methodologies available. Choosing the appropriate methodology allows a good covering of the simulation domain while keeping the number of geometries as low as possible. In the following the most used methodologies in numeric simulation will be explained.

In order to perform a parameter study, one or more variables are modified in a predefined range in order to find the degree of correlation of the variables with the outcomes. Two of the most widely used methodologies to choose the values of the variables are fully factorial experiment and latin hypercube sampling. Apart from methodologies to choose simulations, there are statistical tools like response surface modelling which seek to predict a the outcomes of the whole domain based in the available discrete data.

2.1.1. Fully factorial sampling

A fully factorial experiment is characterized by two or more variables, for which all the possible combinations are calculated. In this way, for a two variable experiment, with three values per variable the amount of simulations is 9. The number of simulations is fix by the following equation $N_{sim} = N_{var}^{N_{val}}$, where N_{sim} is the number of simulations, N_{var} is the number of variables and N_{val} is the number of values. Figure 2-1 represents two different fully factorial experiments. This methodology provides a well structured and organised simulation methodology, which allows to isolate variables in order to find correlations. On the other hand this methodology only works well for a small amount of variables and values, as the number of values and variables increase, the number of simulations increase to a unmanageable number.

This can be a problem also when the simulation domain is too big, as in that case a small step between values is required to get a proper representation of the outcomes, which leads as well to high number of simulations.

2.1.2. Latin hypercube sampling

The latin hypercube sampling, McKay et al.[9] is a sampling methodology which tries, for a given number of simulations, to spread in the given simulation domain equidistantly. In order to achieve this goal the methodology is based in a random stratified distribution. Firstly the range of each variable is divided in a number of sectors equal to the number of simulations, all the sectors have equal length . Then, the simulations are allocated in random sectors for each variable with the condition that each sector for each variable is only allocated once. Then random values are given to the simulation in the given sector. Figure 2-2 represents two different sets of latin hypercube
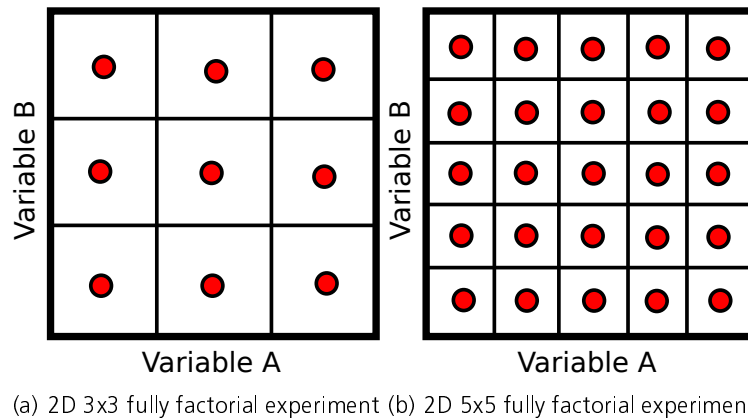
(a) 2D 3x3 fully factorial experiment (b) 2D 5x5 fully factorial experiment

Figure 2-1 Representation of two fully factorial experiments. Note the big increase of simulations even for a 2D case

sampling for five and 10 variables.

This methodology has memory effect, since for each sampling the allocated sectors of each variable must be known. Therefore recursive latin hypercube simulations with no overlapping condition lead eventually to a fully factorial experiment.

Note that two different latin hypercube samplings may lead to two different simulation allocations, Fig. 2-2 represents this phenomenon as well.

(a) 5 variable LHS   (b) 5 variable LHS   (c) 10 variable LHS   (d) 10 variable LHS
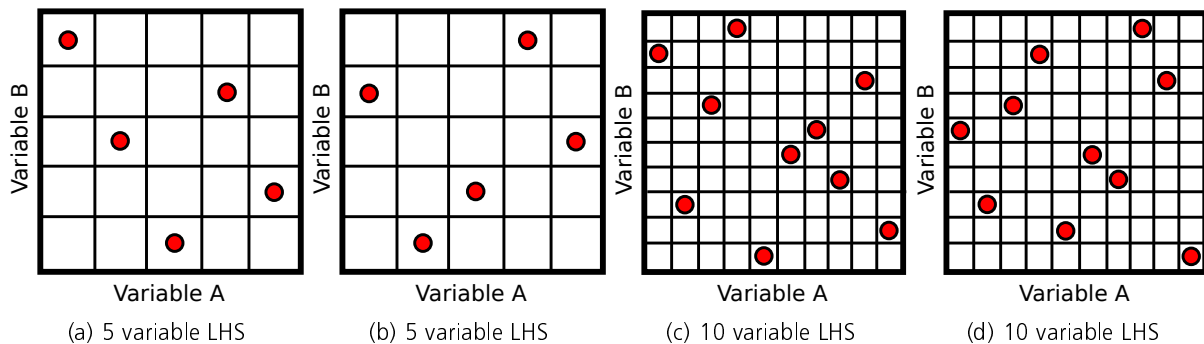
Figure 2-2 Representation of four latin hypercube samplings. Note that two different samplings of the same number of variables may sample in different positions

2.1.3. Response surface modelling

Response surface modelling is a statistical tool which tries to predict the outcomes of a system in a given domain based in discrete results of the study, Antony [2]. The methodology is a polynomial approximation and the degree of certainty depends heavily in the sampling size and the distance between samples of the available data.

Although generating a response surface may be more complicated than other types of experiments, it is very useful to analyse trade-offs and to find low and high spots in the system performance. Additionally the computing cost can be drastically reduced. The advantage of generating a response surface is coupled with the complexity of the problem, as high performance spots may be influenced

by many variables and therefore not be easy to find manually.
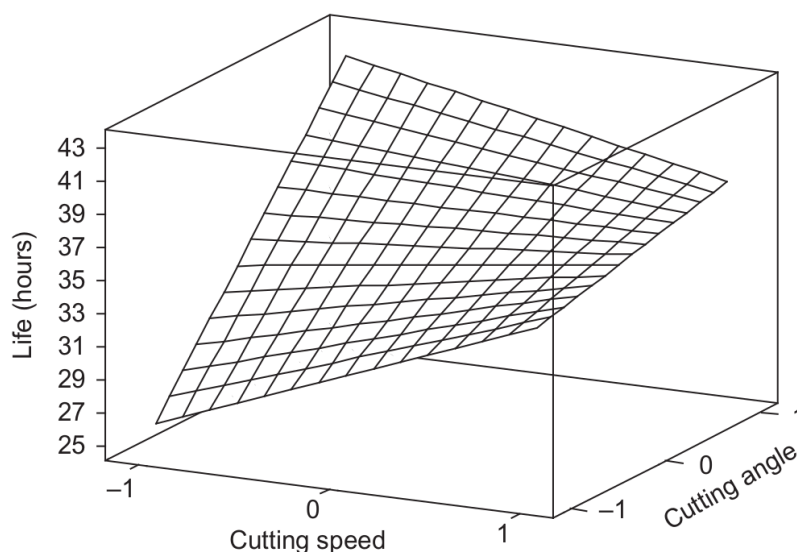
Figure 2-3 Sketch of a response surface of a two varible system. Sketch from Antony [2]

A response surface model can be also used to focus the computing power in the most promising geometries of a domain. In order to do so, the total amount of simulations are shared in different iterations, first a small amount of the total number of simulations is performed, then a surrogate model is built. Based on the predictions of the surrogate model the next batch of geometries are decided. The first surrogate models usually give bad predictions, but as the most significant positions in the domain are populated the predictions improve.

2.1.4. Wave drag and re-compression shocks

As an aircraft approximates to the speed of sound, supersonic regions appear around the aircraft. As the speed further increases, and the Mach number further raises in the supersonic regions re-compression shocks appear at the end of these.

When a re-compression shock appears, there is a flow region in which from the aircraft's perspective the fluid speed reduces abruptly as it goes through. From a global perspective, the fluid going through a re-compression shock is accelerated abruptly. This type of moment exchange is called wave drag, as aircraft's energy is being transferred to the flow field through a phenomena different to pressure drag or friction drag.

The amount of moment exchange depends in the strength, the extent and the angle of the shock to the incoming flow. As the speed increases above the design speed and closer to Ma = 1 the wave drag increases exponentially, even overtaking the whole friction and pressure drag of the aircraft. This point is usually called drag divergence point.

Normal shocks to the flow have the maximum amount of moment exchange. Oblique shocks lead to a reduced amount of moment exchange. Therefore shock de-sweeping at the wing root is coupled with an increase in wave drag.

Re-compression shocks are characterized by their mobility, depending on the free-stream velocity and the surface gradients the re-compression shocks move along the surface.

Re-compression shocks are the source of dynamic phenomena as buffeting or static ones as Mach tuck.

3. Previous work

In this chapter will be discussed the work that it has been historically done regarding NFL transport aircraft, in the following part, will be explained the DLR projects from which this work sets off and finally, a review of will be done of the status at the beginning of the present thesis.

3.1. Historic research

As previously discussed, many work has been invested in laminar research, the earliest known work in laminar flow control (LFC) dates as far back as 1930, a great collection of LFC research can be found in Braslowi and Albert [4]. The first research done in NFL dates from 1980s, while NASA researched with the F-111 by Runyan et al. [16] and the F-14 project by Wagner at al. [24], DLR researched with the VFW-614 by Redeker et al. [14]. The goal of both NASA and DLR was to find the impact of sweep angles in CF instabilities and transition. In 1987 Boeing, under a NASA contract, researched the impact of engine noise in NLF transition by Runyan et al. [17]. In DLR, since the late 80s, many projects have been focused towards NLF wings, nevertheless the most important for the thesis are Seitz et al. [18] and Seitz et al. [19]. Both studied a fuselage-wing configuration, as in the present work. The results and some geometry of Seitz et al. [19] are the starting point for this study.

3.1.1. Laminar glove

As previously discussed, in the 80s an experimental campaign took place in DLR, in which first a laminar glove was developed, flight tested and analysed by Redeker et al. [14] and Horstmann et al. [7]. The main concern was to study the effect of cross-flow transition (CF) and attachment line transition (ALT) on laminar profiles at high reynolds numbers and the interaction between the Tollmien-Schlichting (TS) and the CF instabilities. Apart from that, the Pfeninger-Poll criteria for avoiding ALT transition was put to the test and discovered that it had a good agreement with the ALT transition in free flight. References for the criterion are Cumpsty and Head [5], Pfenninger [12] and Poll [13]. Additionally, research regarding surface disturbance and engine noise influence was performed. They found out that while the engine noise had a little influence, the roughness in the region between 5% and 20% had a strong effect in premature transition.

3.1.2. LamAiR

Based on the findings of previous research, and the availability of new design tools, the LamAir project by Seitz et al. [18] had as goal the design of a NLF short range transport Aircraft. In order to achieve such a goal, firstly a preliminary design tool was used to define the size, design point operation and the reference aircraft, which was based on an Airbus A320-200. The design focus was centred in forward swept wings, due to the previous discussed low leading edge sweep advantages for NLF. In order to design the wing 2.75d inverse design tools were used. Additionally, an aerodynamic-structure coupled study was performed, in which the Carbon Fibre Reinforced Plastics (CFRP) performance was evaluated and optimized to counteract the forward swept wing structural

misbehaviour by aeroelastic tailoring. A range of operations were analysed and a wing-fuselage configuration was designed. As final part of the design 3d analyse were performed in which was clear that a 3d design was necessary due to the shock desweeping. At the time there was some remaining questions, like the insect influence at start and landing or the high lift system. For the LamAiR project the smart droop nose of Monner et al. [10] was chosen, which had the advantage that upper and lower surface had a high lift system without gaps and therefore in both surfaces could be achieved natural laminar flow. On the other hand, the smart droop nose could not achieve the same $C_{L,MAX}$ as a modern turbulent high lift system, which meant that the wing had to be designed larger than the optimum for the cruise flight in order to achieve the same landing and start distances as the reference aircraft. An additional remaining question at the time was if the trade off of the suboptimal cruise wing surface was compensated by the extra natural laminar flow of the under side of the wing.

In order to counteract the strong 3d effects encountered, a belly fairing was constructed. The design strategy followed was a 3d inverse design in TAU. From the CFD results, grid modifications were performed to achieve a pre-set pressure distribution. As Kruse et al. [8] shows, the development of the belly fairing led to a flow improvement in the fuselage proximity. The 3d effects could be counteracted to the point in which the shock almost followed the desired isobar distribution.

3.1.3. TuLam

Departing from the LamAir Project, the goal of the TuLam project by Seitz et al. [19] was to firstly come with a solution for the remaining questions of the LamAiR project and then to improve the performance to achieve a final development of the NLF transport aircraft. During TuLam project the high lift system changed from the smart leading edge to a Krueger flap designed during the DeSiReH project by Strüber and Wild [22], this design choice did allow to reduce the wing surface to the cruise optimum, with the trade-off that the high lift steps would only allow natural laminar flow in the upper surface. Additionally, due to insect shielding effect of the krueger flap at take-off and landing, an open problem of the LamAir project was solved. The main design challenge which was tackled in the TuLam project was the 3d effects of the wing fuselage integration. In order to achieve an isobar distribution along the wingspan for the new wing, new parametric airfoils were introduced in the region close to the fuselage while the belly fairing was kept constant. A 3d inverse design based in the structured RANS solver FloWer, optimized the airfoil parameters. The belly fairing used was the one developed for LamAir project, despite the chord reduction. The results showed an overall improvement from the previous design despite the under side of the wing was turbulent.

Due to the findigs of Streit and Hoffrogge [21], that the strong 3d effects are very difficult to compensate only with the wing profiles, the results remained to be corroborated with a high fidelity method and a fine grid. Based on these results a decision should be taken if a new belly fairing design is worth to be considered.

3.2. Current status

As previous discussed, one of the following parts of the DLR NLF design consisted in gathering the up-to-the-date research and perform high fidelity RANS analysis which would provide a good overview of the research standpoint. After the high fidelity analysis was performed, it was clear that despite the performance increased substantially from LamAiR to TuLam, there was still work to do regarding 3d integration. To further develop the NLF configuration, a 3d geometry based in the TuLam geometry was constructed. The wing and the fuselage are from the TuLam project but have been designed parametric to allow a parametric study. A few preliminary tests have shown, that the belly fairing has a big influence area which extents up to the 30% of the wingspan, and therefore exerts a big impact on the aircraft performance. These findings have been the set off point for this study. In the following the results found will be discussed.

3.2.1. Geometry definition

In order to assess the starting point was important to to set a trustworthy baseline. In order to do so, the LamAir, TuLam and other three geometries were constructed, meshed and calculated. The goal of the three extra geometries was to test the influence extent of the belly fairing in the aircraft performance. The nomenclature used for the geometries was defined as reference geometry, 'RG1' for the LamAiR configuration and 'RG2' for the TuLam configuration. Both configurations had the afore mentioned LamAiR belly fairing, which is not parametric. Besides the already studied geometry three geometries based in a parametric belly faring were considered, the nomenclature used for these geometries is starting geometry 'SG', test geometry 'TG1' and 'TG2'. Each of the geometries had a different goal. RG1 and RG2 had as task to define the starting point. For SG, the main goal was to create a symmetry plane effect, that is to say, in the upper side of the wing, was intentionally created a quasi constant gradient from the belly fairing perspective, so that the wing gradients had no additional influence. For TG1, the belly fairing geometry was kept constant and moved backwards so that the accelerations of the 'growing' part of the belly fairing played a role in the suction side of the wing, the main goal was to observe what kind of influence could be expected from two completely different belly fairings. For TG2 the goal was to create a belly fairing based in the flow found outside of the 3d influence zone, the mindset behind this design is that if a 2.75d flow can be achieved by the belly fairing, then the pressure distribution should follow an isobar distribution and therefore the shock de-sweeping should be suppressed. All geometries have the same wing layout. Furthermore, all current and future geometries apart from RG1 have the same wing, which was developed during the TuLam project. A secondary task of this previous study was to generate values for the variables of the parametric belly fairing, which would be very useful for later research.

3.2.2. Reference geometry performance

All the geometries were analysed at the cruise conditions of Ma = 0.78, C_L = 0.52 and FL 350. The results obtained from the LamAiR i.e. RG1 geometry were not promising. At this point it is worth to remember that the LamAir original wing area was larger than TuLam, which leads to an analyse outside of the original LamAir design point. At the mentioned flight conditions the RG1 geometry had a strong shock at the wing root already at a the 10% of the chord. The angle of attack was

too high for the cruise flight, which leads to the conclusion, that the desired C_L is at the limit of the geometries performance. Due to the early, almost perpendicular shock, a strong separation takes place in the wing root section. The performance metrics for this and the following geometries can be observed in Table 3-1

The TuLam i.e. RG2 results supported partially the results obtained by the Tulam project, a high performance was obtained. Nevertheless a discrepancy with the TuLam results were found in the root region, up to a η_W of 0.2, a shock de-sweeping takes place, which leads to think that there is still room for improvement.

For SG geometry a close behaviour to the RG1 was observed. Firstly the geometry did not converge despite the high iteration number. While for most geometries 10000 iterations was enough to achieve an acceptable convergence, it was observed that low performing geometries took much longer. A plausible source for the slow convergence may lay on the angle of attack iteration process. When a geometry does not achieve the desired lift coefficient the angle of attack is increased. In low performance geometries this point may never be achieved. This behaviour can be observed when the final lift coefficient has not achieved the desired lift coefficient despite the angle of attack is high. Since the performance of SG was not good and the flow was already separated, the geometry was not further calculated.

As previously mentioned TG1 is the same belly fairing as SG but moved backwards. The performance obtained is as in SG very low, a premature shock almost normal to the incoming flow for a large portion of the wingspan, a big shock induced separation, low performance and high angle of attack.

TG2 gave promising results, which as a recap was based in the 2.75d flow in the middle of the wing. Good convergence was achieved quickly, and a slightly lower glide ratio in comparison with RG2. While in TG2 shows improvements at the shock de-sweeping region in comparison with RG2, the region is still not small, reaching up to η_W of 0.18. On the other hand TG2 shows a worse performance towards laminar flow, the total surface is reduced in comparison with RG2.

Summarized from this preliminary analyse the outcomes are clear, a belly fairing has a huge impact in the aircraft performance. A good design may support a proper wing design to even better performance, a bad design may even reduce the $C_{L,MAX}$ below the cruise lift coefficient. Despite the RG2 performance was not fully achieved, the ease in which TG2 achieved a close performance leads to believe that a high performance gain may be achieved through the work. This performance was achieved despite inherent deficiencies, such as the manual design, used for TG2 and implicit methodology mistakes like the limitations of the parametric belly fairing used. More complex and systematic methodologies may achieve even better performance.

3.2.3.   Summary of preliminary study

The preliminary work has given numbers to the importance of a suited belly fairing for an proper performance. Furthermore a limited dataset of values for the parametric belly fairing and the performance metrics has been generated. Additionally, it was measured the wingspan extent of the belly fairing influence, which has been feed back in the mesh generating process to ensure a high mesh resolution in the influence area. The findings of the preliminary study have been continued through this work in order to further understand the importance of the belly fairing in the wing body integration performance.

Flow

(b) RG1   (c) RG2   (d) SG   (e) TG1   (f) TG2
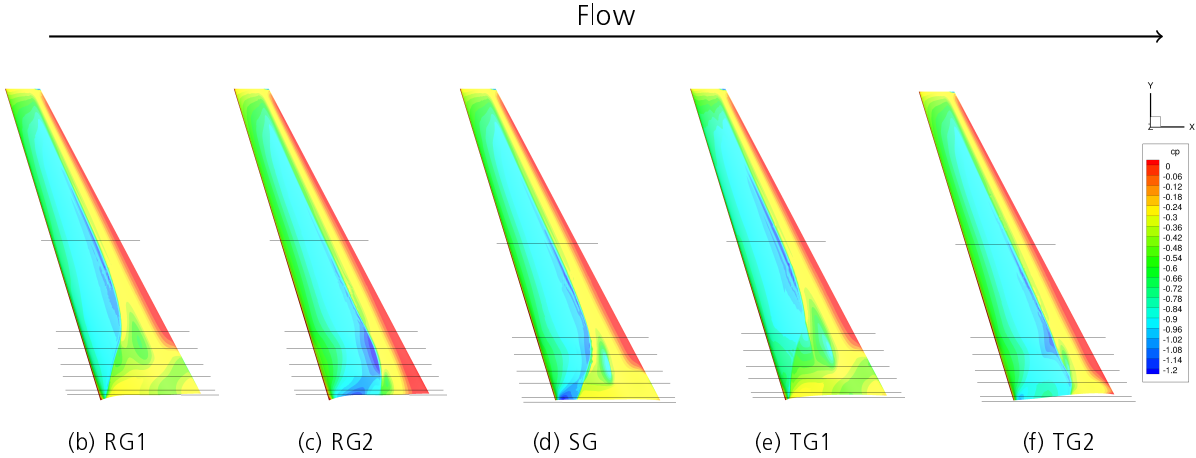
Figure 3-1 C_P distribution for the five different belly fairing / wing geometries at constant lift

Table 3-1 Performance metrics for the preliminary geometries

Geometry	$\alpha\ [deg]$	C_L	C_D	E
RG1	1.91	0.5198	0.0365	14.2410
RG2	0.77	0.5200	0.0228	22.8370
SG	1.05	0.5007	0.0279	17.9462
TG1	1.86	0.5198	0.0377	13.7877
TG2	0.71	0.5198	0.0234	22.3136

Flow

(b) RG1   (c) RG2   (d) SG   (e) TG1   (f) TG2
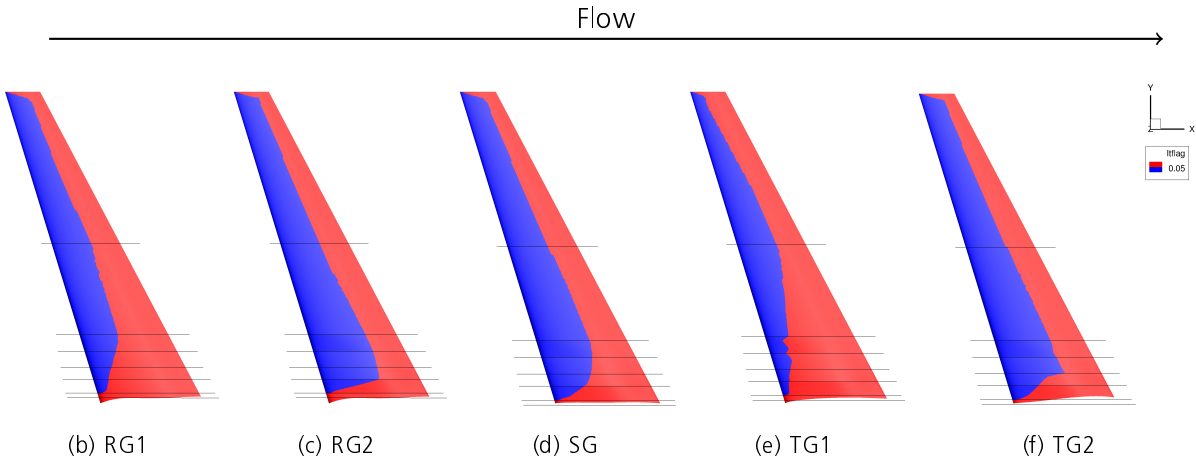
Figure 3-2 Laminar extension for the five different belly fairing / wing geometries at constant lift

Flow

(b) RG1 (c) RG2 (d) SG (e) TG1 (f) TG2
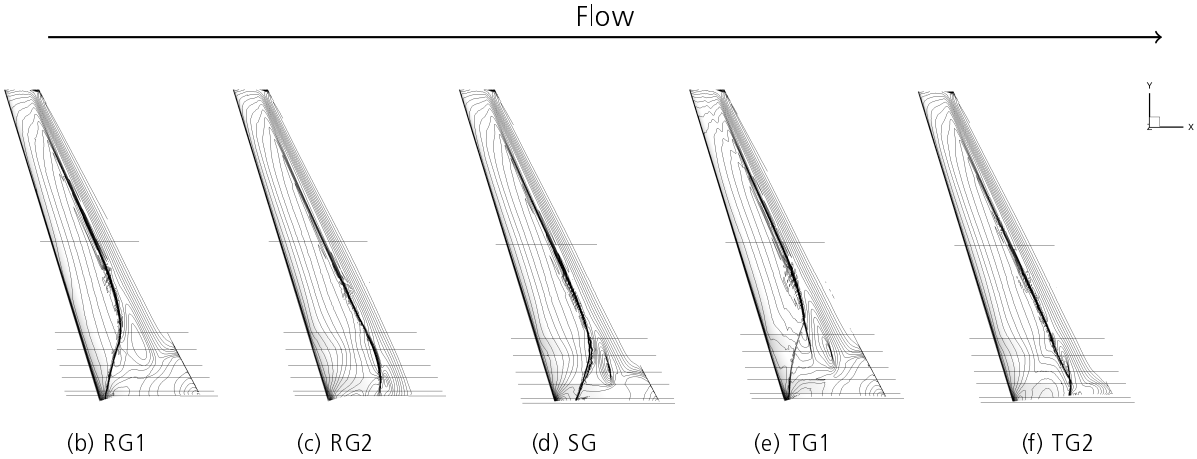
Figure 3-3 C_P level curves for the five different belly fairing / wing geometries at constant lift

4.   Methodology

In this chapter the process followed from the input files to the CFD results will be described. Firstly the focus will be centred in the main configuration of the aircraft, the CAD-parametric model and the geometry generation. The next important point is the grid generation, how it is generated and which steps where taken to ensure a certain trustworthiness of the grid despite no experimental data is available for validation. Then follows a description of the configuration used in TAU for the simulations, especially in the parameters used for NLF. After that, the methodology of the post-processor will be discussed. Finally, the methodology of the parameter study will be explained.

4.1.   Calculation methodology

In this section the geometry generation, the parametric model, the mesh generation, the mesh independence study and the tau configuration will be discussed.

4.1.1.   Geometry structure and generation

In order to perform a parameter study it is necessary to define an appropriate methodology for the geometry generation. As part of the performance optimization, the wing as well as the belly fairing was parametric constructed, which allows to accomplish a positive feedback between wing and belly fairing if both are optimized. In this study the work will be focused on the belly fairing, future work may be focused in the wing once a proper belly fairing design is achieved. In an ideal case both belly fairing and wing would be considered at the same time, but the high number of degrees of freedom in both the belly fairing and the wing lead to a too complex and time consuming numerical experiment.

The geometry has been constructed in Catia V5. The parameters have been linked with construction tables, which together with visual basic macros has enabled a quick method to export a high number of geometries.

As previously discussed, the fuselage has been taken from the TuLam project, which is similar to an Airbus A320. The fuselage geometry is not parametric and does not have a tailplane, pylons or engines.

4.1.1.1.   Wing

Some design considerations have been taken to avoid overcomplicating the geometry generation. The wing layout is fix as a single trapezoidal shape in which leading edge sweep can be modified. Further layout parameters such as taper, dihedral and wingspan can be tuned as well. More complex layouts have not been considered since the wing layout is defined and only small variations are expected. Additionally, twist and airfoil sections have been implemented in a more flexible configuration, which is necessary for future wing development. Along the wingspan, the different profile positions are independently defined, with help of an η_W parameter for each profile, which defines the position of the profile along the wingspan, η_W takes a value of 0 for the wing middle plane and

1 for the wing tip. For the wing geometry of the TuLam project six different airfoils were used. One of them is present in two different positions, profile 6 and 7. The different profile positions of the wing are displayed in Fig. 4-1.

-17°

-27° 48'

Profile 7, η=1, y=17000mm

Profile 6, η=0,56, y=9520 mm

Profile 5, η=0,294, y=4998 mm

Profile 4, η=0,24565, y=4176,05 mm

Profile 3, η=0,16332, y=2776,44 mm

Profile 2, η=0,12331, y=2096,27 mm

Profile 1, η=0,10988, y=1868,02 mm

1868,02 mm
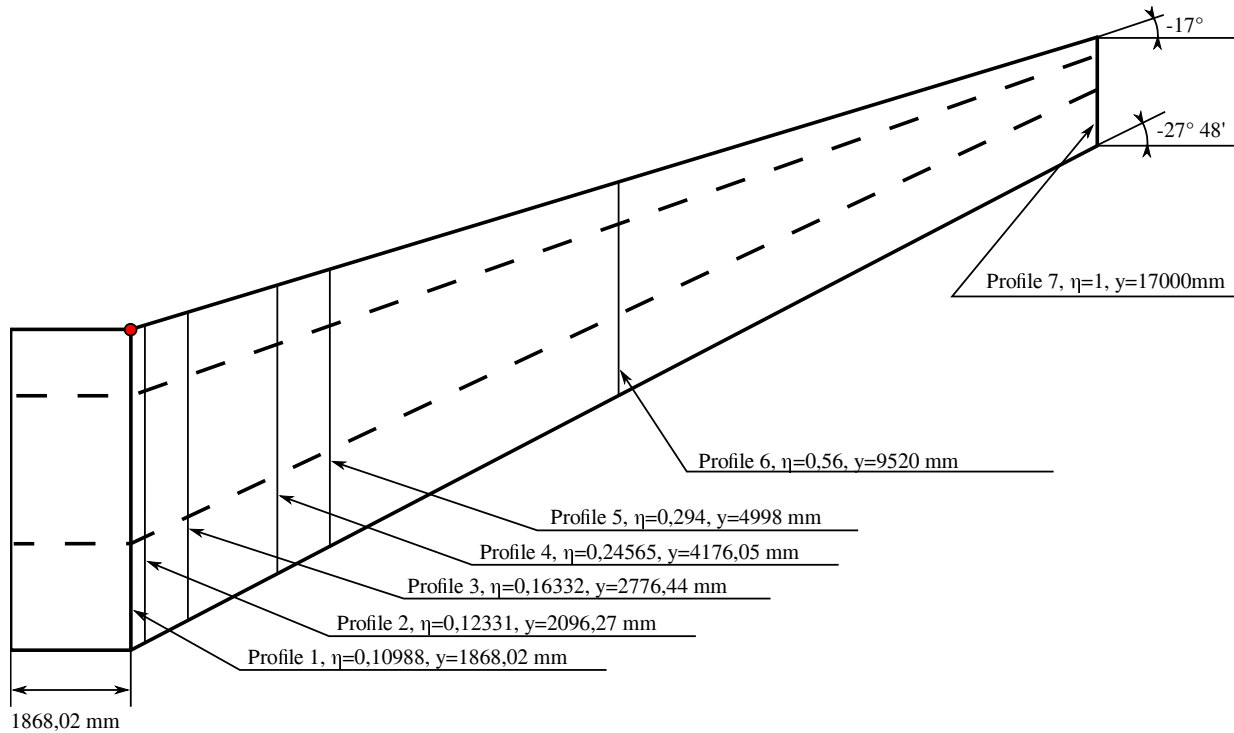
Figure 4-1 Sketch of the wing layout, 7 profile have been used to generate the wing geometry. The red point defines the reference point.

Additionally, each profile has an independent twist, which translates in a local angle of the airfoil relative to the X axis. Together with the airfoil position different twist distributions can be accomplished. In the region between two different profiles the airfoil shape and the twist is interpolated linearly. This means that the surface has a curvature discontinuity at the profile positions. In order to provide a proper reference which can be used either for the wing or for the belly fairing, a reference point has been defined on the leading edge of the first profile.

4.1.1.2. Belly fairing

The methodology choosen to generate the belly fairing is in comparsion to some literature much simpler. Song and Lv [20] used a 4 cross-section belly fairing with 10 points each. In comparision, the 5 point, 4 degree B-spline used in this work has reduced complexity. Figure 4-2 shows a sketch of the B-splines used for the belly fairing generation. This methodology is based in previous work done by Arno Ronzheimer in backward sweept wings [15].
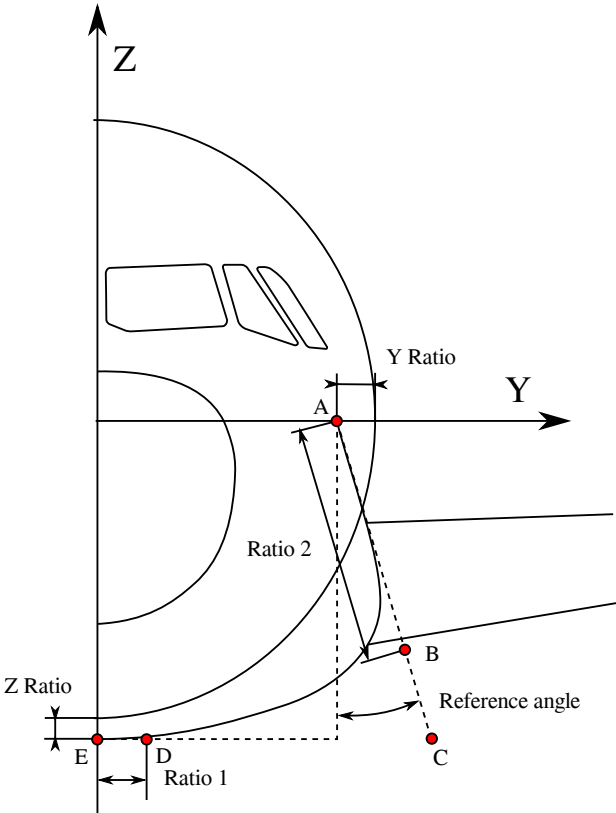
Figure 4-2 Sketch of the parameters used for the belly fairing generation. Each cross-section is a four degree B-Spline contained in the ZY plane. The represented parameters (Z Ratio, Ratio 1, Ratio 2, Y Ratio and Reference Angle) define the position of the 5 points (A,B,C,D,E) for the spline.
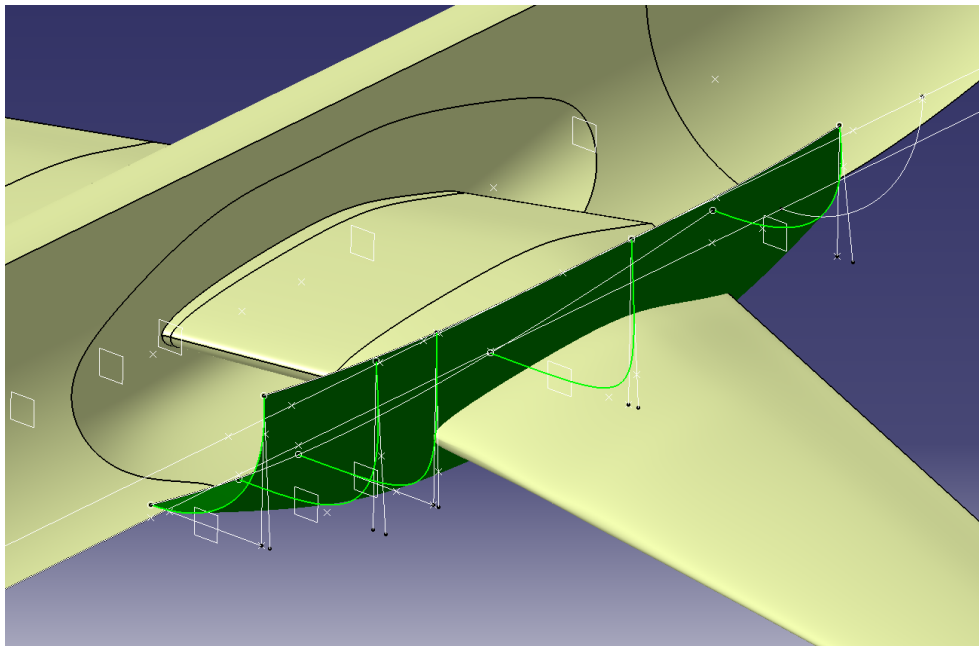
Figure 4-3 Representation of the belly fairing generation

The belly fairing surface is generated with help of the afore mentioned splines, which generate a defined number of cross-sections in the YZ plane with individual profile curve and two additional guide curves, one contained in the XY plane which connects all the A points of the different cross-sections and a second one contained in the XZ plane which connects all the E points of the different cross-sections. Additionally as Fig. 4-4 shows, a tangency imposition has been introduced in the third cross-sections of the represented 4 cross-section belly fairing, which seek to fix the maximum thickness of the belly fairing in the aforementioned cross-section. This tangency is only introduced in the XY contained guide curve, at the cross-section closest to the expected re-compression shock, which for good geometries is expected to be between 60% and 70% of the chord. This measure aims to create a direct influence to the shock with the cross-section variables.
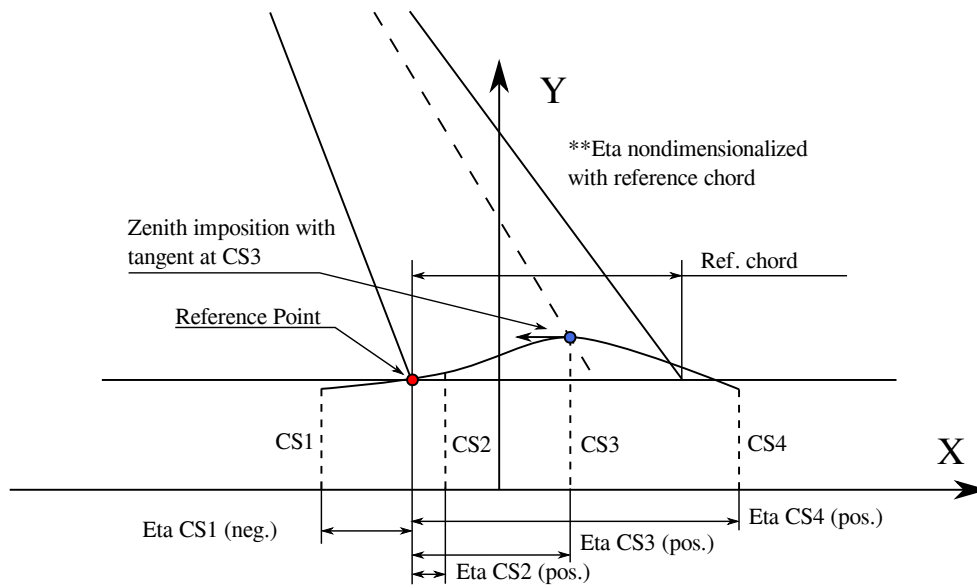
Figure 4-4 Sketch of the parameters used for the belly fairing generation. Detailed representation of the parameter η_{BF}

Since no previous data of a belly fairing is available, there is the uncertainty if a 4 cross-section belly fairing is enough for a transonic design. Due to the supersonic region in the suction side of the wing, a 5 or even higher cross-section count belly fairing may be necessary to achieve optimal performance. Fig. 4-5 shows a 5 cross-section belly fairing, which can achieve with good control a supersonic acceleration between cross-section 2 and 3. Based on this assumption a second belly fairing geometry with 5 cross-section was created, which in the future will be used to assess the performance difference and the computational cost difference between both geometries.
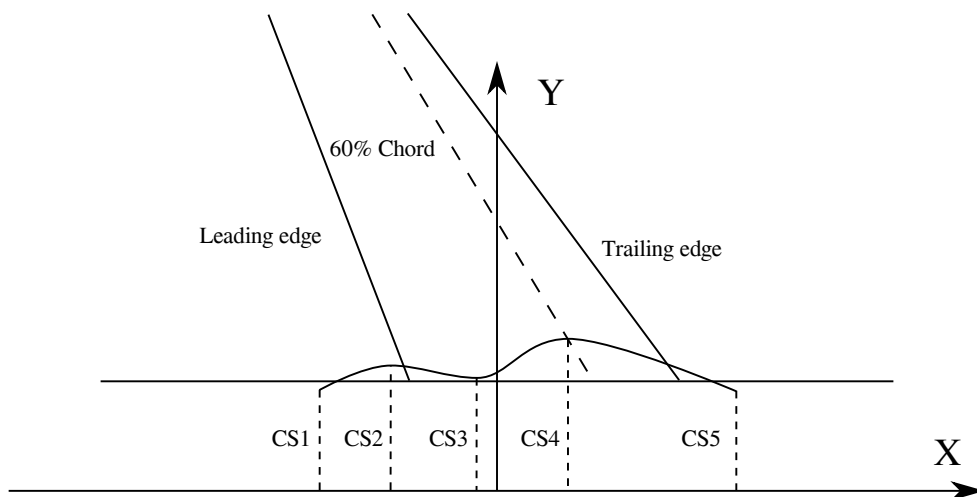
Figure 4-5 Sketch of the parameters used for the belly fairing generation. Detailed representation of the parameter η_{BF}

The cross section position along the X axis is set with help of a η_{BF} parameter. In the case of the belly fairing the η_{BF} parameter refers to the chord length of the first wing profile, which has a
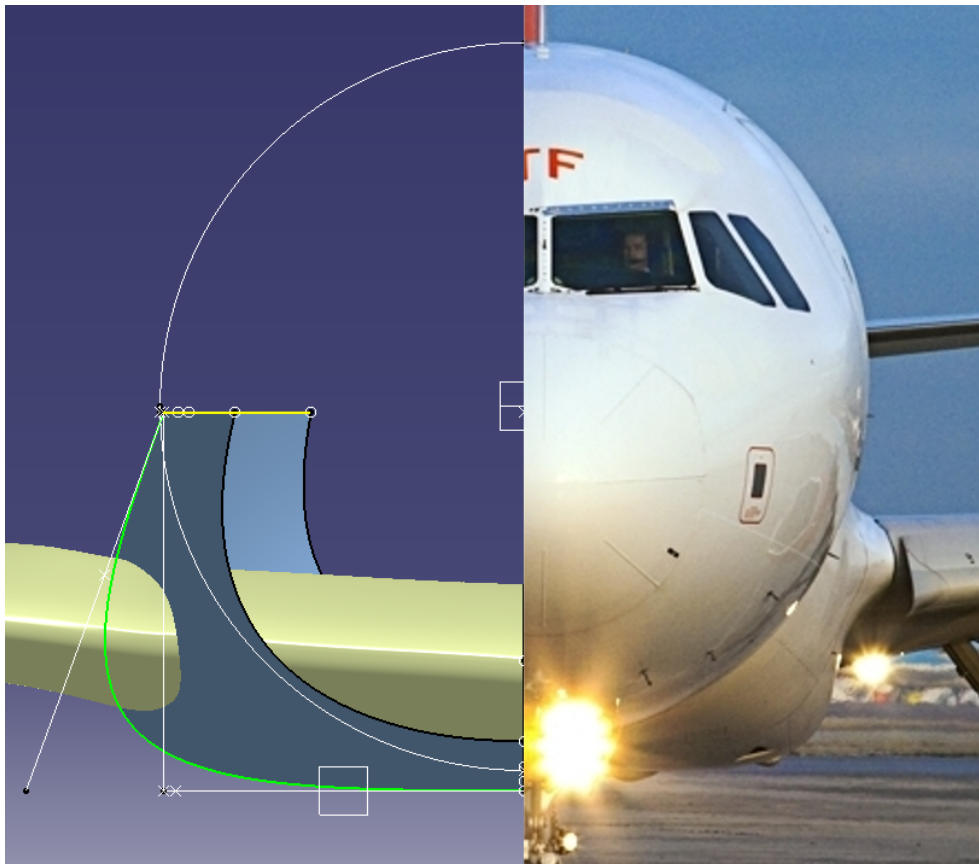
Figure 4-6 Side by side representation of a A320 and TG2 geometry, A320 photo obtained from [1]

length of 5080.02 mm. A positive value of η_{BF} means that the cross-section is past the reference point, towards the rear of the fuselage. A value higher than 1 means that the cross-section is past the trailing edge of the wing. A negative value of η_{BF} means on the other hand that the cross-section is prior to the reference point, towards the nose of the fuselage Fig. 4-4 provides a graphical representation of the η_{BF} parameter on a 4 cross-section belly fairing.

In order to simplify the cross-section generation the parameters have been defined using parameters that can be easily coupled to geometric properties. The parameters are represented by Fig. 4-2. Y ratio and reference angle influence the cross-section size in the Y direction. Z ratio influences the size of the cross-section in the Z direction and finally, Ratio 1 and 2 influences the roundness of the cross-section for the pressure and the suction side respectively.

In the following the coupling between the points and the parameters is explained. Point A is fixed on the Z axis with a value of zero, the Y Ratio defines the relative position of the A point along the Y axis. A value of zero means that the point is right at the fuselage. A value higher than 0 is not feasible because it leads to a non watertight belly fairing. A value of -1 means that the first point is in the center of the fuselage. The point E is in the same way as point A fixed on the Y axis, its position in the Z axis is defined with help of the Z ratio, which influences the maximum depth of the cross-section, as the B spline has a Y axis tangency on the E point. On the same Z position as
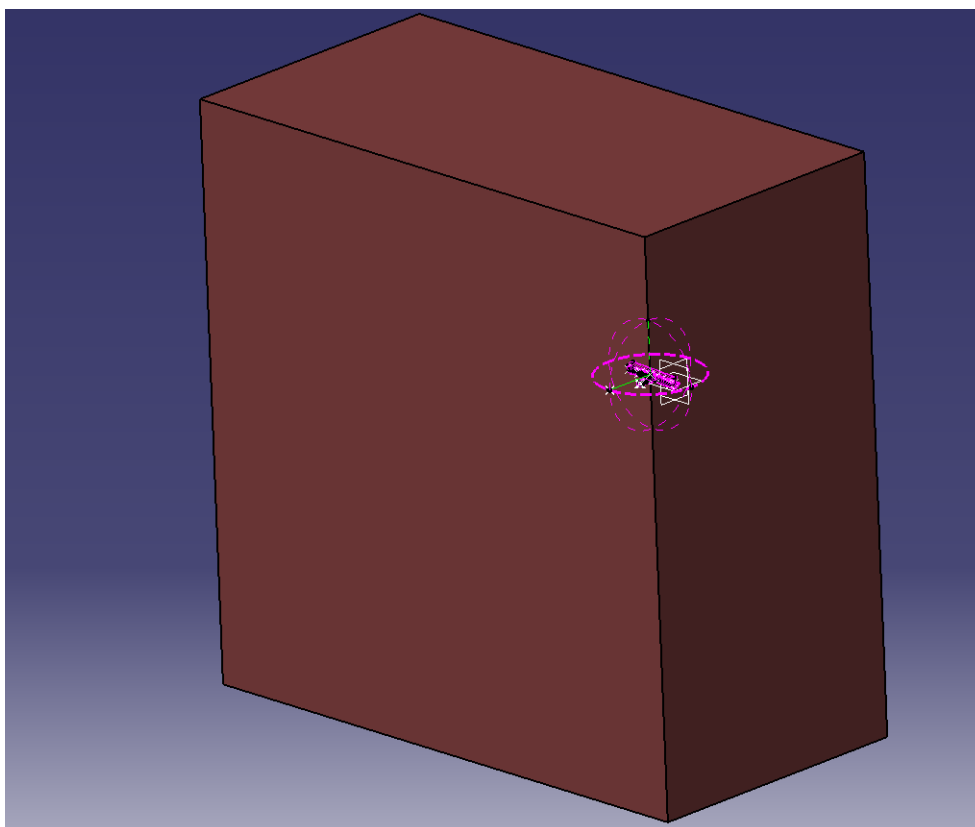
Figure 4-7 Domain representation

the E point are the point D and C, the position of C is defined by the line AC, which starts from point A with the angle defined by the parameter reference angle and projects up to the Z position of point E. The actual position along the line EC of D is fix by ratio 1, which indicates the relative position, a value of 0 set the point at the same position as E and a value of 1 sets the point at the position of C. The position of B is fix along AC in the same fashion with help of Ratio 2. The simplified methodology of the cross-section generation reduces the cost increase when going from a 4 cross-section belly fairing to a 5 one.

4.1.1.3. Farfield definition

The simulation domain in numerical simulation can have a negative effect if is not properly defined. For this study a simulation domain of 80 times the reference profile length (5080.02 mm) was chosen in the X and Z directions. In the Y direction the domain length is 40 times the reference profile length since only half aircraft is being simulated. A representation of the domain can be found in Fig. 4-7.

4.1.2. Grid generation

Due to the complexity of the geometry a hybrid grid has been used. In the previous stages of the work, as the reference geometry performance was assess, Centaur was used to generate the grids, but later on was decided to use Solar for this work. The quasi structured surface grid, aligned with

the flow which solar provides allows a better prediction of the flow compared to centaur. Based in the findings of the mesh independence study the final mesh used for the simulations has an approximately size of 55 million nodes. In the following, an in depth view of the mesh generation will be described.

4.1.2.1. Centaur and solar grids

Centaur was used at the beginning due to the intuitive user interface and the availability of grid generation examples and tutorials. Based in the in house know-how and the support of Stefan Melber it was decided to shift to solar for the grid generation, which as a main advantage offers hexaedron elements on the prisms layer and quad elements on the surface, compared to the pentahedron elements in the prisms layer and the triangle elements on the surface of centaur.

The main advantage of quad elements is better fitting of the grid to the flow field. In simply geometries such as the fuselage, the nodes lay aligned along the flow streamlines. In more complex geometries as the wing with taper, the quad elements fit very well in the leading and trailing edges and provide a reasonable good grid through the wing taper.

All together due to the better fit of the grid to the flow field better exactitude can be expected from the solar grids for the same amount of nodes.

4.1.2.2. Mesh independence study

One of the most critical parts of computational fluid simulation is validation. The high degree of influence that non validated methodology can assert makes methodology validation one of the critical tasks to solve. Optimally the validation is carried over with experimental data from a wind tunnel with similar configuration and similar flow field conditions. Since the NLF configuration is a novel configuration, no experimental data is available. Despite not being the optimal validation methodology, in order to ensure a minimal trustworthiness of the results when no experimental data is available, a common practice in computational fluid dynamics is to perform a mesh independence study, in which the simulation grid is refined until no further influence due to the grid in the performance parameters can be observed. An additional consideration which has to be taken into account since the TuLam configuration is a transonic aircraft, are shock related influences, such as shock discretization or grid - shock coupling. In order to counteract this phenomena mesh refining methods are used, the working principle is that firstly the simulation is ran until convergence, then, where high gradients of static pressure are found, like at the re-compression shock position, the grid is locally refined and further calculated. Due to the additional complexity and computational cost no adaptive mesh refinement has been implemented.

A grid independence study give some degree of trust in the grid, but ultimately the whole methodology used in this work will be validated once the experimental data is available. All the configuration which can not be indirectly validated as the grid has been configured based in common practices in transonic aircraft and laminar flow experiments from previous work in DLR.

The configuration used in this work has been refined using this methodology in which special care was taken to refine the root region of the wing. Additional considerations where taken to ensure a high grid resolution in the belly fairing influence area, which was carefully measured during the previous phase of this work, as the performance of RG1, RG2 and the test geometries was assessed,

to ensure a decoupling of the grid resolution from the obtained results.
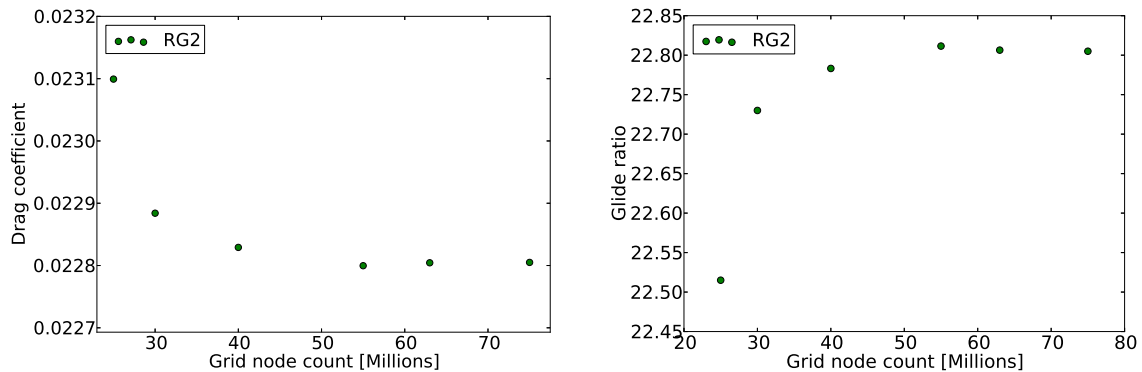
(a) Influence of the grid node count on the drag coeffi-
cient

(b) Influence of the grid node count on the glide ratio

Figure 4-8 Results of the grid convergence study. 55 million grid is the lowest node count grid with no performance influence

At this stage only the geometries described in Chapter 3 were available. Starting from a 25 million node grid a successive refinement of the grid was performed in the five geometries of the preliminary study, until no further refinement had an effect on the performance. At the same time, an assessment in grid generation time and simulation time was performed in order to provide a estimated simulation time per geometry.

The names given to the different grids are derived from the methodology used to generate them. For the first 25 million grid no volume sources were used, also known in centaur as geometric sources, therefore the name used is SUR. For the refined version of this grid volume sources were used, therefore the name chosen was VOL. For the subsequent grids the source length was scaled and the factor was included in the name. In this way the names VOL9, VOL8, VOL75 and VOL7 came to stand, meaning that VOL9 has a 90% source length as VOL and therefore a higher node amount. Table 4-1 displays all the useful information about the different grids. An overview of two different grids can be found in Fig. 4-9.

Grid information						
Grid name	SUR	VOL	VOL9	VOL8	VOL75	VOL7
Node number [Mill.]	25	30	40	55	63	75
Solar runtime [h:mm]	0:30	0:45	1:00	1:40	2:00	5:40
Smooth_taugrid runtime [h:mm]	1:00	1:30	2:00	3:00	4:00	4:45
Tau runtime [hh]	21	28	37	39	45	43
Cores used in tau simulation	96	96	96	128	128	160

Table 4-1 Detailed description of the studied grid densities and the computational costs associated

It was found that depending in the geometry using a grid any finer than VOL8 would either not provide any advantage or produce convergence problems, therefore was decided to base final grid in VOL8 with a total amount of around 55 million of points, which is a high, but in the expected region for a high resolution grid of half aircraft. Figure 4-8 displays how finer grids do not have a big impact in the geometry performance other than some noise.

<table>
<tr><td>(a) Centaur grid, 10M nodes</td><td>(b) Solar grid, 55M nodes</td></tr>
</table>
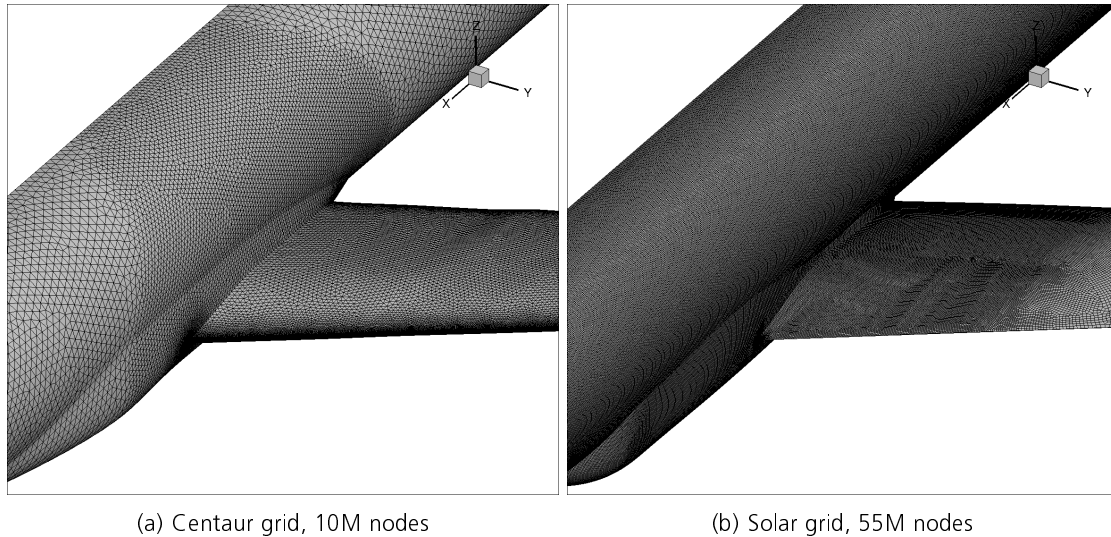
Figure 4-9 comparison of centaur and solar grids. triangle surface elements versus quad surface elements

4.1.2.3.   y+ values

Another concern to ensure a proper grid, is the discretization of the boundary layer region. For the present study no wall functions have been used, therefore it has to be ensured that the first nodes of the grid are in the viscous sub-layer. This is ensured with help of the non dimensional y+, as long as the value is around 1 the viscous sub-layer is properly captured. For the chosen grid the value of y+ ranges between 0.02 and 0.32. The reason why this values are smaller than necessary is because they derived from the methodology used in the mesh independence study. For future work a better distribution of the nodes would lead to a better mesh.

An additional reason for the low values found in the upper side of the wing is that the y+ values are dependent on the friction velocity which is dependent on the wall shear stress. Laminar flow is characterized by the low wall shear stress which leads to very low values of y+.

A representation of the y+ values on the wing surface can be observed in Fig. 4-10. On the wing root turbulent region can be observed the highest values of y+.
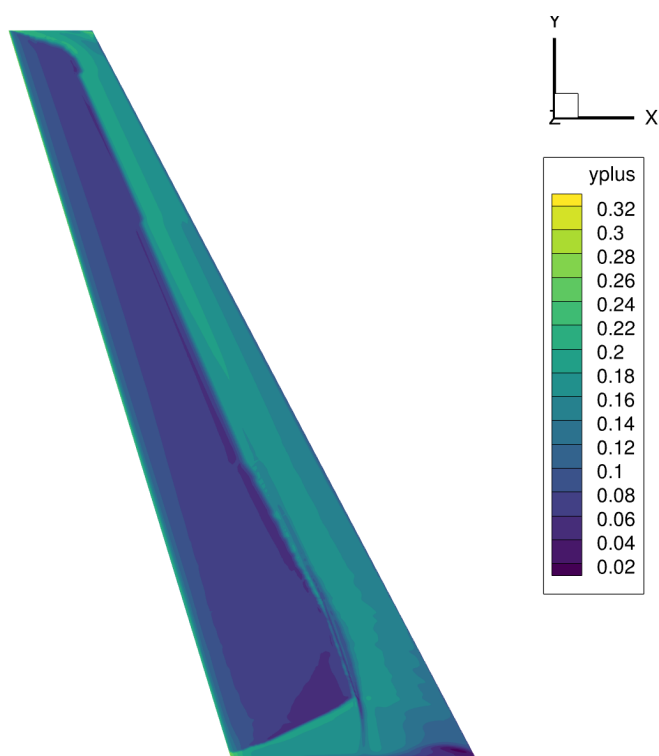
Figure 4-10 Representation of the y+ values along the wing suction surface

4.1.3.   Tau

The DLR RANS solver TAU has been used for the work. The turbulence model used is Spalart-Almaras. Additionally, the laminar module was used, which allows not only to study laminar boundary layers with the reduced friction drag, but to predict the laminar extent according to the flow field conditions. For this work the laminar flow field was focused in the wing, no laminar simulations were performed in the fuselage. In order to achieve the closest possible results of the laminar transition prediction some considerations were taken, such as fuselage boundary layer and turbulent wedge. A representation of the fuselage boundary layer and how it was implemented can be found in Fig. 4-11.

In order to calculate the Fuselage boundary layer thickness at the leading edge of the wing the turbulent flat plate equations were used.

The laminar boundary layer implementation of TAU allows to impose a region in which no additional turbulence is generated and the friction coefficient is lower, like in a laminar flow field, on top of it, based in the pressure distribution of a surface, a boundary layer stability analysis can be performed in order to identify for the current flow field conditions, where the transition takes place. Although this methodology is acceptable for surfaces in low turbulence flow, it has to be taken in consideration that a high incoming turbulence will lead to a turbulent boundary layer, as it can be expected in a surface on the wake of another body or a surface in a high turbulent flow.

Therefore turbulent flow can be expected in the region influenced by the fuselage boundary layer.

Atmospheric boundary layer can also be a trigger for turbulent flow.

4.1.3.1. Laminar imposition

The laminar module of tau offers two different methodologies that can be used to model the laminar boundary layer. Transition imposition and transition prediction. As the names suggest, transition imposition allows to simulate a surface of the geometry as a Laminar flow, independently of the flow field. In transition prediction, a boundary layer stability analysis is performed, and the transition position is automatically set according to the N-factors. In order to use the transition prediction a prior laminar region has to be defined, which is used as an starting point and its based in transition imposition module. Additionally some limitations, like fuselage boundary layer impact or wing tip can be defined, which will be explained in following. Apart from flow field phenomena, the definition of a preliminary boundary layer extent helps with convergence, therefore the preliminary definition must be close to the final solution. Due to the high amount of previous work regarding laminar wings, the laminar extent in a 2.75d case is available and expected to be at a position close to $x/c = 0.6$, where the re-compression shock takes place.

A common Phenomena when transition takes place in a point is a downstream wedge propagation of the transition due to the flow field instability propagation. For the fuselage-wing configuration considered in the present work, the free stream low turbulence flow allows a big extent of the laminar boundary layer, but in the region close to the fuselage, the already turbulent boundary layer coming from the fuselage leads to a small region with turbulent flow. On this region not only the area respective to the fuselage boundary layer is turbulent, but a wedge propagation on the surface is provoked. Since no matter what, the flow is already turbulent in this region, a turbulent profile with focus in low wave drag can be used for this region in the wing with no penalties. In order to model this behavior the boundary layer thickness for a flat plate with the length of the distance from the fuselage nose to the wing root leading edge was calculated. At the wing roots leading edge the fuselage boundary layer thickness was used for the starting point of the turbulent wedge, which follows a fix spreding angle of 12 degrees based in in the findings of Fisher [6]. At the wing tip the turbulent wedge starts at the wing tip leading edge an spreads with an also fix 12 degree. A diagram of the defined boundaries for the transition module is shown in Fig. 4-11.

The preliminary boundary layer is defined with help of a polyline. A user defined number of points are allocated in the laminar surface, and the points are linearly connected. The points do not have to be on the surface, but should be as close as possible.

4.1.3.2. Laminar prediction

Starting with the laminar boundary layer imposition data, the boundary layer extent can be calculated with help of the laminar boundary layer prediction module. In order to do so, a boundary layer stability analysis is performed in the discrete poly line points used for defining the the laminar region.
The laminar prediction module allows to define four different behaviours for the discrete points, which will be explained in shortly. Then, the N-factors are calculated for each of the points and the transition is updated to the new position depending on the point behaviour.
The four different behaviours refer to how the transition position is updated and the options are:
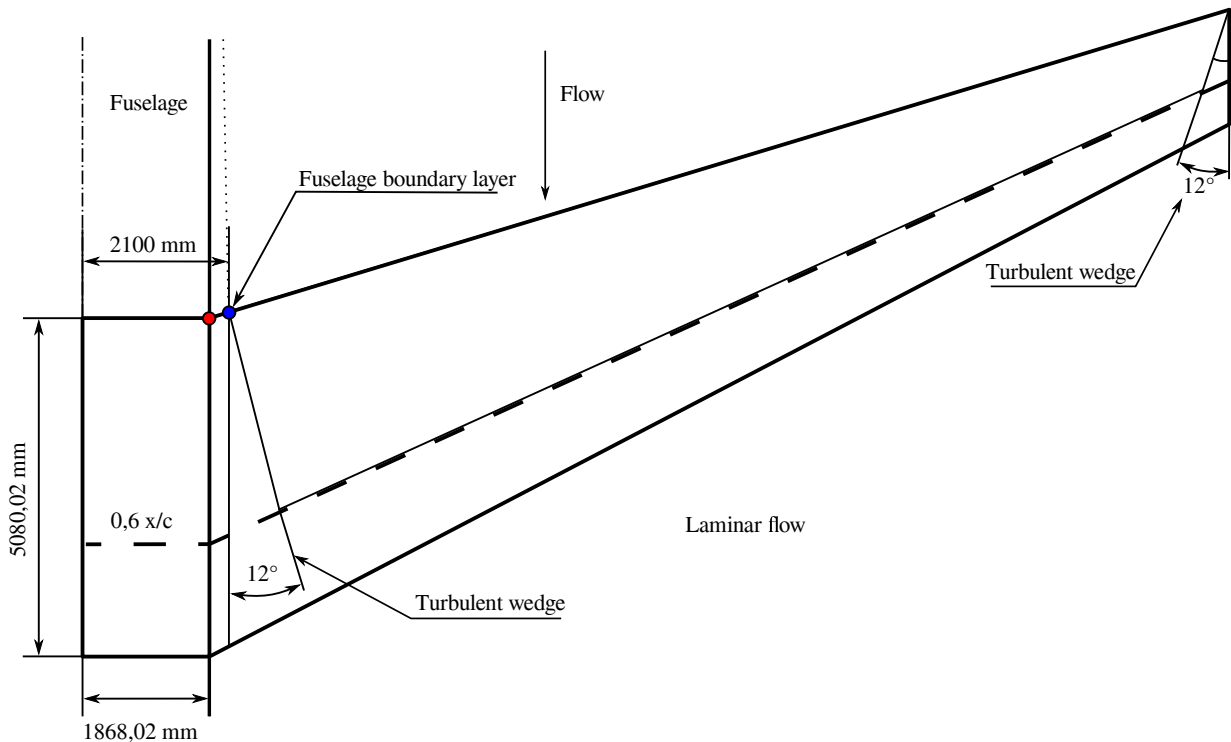
Figure 4-11 Sketch of the pre-set laminar layout for calculation. the turbulent wedge of fuselage and wingtip are considered.

fixed position, free position, upstream free or downstream free. Free and fixed position are self explanatory, in a surface with leading edge transition, such as the afore mentioned fuselage boundary layer meeting point, or downstream of the engines pylon, a fix transition can be imposed with the fixed position option. In a clean surface with low turbulence inflow and no gaps or steps that may provoke a premature transition, such as the middle part of the wing, free transition may be used, departing from the pre defined position the transition position is updated to the stability analysis position, whether upstream or downstream.

Upstream free movement is useful to impose a maximum extent of the laminar region, in this way departing from the laminar imposition the laminar region may be reduced if the stability analysis reveals a transition position upstream of the defined position, but not increased if the stability analysis reveals a transition position downstream of the defined position. This behaviour is useful to model gaps or steps in a surface, as usually they have a thickness higher than the critical thickness for transonic aircraft and therefore lead to a transition. For our case study, this behaviour is used to model the turbulent wedges, by connecting the first fix transition point to a upstream free point with a 12 degree wedge the minimum angle of 12 degree is ensured. This wedge was defined with extra length, to ensure that the stability takes over in the outer part.

Downstream free condition works in the same way as upstream free, but only allowing an increase
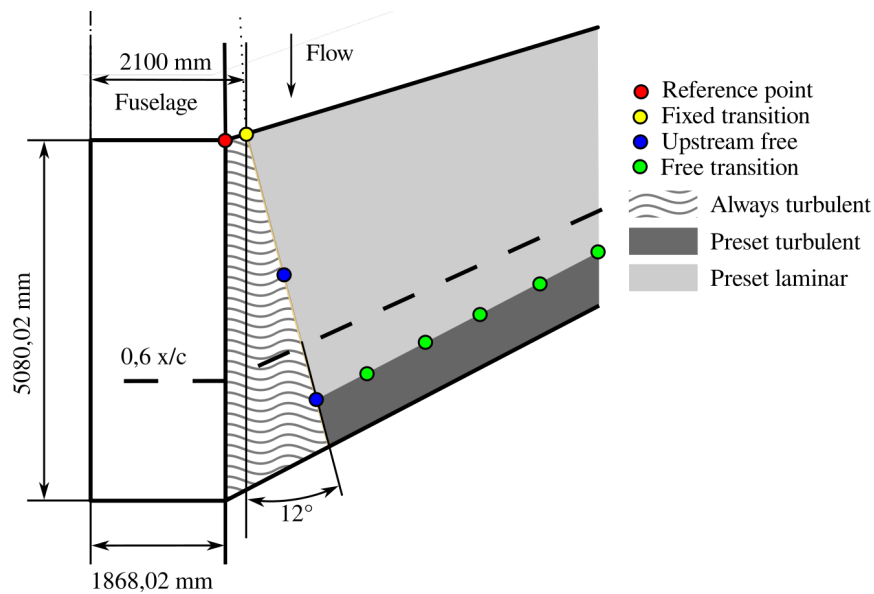
Figure 4-12 Representation of the polyline point behaviour of the laminar prediction module. The area represented is the wing root. The methodology used to achieve a turbulent wedge with a minimum spread angle of 12 degrees is shown.

of the laminar boundary layer extent. This is useful when boundary layer control is used. This behaviour wont be used along the work. Figure 4-12 shows the three different points used in this work and how the affect to the laminar extent in the wing surface.

The laminar boundary layer module is based in the afore mentioned stability analysis, firstly the envelope of the N factors for the different frequencies for CF and TS are calculated, then the values are compared with the limit values, and a transition is found if N-factors limits are surpassed. In design point conditions, the N-factors do not surpass the limits if the wing profiles are properly designed, nevertheless, in some cases, the suction gradients are not high enough, which leads to a rapid grow of the N-factors and a transition. This phenomena happens when the profile is in a high angle of attack or sometimes when the 3D influences in the wing root are big enough. Otherwise, the transition takes place at the shock position, the high pressure gradients on the re-compression shock leads to an automatically transition.

The transition prediction module works in a iterative manner, firstly, in order to ensure convergence the simulation is carried out only with the transition imposed and no updates are made in the laminar boundary layer. After a user defined iteration number, for this work 3000 iterations, the transition prediction module takes over, the boundary layer stability analysis are done, the transition positions are updated in the simulation, and then the simulation continues. After the residuals have converged, additional stability analysis are made in a user defined interval. For this work an interval of 500 iterations was chosen. In this way the boundary layer analysis are carried over from iteration 3000 to iteration 9500, leaving a final 500 iterations to ensure a proper convergence.

4.2. Results processing

Due to the high number of variables in the belly fairing generation and the successive optimization of the belly fairing geometries, there will be a high amount of geometries and results. In order to allow the handling of the shear amount of results it has been developed a bash script, which firstly generates the wing surface data using tecplot, then extracts the different performance metrics from the TAU outputs and generates the pressure distributions plots along different positions in the wing. Finally all the gathered data is put together in a standard document which allows a quick overview of the geometry performance. In the following the different parts of the post-processor will be explained.

4.2.1. Performance Metrics

The most important performance metrics are as usually considered the drag coefficient and the lift coefficient. Despite all the geometries are calculated at a constant lift coefficient, sometimes, due to convergence reasons, the achieved lift coefficient may vary a few lift counts, therefore from the obtained metrics the glide ratio is calculated, defined as:

$$E = C_L/C_D$$

The usage of the glide ratio accounts therefore for these small discrepancies.

Since the main goal of this work is centered in the wave drag reduction, a tool developed by Thomas Streit has been used to assess the wave drag. The working principle of the tool is based in discrete sections along the wingspan. On the given sections the pressure coefficient is analysed in order to find the shock position and the shock strength. Once the shock position is available, the shock extent is mapped on the wing by joining the different shock positions in the available sections. Based in the maped shock position, the angle of the shock to the free stream and the shock strength, the wave drag can be obtained.

Apart of the glide ratio and wave drag coefficient, the angle of attack, the lift and drag coefficient are shown as well. It was found that for some bad belly fairing geometries, the re-compression shock is normal to the flow for a large region at the wing root, leading to a zone with reduced suction and high wave drag. Since the calculations have been done at a constant goal lift coefficient, tau tries to compensate by increasing the angle of attack. Bad geometries are therefore characterized by a high the angle of attack and high drag, in some of them the goal lift is not achieved.

4.2.2. Aerodynamic postprocessor

Most of the preliminary assess of the geometries performance is based in the performance metrics, as they give a good overview of the geometries and many geometries can be displayed at the same time. Additionally performance metrics allow to find correlations between variables and performance. Nevertheless and aerodynamic post-processing of the wing is also done, which allows to correlate the performance metrics with the flow field.

Two different approaches were taken for this post-processing, surface representation and discrete profile plotting. Firstly since the main goal of the study is to reduce the region in the wing root where the shock is normal to the flow, the upper surface contours are processed and represented. While this methodology does not give exact values, provides a good overview of the the flow field behaviour. The level curves are represented for the pressure coefficient, with constant intervals of 0.06 from a value of 0 up to a value of -1.2. A representation can be found in Fig. 5-10(b). This gives a good overview of the shock position an its orientation. Additionally the same contours are shown where the values of the C_P are represented according to a colour schema, which represents maximum suction and re-compression zones. Suction zones after the re-compression shock are also very well represented. A representation can be found in Fig. 5-10(c). Lastly, a representation of the laminar boundary layer extent shows if the laminar extent has been affected by the geometry performance. A representation can be found in Fig. 5-10(a). In some geometries can be expected a small reduction of the laminar boundary layer extent, which may be overcompensated by a good shock position leading to a overall good performance. In the best case scenario no trade off would happen.

(a) Laminar extent for RG2   (b) C_P level curves for RG2   (c) C_P contours for RG2
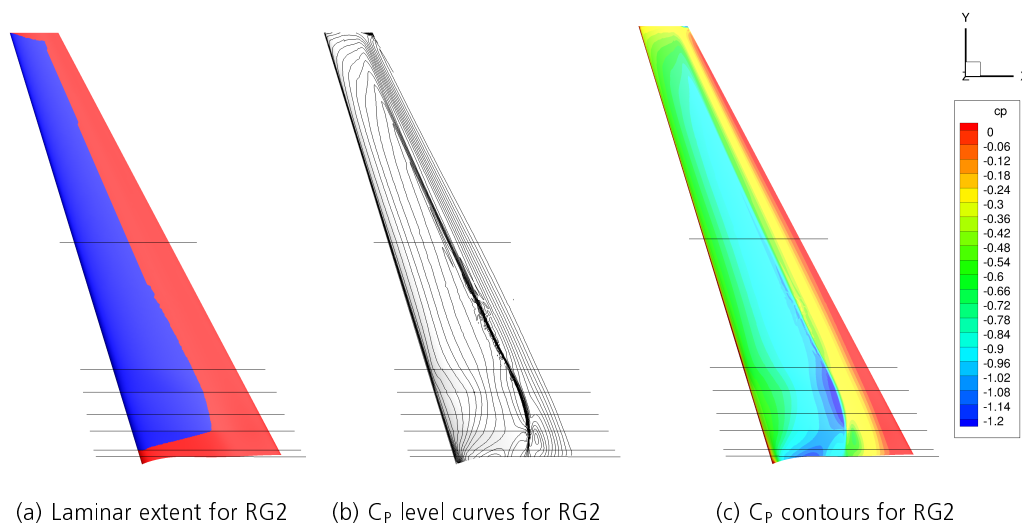
Figure 4-13 Example of the output of the surface aerodynamic post-processor for RG2

In order to complement the surface data, C_P distributions along the wing chord are represented at the positions where the different wing profiles are located. This methodology seeks to provide more exact data, the chord position along with the C_P distributions, the N-TS and N-CF factors, the transition position and the shock position are shown.

The whole output of this post-processor is shown in Fig. 4-14. Since the wing geometry is constant, this post-processor allows a good comparison between different geometries, which gives overview of the extent of the 3D effects. This methodology has been used in Fig. 1-4 to compare RG1 and RG2.

The tool used to calculate the wave drag, provides as well as the wave drag coefficient, different intermediate data which is very useful for debugging. Firstly, the shock position found for each section is shown, represented in Fig. 4-15(d), then, the local drag coefficient produced in each

(a) Profile 1, $\eta = 0.10988$ (b) Profile 2, $\eta = 0.12331$ (c) Profile 3, $\eta = 0.16332$ (d) Profile 4, $\eta = 0.2$

(e) Profile 5, $\eta = 0.24565$ (f) Profile 6, $\eta = 0.294$ (g) Profile 7, $\eta = 0.56$
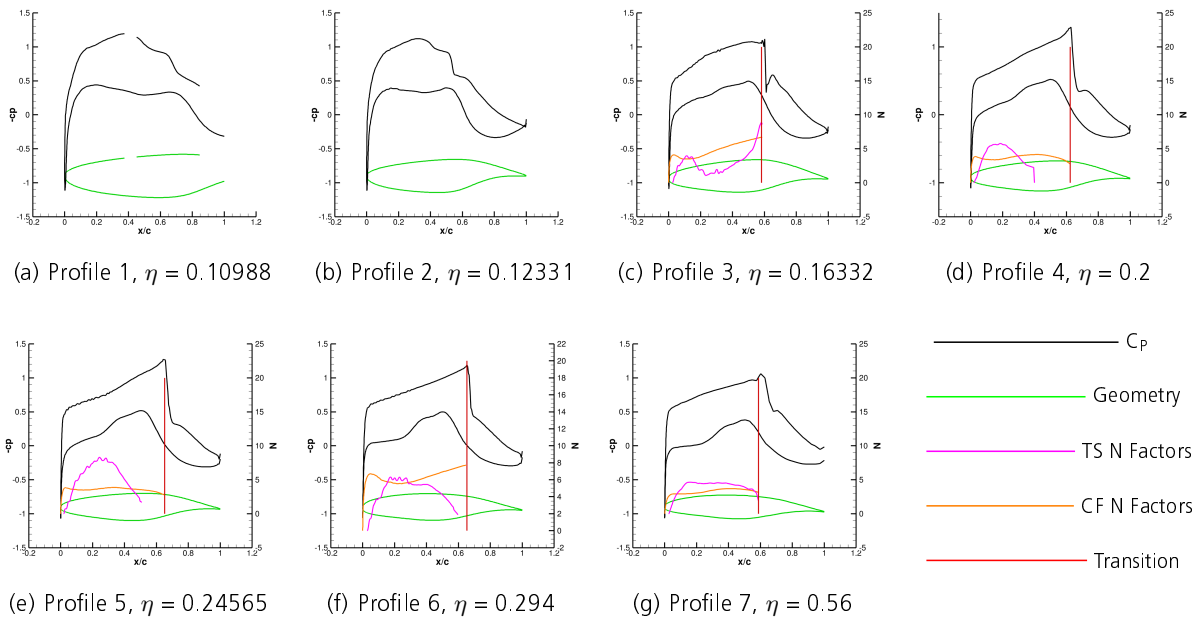
Figure 4-14 Example of the output of the discrete aerodynamic post-processor for RG2

section, represented in Fig. 4-15(a), the local force produced at each section, represented in Fig. 4-15(c) and the local sweep is displayed, represented in Fig. 4-15(b). For all the calculated values three different values are shown, which are correlated to three different methodologies. The simplest methodology assumes a isobar distribution, that is to say, the sweep for each section is linearly interpolated between leading edge and trailing edge sweep, based in the shock position along the chord. For the second methodology, the different shock positions are joined together and the real sweep angle to the free steam is calculated. The third methodology is based in the second but smoothing is used to reduce the peak values derived from the discretization.

Finally, also due to debugging reasons, the angle of attack and the drag coefficient evolution along the simulation iterations is displayed. This provides a quick overview of the simulation if needed. A representation can be found in Fig. 4-16. This data is specially useful for bad performing geometries as the angle of attack diverges due to the incapability of achieving the goal lift coefficient.

Despite the aerodynamic post-processor is automatically generated for all the geometries, it is used as a complement to the performance metrics and is only checked for the best and worst geometries.

4.3.   Reverse engenieering

Although there is no previous parametric belly fairing, the inverse CFD belly fairing of the LamAir project is available. In order to start the simulations in a somewhat known territory, based in the good performance of RG2, the starting parameters of the parameter study where chosen based in the RG2 geometry. The parameters chosen where inspired as well in TG2, which is the belly firing based in the 2.75d flow field of the middle of the wing. Both geometries were considered for the initial parameters because both geometries have good performance despite the geometries are very

(a) Local wave drag coefficient

(b) Local sweep

(c) Local wave force

(d) Representation of the schock position on the wing surface
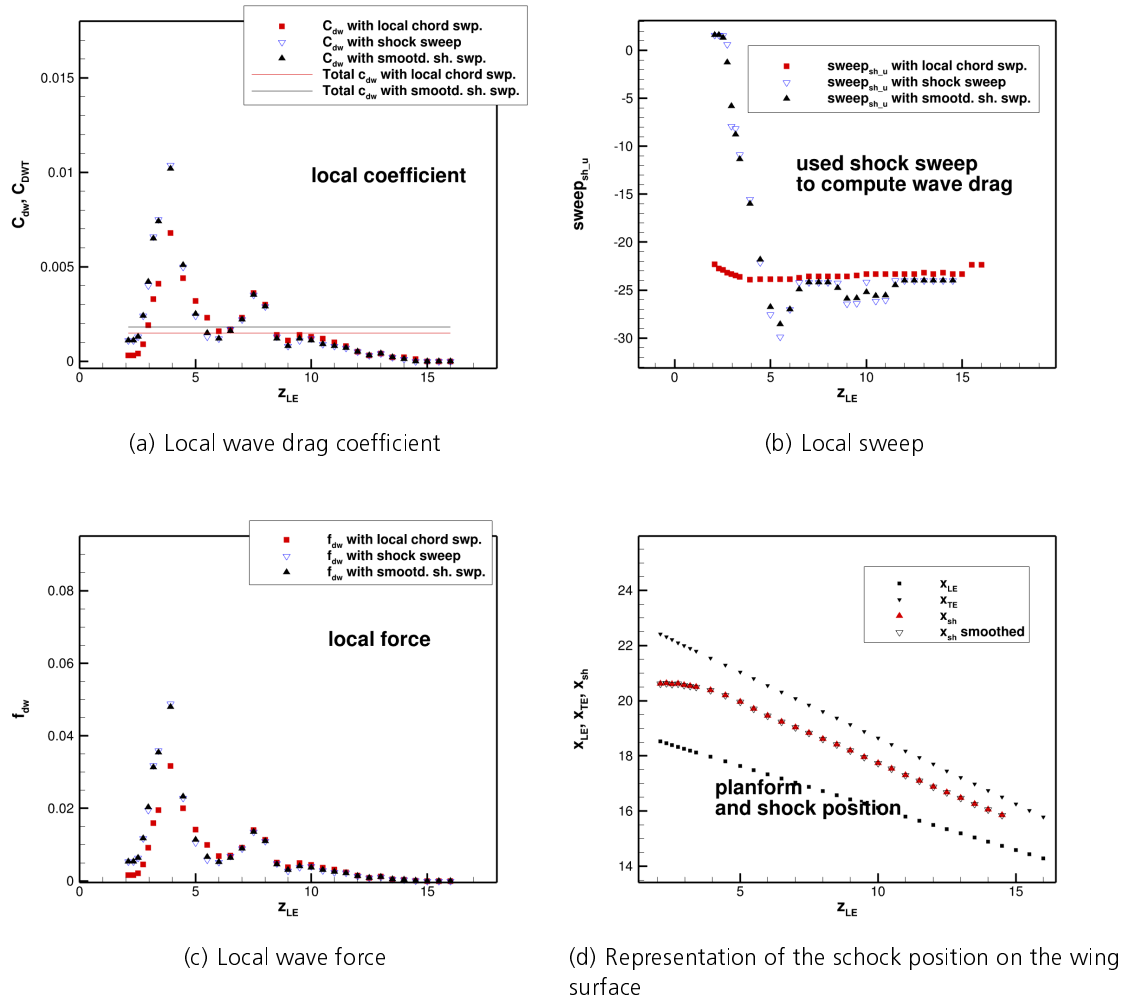
Figure 4-15 Example of the graphic output of the wave drag post-processor for RG2

different, which suggest that there is a big geometric domain in which good performing geometry can be found.

In order to extract the approximate parameters of the RG2 geometry, firstly a visual analysis of the belly fairing was performed. The RG2 belly fairing is characterised by a S-shape, therefore is difficult to replicate the geometry with a four cross-section belly fairing. Nevertheless, based in the visual analysis the high and low spots were found and a plane was set at the positions. By performing a interference operation the cross sections were extracted. Although not necessary for the approximate parameter extraction, a surface was generated with the extracted profiles to check for deviations. Once the interference cross-sections were available, the parameters of the belly fairing were modified until the parametric profiles were as close as possible to the extracted ones. Table 4-2 shows the extrapolated parameters of the RG2 geometry and Table 4-3 shows the parameters of TG2
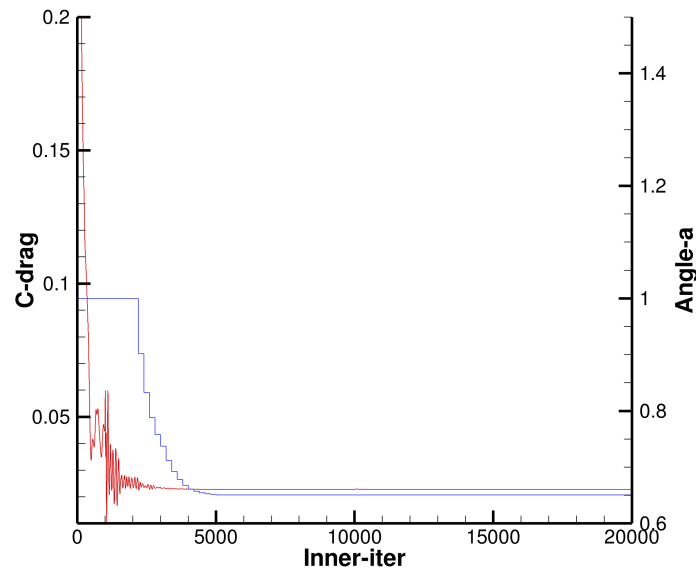
Figure 4-16 Example of the drag coefficient and the angle of attack variation along the simulation iterations for RG2

4.4.   Parameter Study structure

As it may be expected, the high amount of degrees of freedom and the lack of information, regarding which parameters should be investigated or the the parameter bounds for the chosen methodology lead to a shear amount of geometries, which are neither economically nor time feasible, therefore, some decisions have to be taken to provide a manageable amount of simulations.

As previously discussed, the availability of two very different geometries with high performance, offered a starting point for the parameter study, nevertheless this does not guarantee that the absolute optimum is in the chosen domain.

Despite the available geometries, the numbers of degrees of freedom had to be reduced.   The

RG2 belly fairing						
Cross-section	η_{BF}	Y Ratio	Ref. Angle	Ratio 2	Z Ratio	Ratio 1
1	0.254	0.0845	3.96	0.1	0.01	1.0
2	0.631	0.0633	1.01	1.0	0.01	0.9
3	1.196	0.0215	3.22	0.0	0.01	0.95
4	1.634	0.0385	1.46	0.8	0.01	0.9

Table 4-2 Extrapolated parameters obtained from the RG2 belly fairing. Cross-section 1 has a maximum discrepancy of 0.288 mm. Cross-section 2 has a maximum discrepancy of 1.409 mm.

TG2 belly fairing						
Cross-section	η_{BF}	Y Ratio	Ref. Angle	Ratio 2	Z Ratio	Ratio 1
1	-0.7123	0.206	13	0.247	0.082	0.157
2	0.0416	0.05	4	0.75	-0.031	0.6
3	0.7014	0.01	20	0.43	-0.056	0.7
4	1.3612	0.08	11	0.3	0.01	0.6
5	1.9267	0.415	10	0.237	0.307	0.357

Table 4-3 Parameters used in TG2 for the belly fairing generation

first assumption taken was regarding the belly fairing methodology, in order to start with lower complexity it was decided to limit the simulations to a 4 cross-section belly fairing. Nevertheless if all the variables are considered, a 4 cross-section belly fairing has 24 different variables, which is still way too high.

Therefore some consideration has been taken to design a low variable belly fairing. Since the most performance influence is expected in the suction side of the wing due to the supersonic flow field a four cross-section belly fairing was chosen, from which only the second and third cross section will be modified. Furthermore, since two complete cross sections are still 12 variables, only the parameters which influence the suction side of the wing (Reference angle, Y ratio and η_{BF}) are going to be considered, which lead to a total number of 6 variables.

4.4.1. Simulation strategy

Once the number of variables has been defined, the simulation strategy has to be considered. In order to further simplify the starting simulations, it was decided to only consider the second cross-section of the belly fairing, then, with the best performing second section, perform a design space exploration of the third cross-section.

While this methodology provides two easy manageable 3-variable parameter studies, is important to point out that the geometric domain is being reduced to a small part of the original size, Fig. 4-17 provides a visual representation of this phenomenon.

The smaller lined square represents a four variable design space exploration (for example a 4-cross-section belly fairing in which only η_{BF2}, η_{BF3}, RW2 and RW3 is considered) which has been divided in two 2-variable design space exploration, represented in dark grey, the ignored geometries are represented in light grey. The larger lined square represents a six variable design space exploration (for example a 5-cross-section belly fairing in which only η_{BF2}, η_{BF3}, η_{BF4}, RW2, RW3 and RW4 is considered) which has been divided in three 2-variable design space exploration. On the right hand side of the representation, the real numbers for a 3-dimension (variable) 3 value, four cross-section belly fairing, and a 3-dimension (variable) 3 value, five cross-section belly fairing are shown. The main outcome of this representation is to show the diminishing returns of this methodology for simplifying complex geometries.
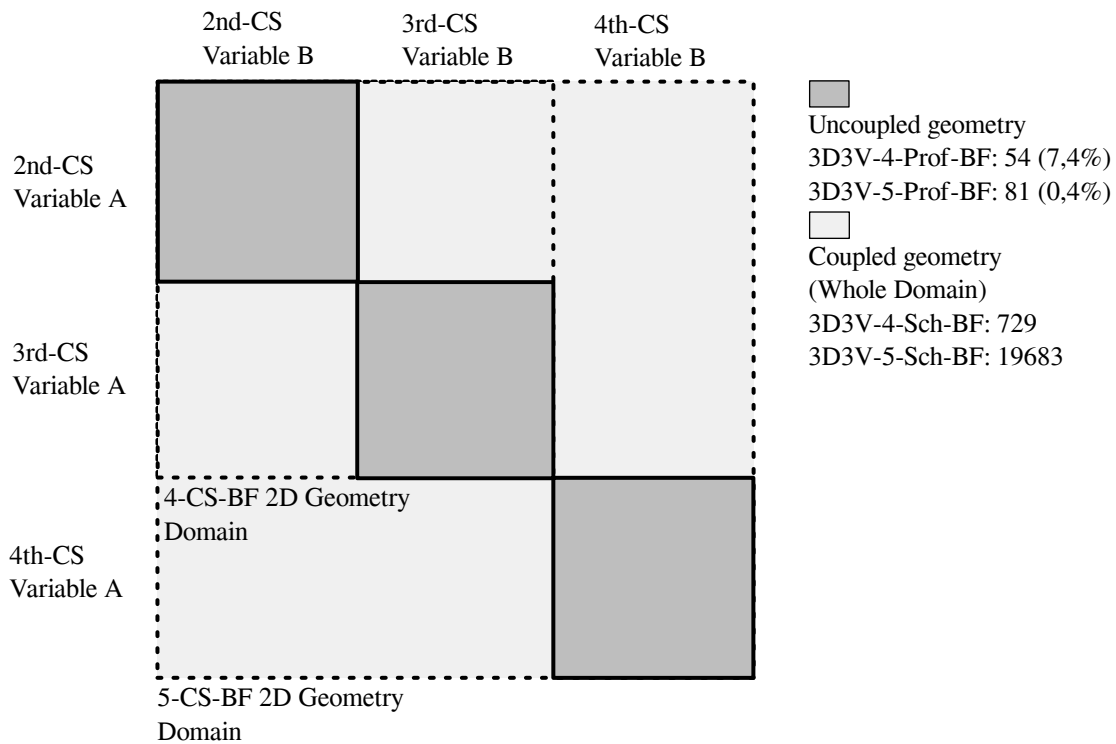
Figure 4-17 Graphic representation of the limitations of the isolated approach. In order to reduce the parameter study complexity the cross-sections in the first stages are studied independently. For a geometry with 4 cross-sections, 3 variable (3D) per cross-section and 3 values per variable this approach only covers 7.4% of the possible geometries in the domain, for the geometry with 5 cross-sections under the same conditions only 0.4% of the possible geometries in the domain are are covered. **NOTE: the graphic representation is limited to a 2 variable (2D) representation while the values are calculated for a 3 variable (3D) geometry.

Although the diminishing returns of this methodology for complex geometries as 5-cross-section belly fairing are a clear disadvantage, they offer a big advantage for more simple geometries like a 4-cross-section belly fairing. The main advantage relies in the limitation of the number of geometries, which at the beginning of the work was a critical, since the bounds of the variables were still to be defined, while still covering an acceptable region of the geometry domain. Furthermore, the isolated simulation or stepped approach allowed to apply a variable-bounds iteration process. As already mentioned, for this work there was no reference regarding variable bounds, by firstly performing an stepped simulation, the bounds and even the variables considered could be easily modified if necessary or beneficial.

This stepped approach is represented by Fig. 4-18, first a probing study is performed on the second cross-section, then depending in the results, either the bounds are modified or the third cross section is explored.

Once the stepped approach is finished, in order to cover the whole geometry domain, both cross-sections have to be considered at the same time. Based in the results of the stepped approach it was decided to only consider five variables: η_{BF2}, RW_2, YR_2, η_{BF3} and RW_3. Two main reasons supported this decision, one of them is dramatic reduction of the geometric domain compared to considering six variables. Including YR_3 as well, for a fully factorial experiment with six variables

and three values the number of simulations is 729, if one variable less is considered the number of simulation reduces to 243. The second reason to decide further simplifying the geometry is based in the results of the stepped approach, which will be discussed in the next chapter.
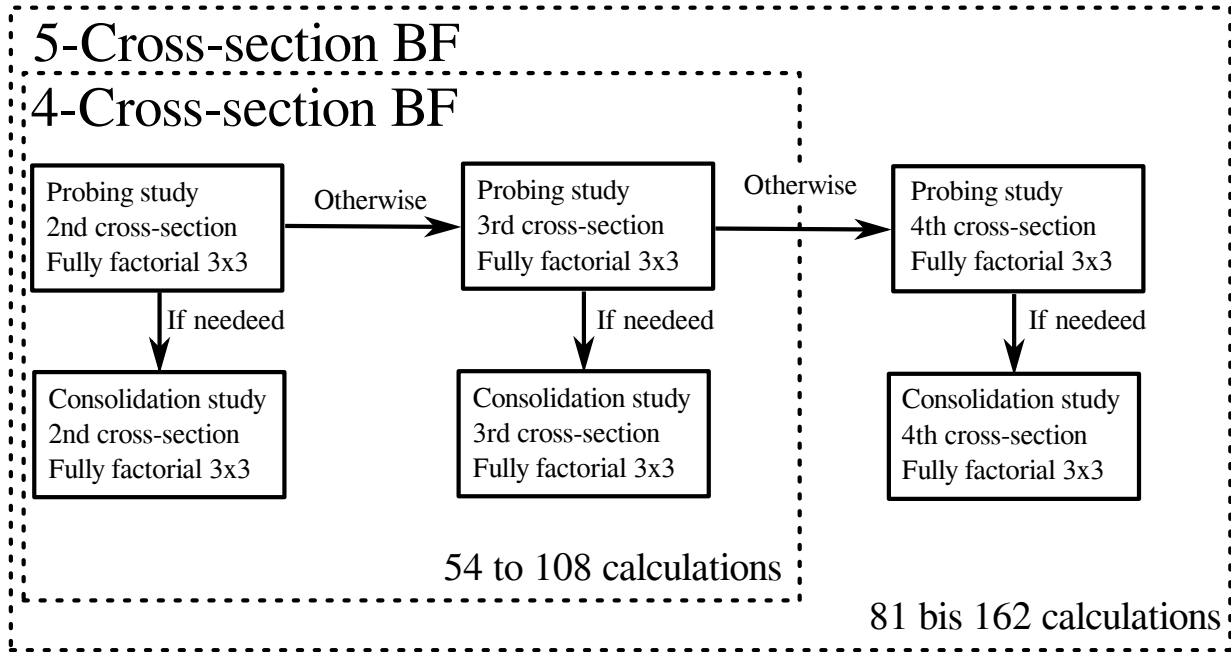
Figure 4-18 Sketch of the stepped methodology, the probing-consolidation methodology provides a flexible methodology that allows an adaptation of the geometry bounds

5. Results

In the following chapter the results will be discussed. Since the methodology of each step depends on the previous step, the methodology close related to each parameter study will be discussed in its corresponding part, with the objective of keeping an easy to follow narrative, which also represents the method in which decisions have been done along the work.

5.1. First parameter study

As previously discussed, the 4-cross-section belly fairing will be simulated in an stepped approach, for this first parameter study only the second cross section will be considered, therefore, all the parameters but the ones to be explored have to be defined and been fixed. Table 5-1 displays all the values chosen for all the parameters but η_{BF2}, RW_2 and YR_2, which will be explored in the first parameter study, and as a recap are the ones which have the most influence in the suction side of the wing.

5.1.1. Parameter study domain

Most of the fix parameters at the first and second section are based in the TG2, due to the good performance achieved. For some parameters, such as Reference angle, the values chosen were less aggressive than in TG2, this decision was based in the parameters extracted from RG2, which were much less aggressive and achieved even better performance. Less aggressive values are expected as well to provide less risk of separation and therefore provide a better overview of the influence of the different variables. The starting values for η_{BF3}, RW_3, YR_3 were even more carefully chosen, as a big influence was expected coming from the cross-section parameters close to the re-compression shock, a wrongly chosen third cross section parameters could lead to a useless dataset.

One of the preliminary hypothesis was that the re-compression shock could be expected to be close to the belly fairing maximum thickness position. This hypothesis is based in the assumption that the supersonic flow above the wing may suddenly re-compress as the shrinking belly fairing provokes a acceleration in the supersonic flow. Based on that hypothesis, the main goal of this work is to influence the shock position at the wing root towards the rear of the wing, from a starting 55% towards a more beneficial 60-70%, therefore the third cross-section which has been chosen to be at a 65% of the chord, has been set up to be the thickest. In order to ensure the thickest cross section, the Y Ratio was keep at the minimum and the reference angle was chosen with a generous 4 degree, which was also found at the thickest in the RG2 geometry. This methodology can be found as well in TG2, which has the thickest cross section at a 70% of the chord, with an enormous 20 degree reference angle. Note that the good performance of such a thick cross-section means that the geometry domain in which good performing geometries can be found is quite big. Nevertheless, choosing a big domain leads either to a low resolution from which is very difficult to find correlations or to a high number of simulations and therefore a high computational cost.

belly fairing fix parameters						
Cross-section	η_{BF}	Y Ratio	Ref. Angle [deg]	Ratio 2	Z Ratio	Ratio 1
1	-0.5	0.2	4	0.25	0.082	0.25
2	n/a	n/a	n/a	0.8	-0.056	0.7
3	0.65	0.001	4	0.8	-0.01	0.8
4	1.4	0.1	8	0.3	0.2	0.357

Table 5-1 Fixed parameters in the first parameter study

5.1.2.   Limits and sampling strategy

As just discussed for the values chosen for the third cross-section, the limits for each variable have to be chosen in a way in which a sensible size of the geometry domain is covered, while the region covered is not too big to keep the resources used low. Based in the already defined values for the third cross-section it was decided that the reference angle would vary between 0 and 4 degrees. The Y Ratio was decided in a first approach that should not be any higher than 0.1, an vary therefore between 0 and 0.1. It was later discovered that with a the low value Y ratio of 0.001 at the third cross section, the methodology used for the belly fairing generation did not allow a value lower than 0.02 at the second cross section, therefore the Y ratio was explored between 0.02 and 0.012. Finally η_{BF2} was decided to be explored between the values of 0, at the root leading edge and 0.3, at a 30% of the wing chord. No higher values were chosen to ensure that the cross section remains in the front part of the wing and to avoid oscillations at the belly fairing generation, since if the second cross sections is to close to the third, big oscillations in the geometries generated may appear leading to useless geometries.

For this parameter study it was decided to use a three value, three variable, fully factorial experiment. The total amount of geometries for a fully factorial experiment of these characteristics is 27. The values that the three variables take for the afore mentioned parameter study with the decided limits is shown in Table 5-2.

First variable values			
Variable	min.	mid.	max.
η_{BF} [/]	0.0	0.15	0.3
Y Ratio [/]	0.02	0.07	0.12
Reference angle [deg]	0	2	4

Table 5-2 Values used in the first parameter study for the belly fairing generation before expanding the domain based in the results found

5.1.3. Limit adjustment

From the stating fully factorial experiment, based in the flexibility of the aforementioned stepped approach, it was decided to expand the simulation domain to ensure that the best performing geometries were inside the limits. The limit expansion was performed manually, and it was decided to expand the simulation domain only in the regions where interesting data was found, rather than continue with the fully factorial approach. The best performing geometries were found for a value of η_{BF2} equal to 0 Y Ratio equal to 0.02 and reference angle equal to 4, which represents the limits of all the three variables. Therefore it was decided to expand the simulations to a value of η_{BF2} equal to -0.15. At the same time for a value of η_{BF2} equal to 0, new simulations with higher reference angles, 6, 8 and 10 degrees were performed. Lastly Y Ratio could not be further reduced as previously discussed, since 0.02 is the minimum which the geometry generation methodology allows.

In order to keep this chapter as compact as plausible the results show already the whole picture with the modifications performed.

5.1.4. Results

The results of the design space exploration are shown in Fig. 5-1. Reference angle shows a big influence in the performance when combined with η_{BF2} equal to 0 and Y Ratio equal to 0.02. From a reference angle of 4 to a reference angle of 6 there is a strong grow in the performance which slowly fades away as the reference angle is further increased.

Note that despite the whole nine geometries of η_{BF2} equal to -0.15 were tried to be generated, six of them gave generation problems. The problem here was the same as previously discussed, the geometry generation methodology. When the Y Ratio is to small the belly fairing has a region of positive Y Ratios between the second and third cross section, leading to a failed geometry. For a value of η_{BF2} equal to 0, the minimum Y ratio that would lead to a proper geometry was 0.02, as the distance between the second and the third cross-section increased, so did the Y Ratio, which has a minimum value between 0.07 and 0.12 for an η_{BF2} of -0.15. The issue will be discussed later on in more detail.

The parameters which were found to deliver the best performing geometry were fixed for the second cross section for the next study.

5.1.5. Best performing geometry

In order to review the progress of along the work, the best geometry has been reviewed. The geometry which achieved the best performance was Geo70, the name is derived from the simulation order and has not a direct link to the parameters, but is important for later comparisons. All the performance metrics have been summarized and compared to the non parametric reference geometry in Table 5-4. Table 5-3 shows the whole parameters used in the Geo70 generation. In Fig. 5-2 the pressure coefficient is represented along the wingspan. One of the first observations that can be made are that Geo70 is a big belly fairing, this is derived from the missing first profile and almost missing second profile. A major difference can be observed at the third profile with respect to the reference geometry, a detailed comparison is shown in Fig. 5-3. While RG2 has a mostly laminar pressure distribution with a following strong shock, Geo70 has an hybrid between a
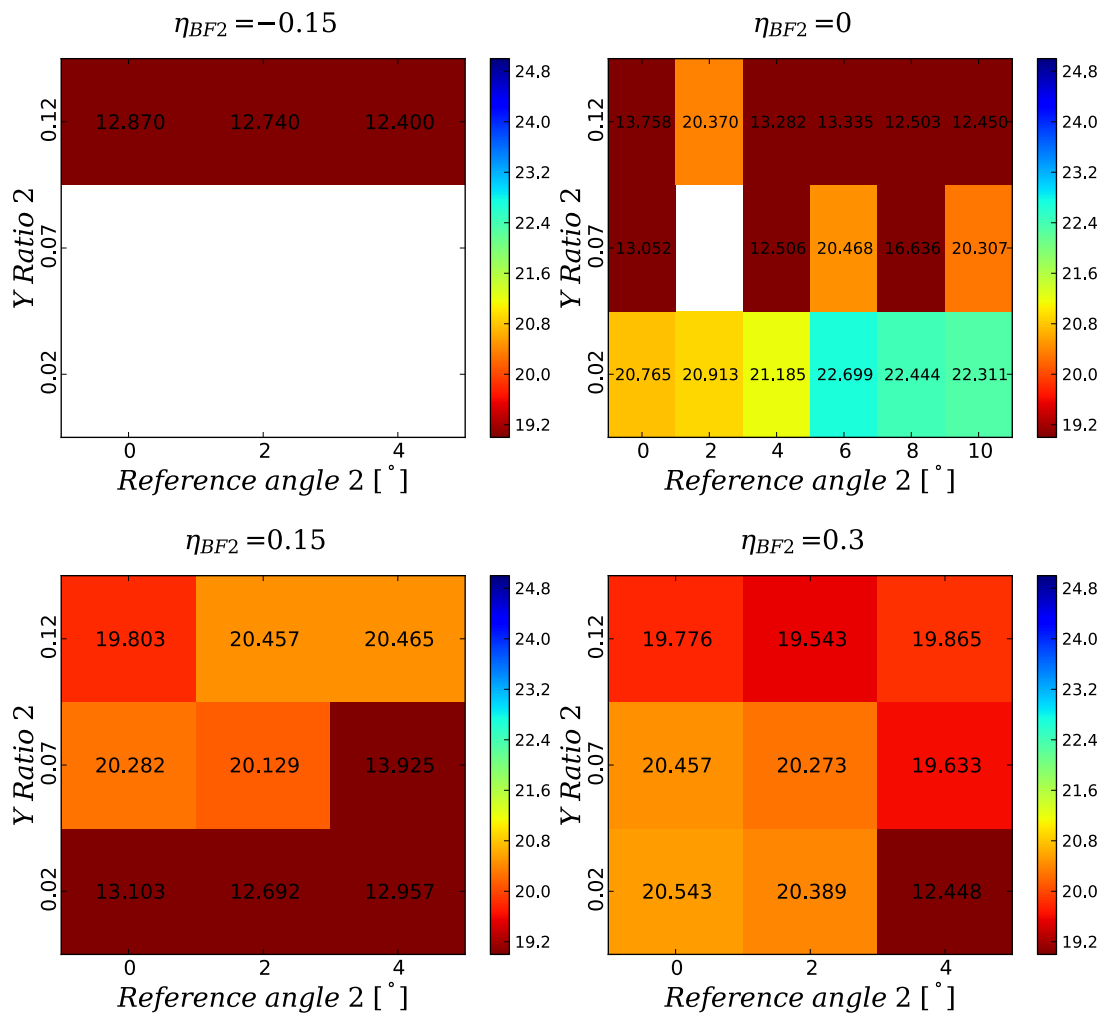
Figure 5-1 Representation of the performance obtained in the first parameter study

laminar pressure distribution and a constant, ever so slightly reducing suction, which is followed by a smaller re-compression shock, a later acceleration and a second re-compression shock. This big difference can be related not only to the 3D effects of the belly fairing but also to the difference between the angle of attack of RG2 and Geo70. It can be observed that in Geo70, due to the constant gradient, the transition takes place earlier, reducing the laminar extent over the wing.

The double re-compression shock at the inner region of the wing present in Geo70 is a clear sign that the belly fairing is still not properly fit to the wing.

Apart from the direct comparisons with RG2, in Fig. 5-4 can be observed that from the position of the sixth profile in the wing there is a slightly de-sweeping of the shock up to the fourth profile of the wing. This this de-sweeping is also represented in Fig. 5-2, while the shock position is at the 65% of the chord length at the profile 6, it has reduced to a chord length of 60% for the profile 4. The de-sweeping of the shock is clearly displayed in Fig. 5-5(b), where it can be observed from a distance of 6 m towards the fuselage the sweep angle gradually reduces, which coincides in Fig. 5-5(a) with the highest local wave drag and in Fig. 5-5(c) with the highest local wave force.

Geo70 belly fairing parameters

Cross-section	η_{BF}	Y Ratio	Ref. Angle	Ratio 2	Z Ratio	Ratio 1
1	-0.5	0.2	4	0.25	0.082	0.25
2	0	0.02	6	0.8	-0.056	0.7
3	0.65	0.001	4	0.8	-0.01	0.8
4	1.4	0.1	8	0.3	0.2	0.357

Table 5-3 Parameters used in Geo70 for the belly fairing generation

Performance metrics

Geometry name	$\alpha\,[deg]$	C_L	C_D	C_{DW}	E
RG2	0.77	0.5200	0.02277	0.0018	22.8370
Geo70	0.81	0.5200	0.02288	0.0023	22.7272

Table 5-4 Performance metics of RG2 and Geo70

(a) Profile 2, $\eta = 0.12331$ (b) Profile 3, $\eta = 0.16332$ (c) Profile 4, $\eta = 0.2$ (d) Profile 5, $\eta = 0.24565$

(e) Profile 6, $\eta = 0.294$ (f) Profile 7, $\eta = 0.56$
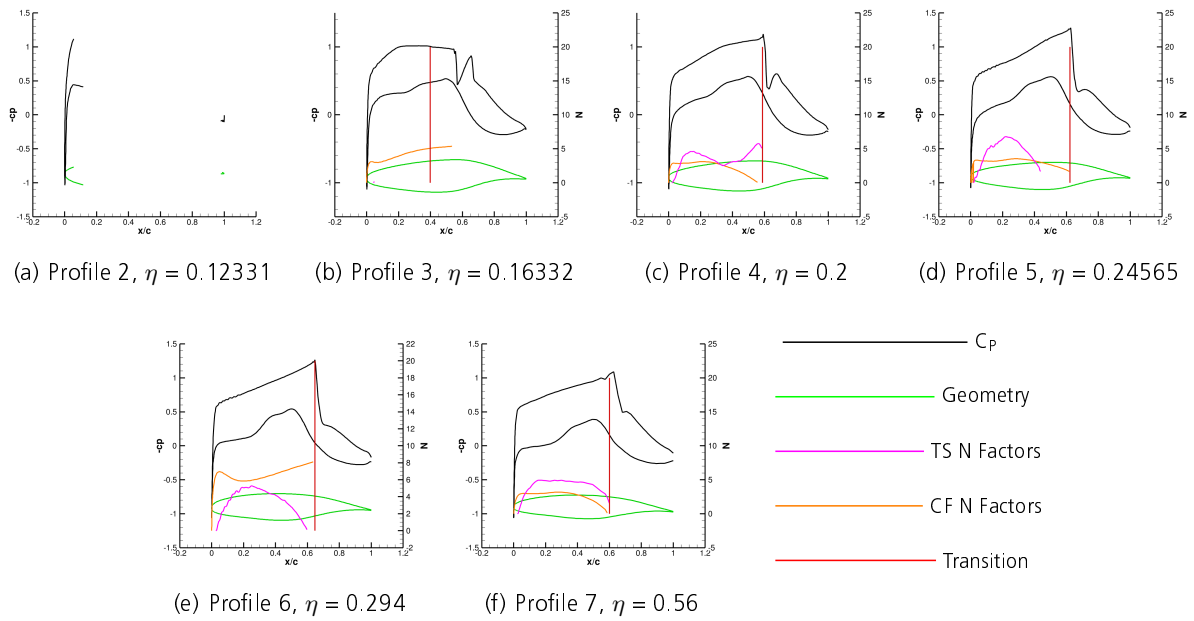
Figure 5-2 Representation of the C_P distribution, the N factors and the transition position along the wing for Geo70

(a) RG2, $\eta = 0.16332$ (b) Geo70, $\eta = 0.16332$
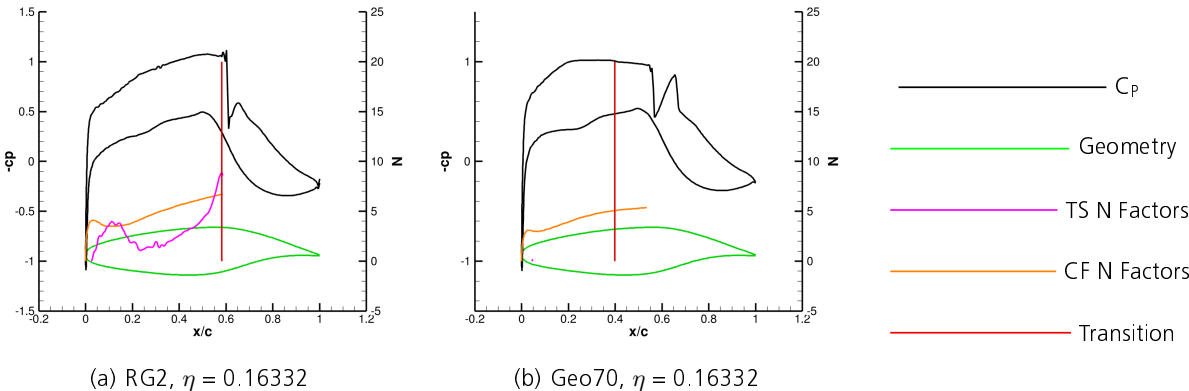
Figure 5-3 Comparision the C_P distribution between Geo70 and RG2 at $\eta = 0.16332$

(a) Laminar extent for Geo70   (b) C_P level curves for Geo70   (c) C_P contours for Geo70
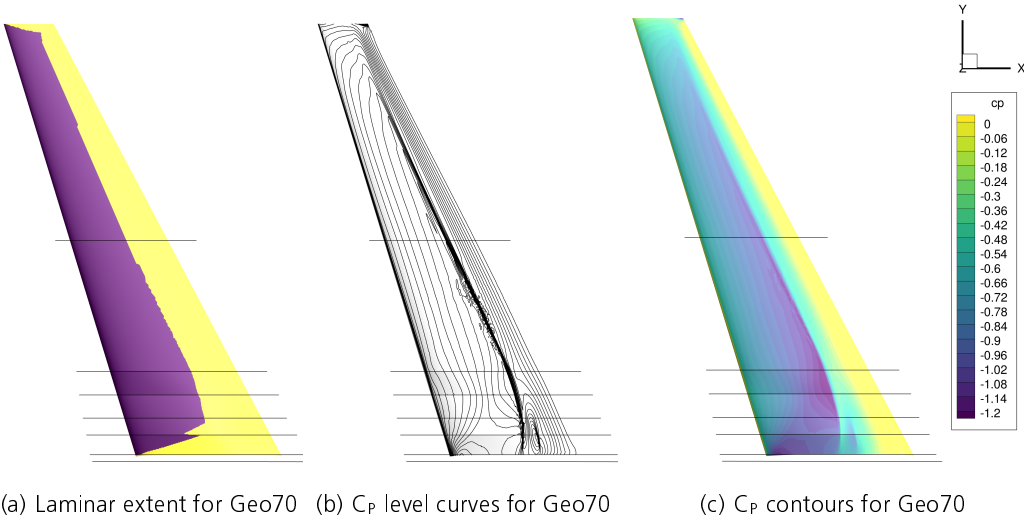
Figure 5-4 Surface contours of Geo70

(a) Local wave drag coefficient

(b) Local sweep

(c) Local wave force

(d) Representation of the schock position on the wing surface
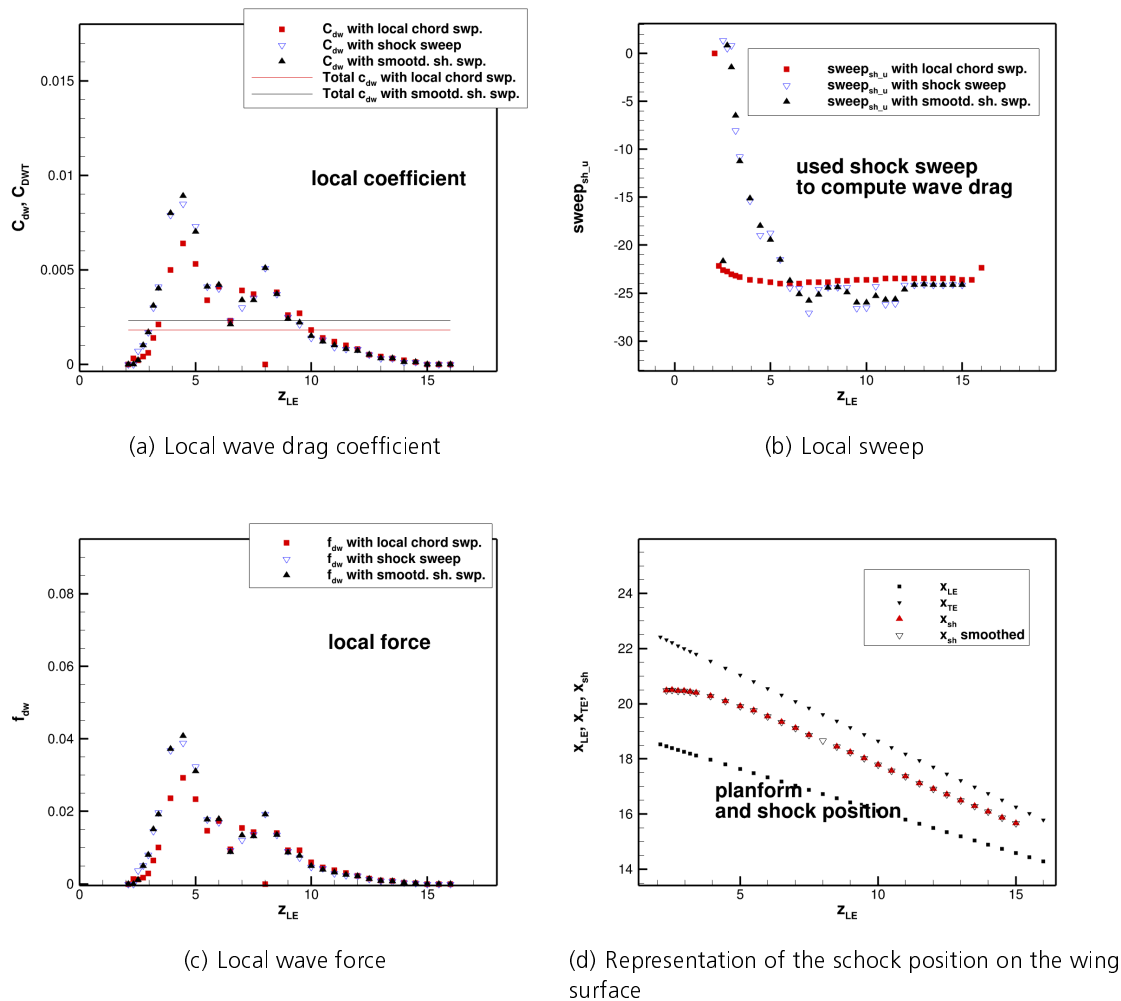
Figure 5-5 Graphic output of the wave drag post-processor for Geo70

5.2. Second parameter study

Following with the stepped approach, the third cross section was explored. The current hypothesis for the belly fairing definition is that the third cross section should be the thickest, in order to trigger the re-compression shock. Furthermore, with the parameter study, it was necessary to test if the η_{BF3} parameter could be directly correlated to the position of the shock. Since no negative values of Y Ratio are possible, and any higher values than the actual chosen 0.001 lead to a thinner cross section, for this design space exploration was decided to only consider η_{BF3} and Reference angle 3, leaving Y Ratio 3 to the value which would lead to the maximum thickness. The values chosen for the second cross section are the values which gave the maximum performance in the previous study. All the other values regarding first and second cross section have been kept constant since the last study. The fixed values choosen for this parameter study can be found in Table 5-5.

belly fairing fix parameters						
Cross-section	η_{BF}	Y Ratio	Ref. Angle	Ratio 2	Z Ratio	Ratio 1
1	-0.5	0.2	4	0.25	0.082	0.25
2	0	0.02	6	0.8	-0.056	0.7
3	n/a	0.001	n/a	0.8	-0.01	0.8
4	1.4	0.1	8	0.3	0.2	0.357

Table 5-5 Fixed parameters in the second parameter study

5.2.1. Parameter study domain, limits and sampling strategy

The same approach used in the first parameter study was used here, with the small difference that an starting point was available, since the results of Geo70 were available. Starting from the parameters of Geo70, for both variables a smaller and a bigger value than Geo70 was chosen, in a fully factorial manner. Since this time only two variables were considered, and one geometry was already simulated this leaded to 8 geometries. The values of the variables to be simulated are displayed in Table 5-6. Based in the results obtained, the simulation domain was again manually extended in the regions which could be expected to give good performance, therefore, η_{BF3} was further simulated for the values of 0.85 and 0.95. Reference angle 3 was additionally simulated for the values of 0, 8 , 10 and 12 degrees.

Starting variable values			
Variable	min.	mid.	max.
η_{BF} [/]	0.55	0.65	0.75
Reference angle [deg]	2	4	6

Table 5-6 Values used in the second parameter study for the belly fairing generation before expanding the domain based in the results found

5.2.2. Results

The gliding ratio of all the simulated geometries is displayed in Fig. 5-6. As the results show, there is for some geometry combinations a good performance plateau, in which as long as the variable varies are not too badly chosen, the performance is good and the variable values have little influence in the performance. Although the domain could have been further expanded, at a value of reference angle equal to 12, some geometries gave generation problems, leading to failed geometries, therefore it was decided to not further expand the domain. Along the other available directions, a value of η_{BF3} smaller than 0.65 started giving bad performance, which can be expected, as η_{BF3} reduces the third cross section comes closer to the second leading to stronger gradients between the second and third cross-section. Lower values of reference angle than 0 were

avoided as doing so means that the belly fairing is smaller at the wing junction than the fuselage, with a sharp angle. This decision seems partially supported by bad performing geometry found at a reference angle of 0 and a η_{BF3} equal to 0.65. No other combination with a value of η_{BF3} equal to 0.65 gives such a bad result. Another reason to not further expand the simulation domain of the third cross section is that when both cross-sections are simulated together, a big domain would lead to a low resolution, which is not desired in this study as it has to set the baselines for further research. Apart from that, there is no reason to not further expand the domain towards higher values of η_{BF3}.

Since no geometry was found with an statistically significant higher performance than the others, Geo70 remained as the best parametric performing geometry, although at the point a big dataset of good performing geometries was available.
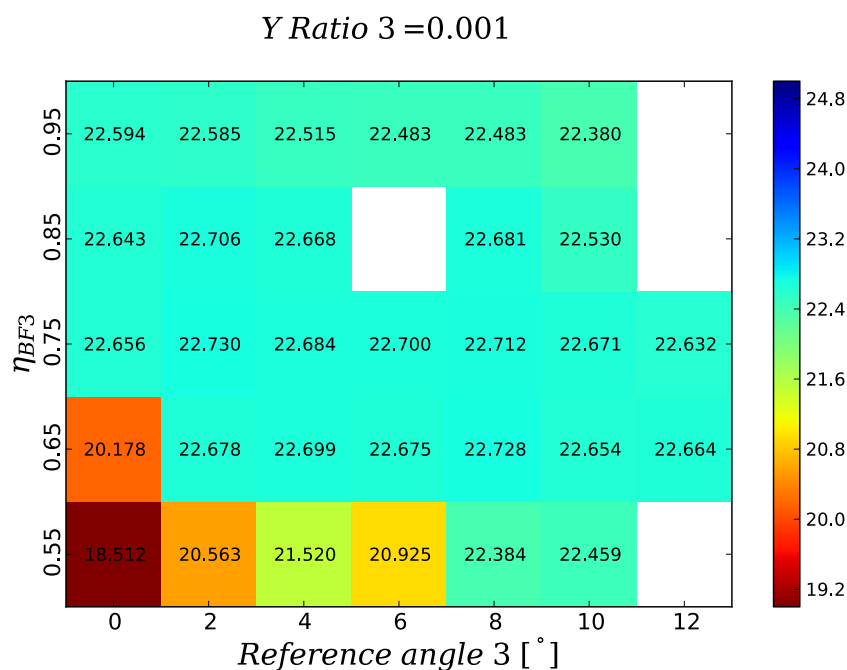
Figure 5-6 Representation of the performance obtained in the second parameter study

5.3. Third Parameter study

Based in the findings of the previous parameter studies, there was now a well defined region for both the second and the third cross section in which better combinations of the parameters could be expected. In order to investigate the multiple not considered combinations, was decided to perform a parameter study in which all the five variables considered in the two previous studies were free.

It is worth to mention the importance of the previous studies, as for this parameter study, the high number of variables lead to a much higher number of simulations, which meant that the region to be studied had to be carefully chosen.

5.3.1. Parameter study domain

All the parameters but the previously studied remaining fix as before. Table 5-7 shows an overview of the fix parameters. The variables considered in this parameter study are η_{BF2}, RW_2 and YR_2, η_{BF3} and RW_3.

	belly fairing fix parameters					
Cross-section	η_{BF}	Y Ratio	Ref. Angle [deg]	Ratio 2	Z Ratio	Ratio 1
1	-0.5	0.2	4	0.25	0.082	0.25
2	n/a	n/a	n/a	0.8	-0.056	0.7
3	n/a	0.001	n/a	0.8	-0.01	0.8
4	1.4	0.1	8	0.3	0.2	0.357

Table 5-7 Fixed parameters in the third parameter study

5.3.2. Limits and sampling strategy

For this parameter study, as for the other parameter studies, it was decided to go for a fully factorial experiment of three values, which leads to a total of 243 geometries. The values chosen for each of the variables are represented in Table 5-8. Despite a higher resolution for Reference angle and η_{BF} would have been desired, the main objective of this study was to cover the whole domain while considering the five degrees of freedom.

Although most of the post processing was already automated at this point of the work, the parameter file for the geometry generation was done by hand, this is important to mention because Y Ratio 2 should have the same values as in the first parameter study: 0.02, 0.07 and 0.12 but a mistake was made and the values 0.012, 0.02 and 0.07 were used.

Variable values for third parameter study			
Variable	min.	mid.	max.
η_{BF2} [/]	0	0.15	0.3
Reference angle 2 [deg]	2	6	10
Y Ratio 2	0.012	0.02	0.07
η_{BF3} [/]	0.55	0.75	0.95
Reference angle 3 [deg]	0	5	10

Table 5-8 Values used in the third parameter study for the belly fairing generation

5.3.3.   Results

Due to the high number of degrees of freedom is not easy to analyse the results of this parameter study. The different variables influence each other and lead to a noisy dispersion from which is difficult to extract correlations. Figure 5-7 represents all the geometries performances for all the five variables studied. For the values studied, only η_{BF3} seem to have a direct impact on the dispersion of the performance results, which concentrates for higher values. This behaviour was observed in more detail by isolating the values of Reference angle 3, the remaining variable of the third cross-section.

As it can be observed in Fig. 5-8, as Reference angle 3 increases, so does the influence of η_{BF3} in the dispersion. The fact that values of η_{BF3} equal to 0.95 give least amount of low performance geometries can be reasoned with that having the third cross section at the wing leading edge reduces the risk of separation, as no adverse pressure gradients are found in the belly fairing at the same time as in the wing suction surface. As Reference angle 3 increases, the third cross section is bigger and therefore the separation risk on the wing is reduced, therefore a Reference angle 3 of 10 degrees together with a η_{BF3} of 0.95 does not lead to separations, which are characterized with a glide ratio below 20. Despite the aforementioned strategy reduces the dispersion of the results and reduces the possibility of flow separation on the wing, in Fig. 5-8 can be also observed that the maximum performance reduces as well. As it will be reviewed in the next sub-chapter, the best geometry is not contained in this combination.

(a) Influence of η_{BF2} in E

(b) Influence of η_{BF3} in E

(c) Influence of Y Ratio 2 in E

(d) Influence of Reference angle 2 in E

(e) Influence of Reference angle 3 in E
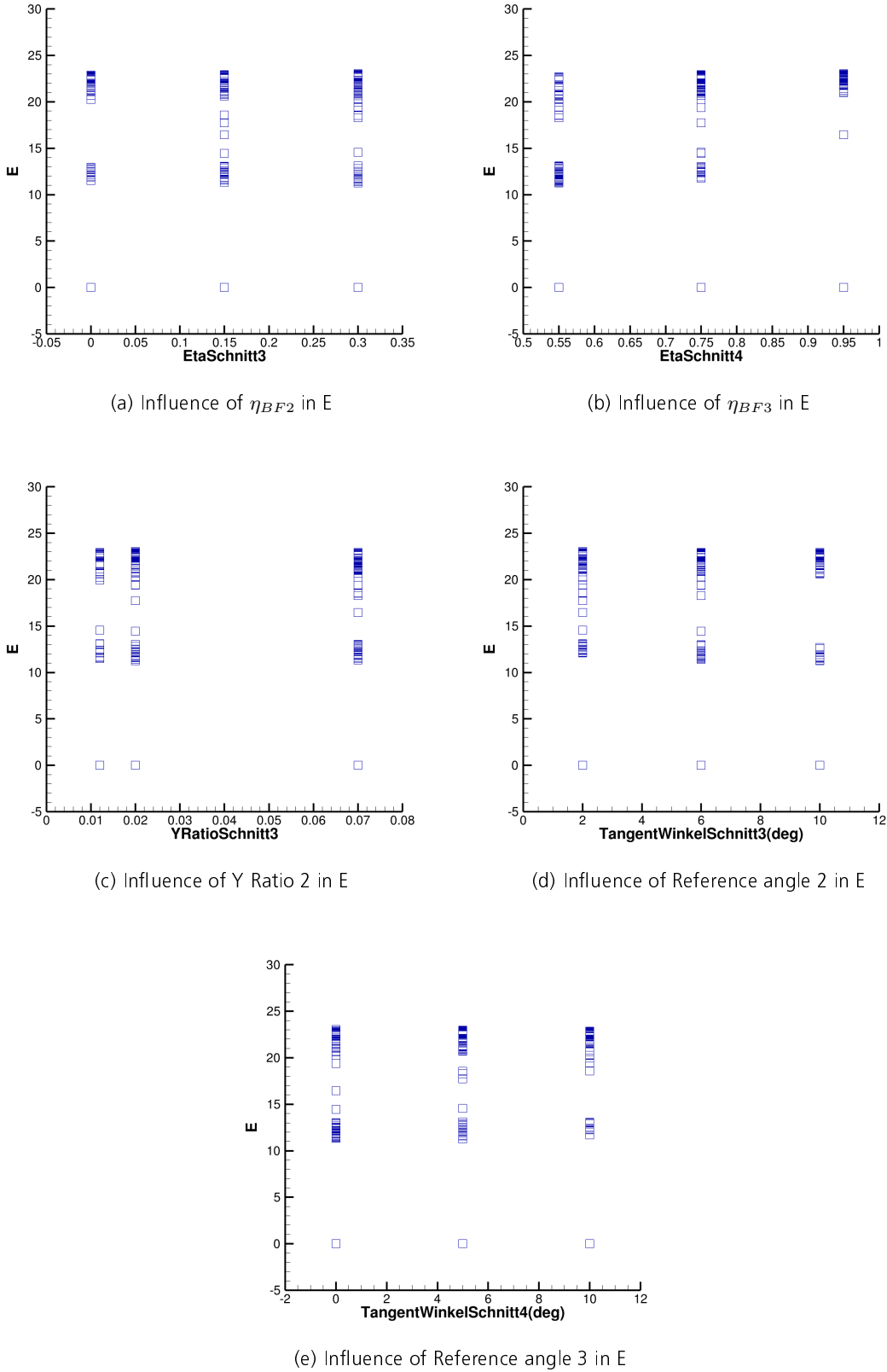
Figure 5-7 Representation of the variable influence in the geometry performance
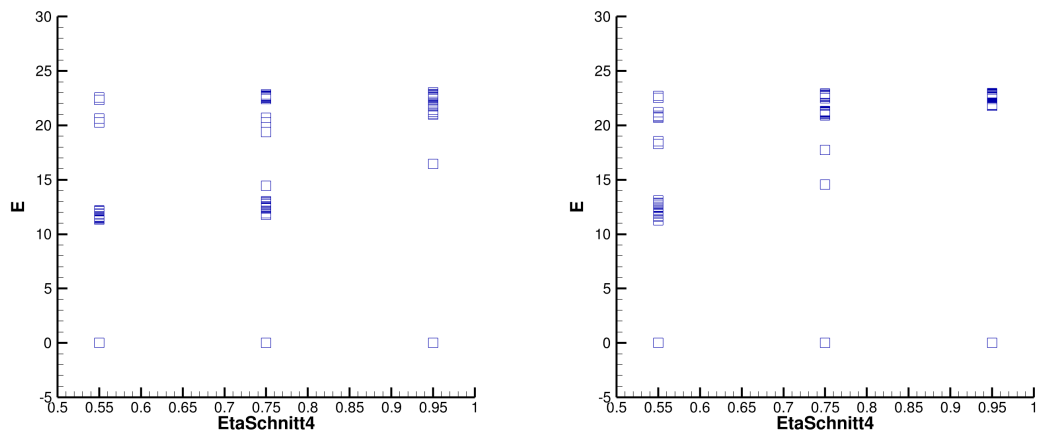
(a) Influence of η_{BF3} in E with Reference angle 3 equal to 0 deg

(b) Influence of η_{BF3} in E with Reference angle 3 equal to 5 deg
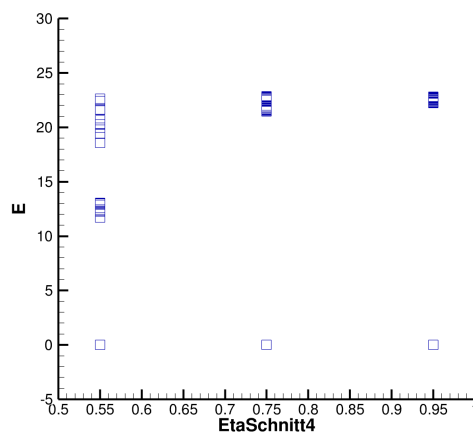
(c) Influence of η_{BF3} in E with Reference angle 3 equal to 10 deg

Figure 5-8 Representation of the influence of reference angle 3 and η_{BF3} in the geometry performance

5.3.4. Best geometry performance

In the same way as in the first parameter study, there has been found a new best performing geometry, Geo267. The performance metrics have been compared with previous geometries in Table 5-9. Compared to the RG2 performance, the wave drag has remained constant, while the drag coefficient has reduced, which suggest an increase of the laminar extent.

Table 5-10 displays the values used for the Geo267 belly fairing generation. One of the first observations that can be made are that in this case, in adverse to Geo70, the Geo267 belly fairing is small, with low values of reference angle, which is at the same time represented in the aerodynamic post-processor with a whole second profile. A second observation of the parameters of Geo267 is that in the same way as in Geo70, the second cross-section of the belly fairing is larger than the

Performance metrics					
Geometry name	$\alpha\,[deg]$	C_L	C_D	C_{DW}	E
RG2	0.77	0.5200	0.02277	0.0018	22.8370
Geo70	0.81	0.5200	0.02288	0.0023	22.7272
Geo267	0.75	0.5201	0.02260	0.0018	23.0132

Table 5-9 Performance metrics of RG2, Geo70 and Geo267

third. This is represented by the bigger reference angle in the second cross-section than in the third. This observation provides an interesting point, which goes against an hypothesis formulated at the beginning of the work, in which was suggested that the third cross-section had to be the thickest, in order to provide a re-compression shock as the belly fairing contracts. Further discussion on the theme will be presented later on in the work.

Geo267 belly fairing parameters						
Cross-section	η_{BF}	Y Ratio	Ref. Angle	Ratio 2	Z Ratio	Ratio 1
1	-0.5	0.2	4	0.25	0.082	0.25
2	0.3	0.02	2	0.8	-0.056	0.7
3	0.95	0.001	0	0.8	-0.01	0.8
4	1.4	0.1	8	0.3	0.2	0.357

Table 5-10 Parameters used in Geo267 for the belly fairing generation

Moving on to the aerodynamic post-processor, represented in Fig. 5-9 and Fig. 5-10, apart from the additional inner profile, Geo267 shows an aerodynamic behaviour closer to Geo70 than to RG2. Despite the broad similitude, when looking in detail, Geo267 shows a better shock position than Geo70, which is also shown by C_{DW}. Geo70 showed a mild shock de-sweeping from the sixth profile inwards, Geo267 shows an still appreciable but more moderate de-sweeping. Furthermore, Fig. 5-12 shows that the double re-compression shock found in Geo70 is in Geo267 single.

The backwards position of the shock implies a lower wave drag, and a larger laminar extension, which accounts to a big drag reduction from Geo70.

(a) Profile 2, $\eta = 0.12331$ (b) Profile 3, $\eta = 0.16332$ (c) Profile 4, $\eta = 0.2$ (d) Profile 5, $\eta = 0.24565$

(e) Profile 6, $\eta = 0.294$ (f) Profile 7, $\eta = 0.56$
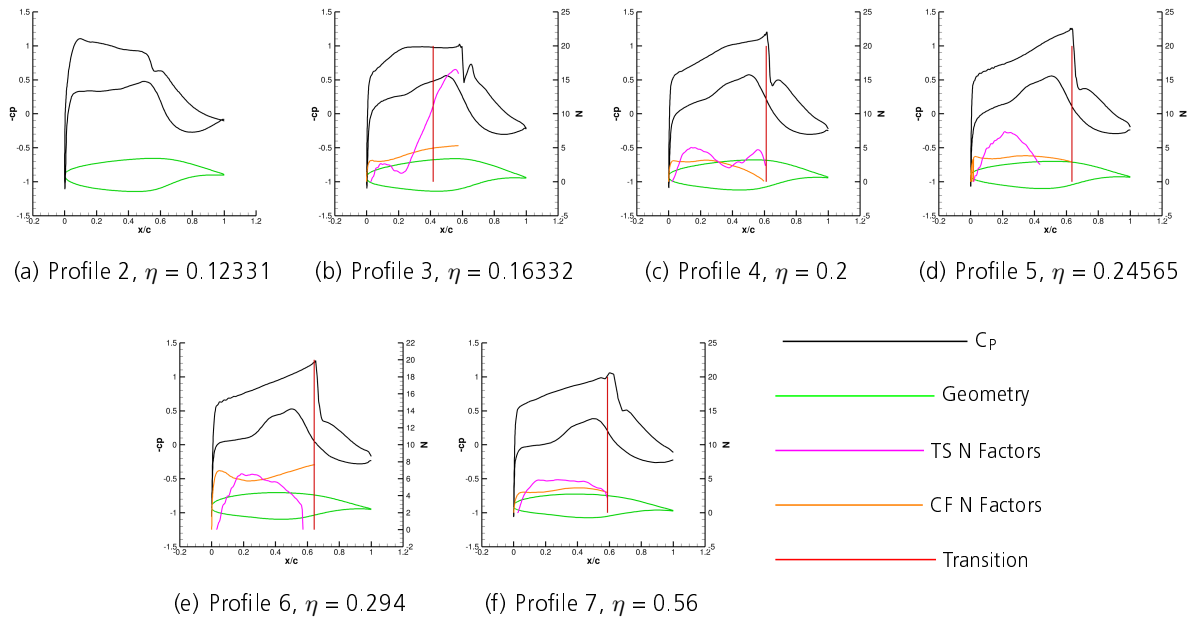
Figure 5-9 Representation of the C_P distribution, the N factors and the transition position along the wing for Geo267

(a) Laminar extent for Geo267 (b) C_P level curves for Geo267   (c) C_P contours for Geo267
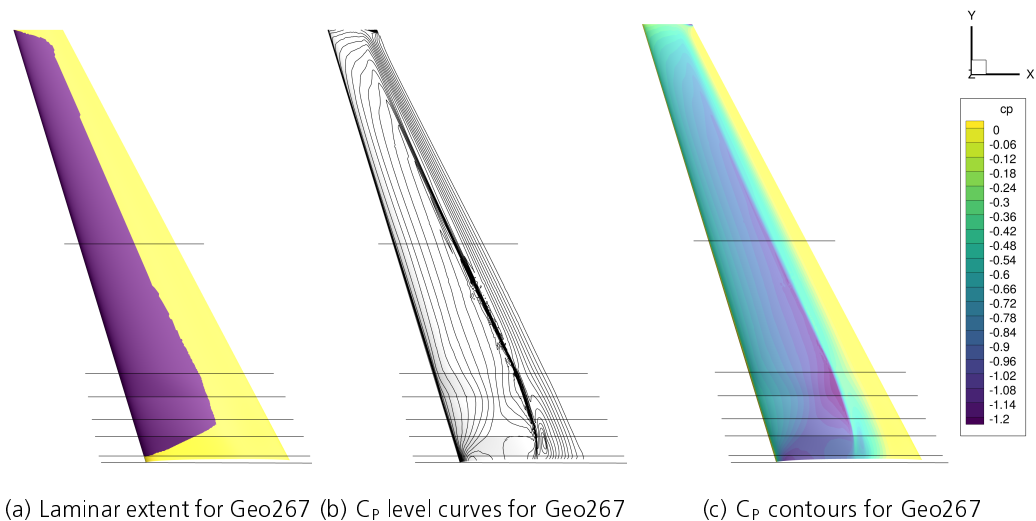
Figure 5-10 Surface contours of Geo267

(a) Local wave drag coefficient

(b) Local sweep

(c) Local wave force

(d) Representation of the schock position on the wing surface
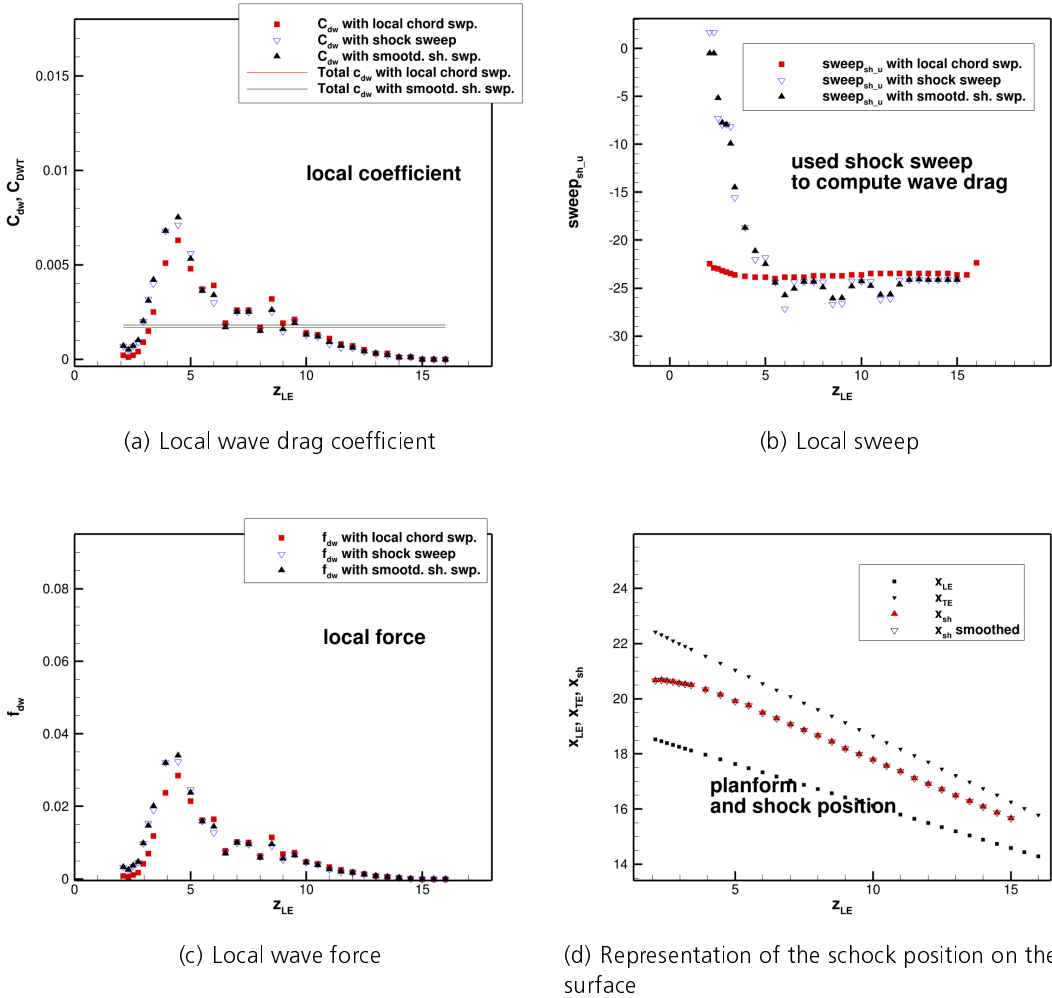
Figure 5-11 Graphic output of the wave drag post-processor for Geo267

(a) Geo70, $\eta = 0.16332$ (b) Geo267, $\eta = 0.16332$
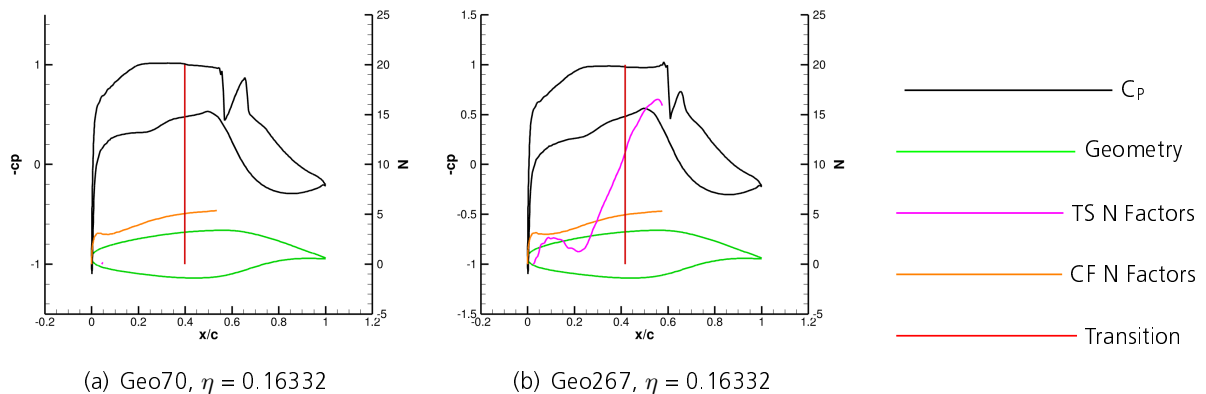
Figure 5-12 Comparision the C_P distribution between Geo267 and Geo70 at $\eta = 0.16332$

5.4. Response surface modelling

At this point, the previous reference geometry performance had been surpassed, nevertheless it was clear that the optimum performance of the four cross section was still to be achieved. The main advantage at this point is that a belly fairing database had been built based in the previous three parameter studies, which enabled the usage of surrogate models.

5.4.1. Methodology

While considering big and complex geometry domains such as the one in hand surrogate models are a very suitable tool in order to improve the available knowledge. Based in the available data a continuous surface of results is built, and can be used to find good performing geometries based in the implicit correlations available in the data. This same procedure could be also done manually as it was made in the three previous parameter studies, but the high number of degrees o freedom make very complicated this task.

The SMARTy tool from the AS-CASE department has been used to generate the surrogate models. Bekemeyer [3] was decisive for the proper implementation of the surrogate models in this work.

In order to find the best geometries is important to ensure that the surrogate model provides a good prediction. In order to do so, first with the available geometries a first surrogate model is built, which usually has poor prediction capability. This happens because in the regions at the furthest of the available geometries bad prediction occur. This may lead to either much worse predictions than real or the other way around. In order to improve the surrogate model performance, additional geometries can be simulated and feedback to a second surrogate model. This process is iterative and the prediction improves with each iteration.

For this work it was decided to build a surrogate model and take a sample size of 30 geometries based only in the best performance achieved. Then the geometries were generated and simulated as in the previous parameter study.

5.4.2. Results

As previously discussed, the usage of surrogate models needs a iterative generation of more surrogate models in order to achieve improvements. Based in the time constraints only one surrogate model could be built. From the sampled 30 geometries there was not one geometry which achieved the good performance of Geo267. On the other hand three good performing geometries were achieved with performance close to the one of Geo267.

In this way the surrogate model just provided a better database for future work rather than finding a better performing geometry.

Future work should be invested in further improving the surrogate model, in order to find the optimum of the methodology.

Performance metrics					
Geometry name	$\alpha \, [deg]$	C_L	C_D	C_{DW}	E
RG2	0.77	0.5200	0.02277	0.0018	22.8370
Geo70	0.81	0.5200	0.02288	0.0023	22.7272
Geo267	0.75	0.5201	0.02260	0.0018	23.0132
Geo358	0.77	0.5201	0.02267	0.0017	22.9476

Table 5-11 Performance metics of RG2 and Geo70, Geo267 and Geo358

5.5. Turbulent performance

A common practice when designing laminar profiles is to test the performance when the profiles are under turbulent flow. Based in profile design for sailplanes is known that turbulent flow in a laminar profile reduces the profiles performance. Along the present work there has been a number of geometries which have not reach the design performance, as the 3D effects have reduced the maximum lift coefficient below the original design. Since laminar profiles could be expected to work in turbulent flow due to mosquito impact or rain, is important to check what kind of performance hit do the best designs take under such conditions.

5.5.1. Methodology

In order to ensure the best outcomes the six best geometries were simulated under turbulent flowfield. The same grids used in the previous laminar studies were used again, but this time the laminar module was deactivated. The geometries selected were chosen by their gliding ratio. Geo267 and Geo294 were so far the most promising but in order to ensure a success outcome all the six geometries available with a glide ratio above 22.90 were simulated. Table 5-12 shows all the geometries tested.

Laminar performance metrics

Geometry name	$\alpha \ [deg]$	C_L	C_D	C_{DW}	E
RG2	0.77	0.5200	0.02277	0.0018	22.8370
Geo267	0.75	0.5201	0.02260	0.0018	23.0132
Geo294	0.76	0.5199	0.02264	0.0018	22.9653
Geo301	0.78	0.5199	0.02269	0.0017	22.9156
Geo356	0.79	0.5201	0.02268	0.0016	22.9293
Geo357	0.77	0.5201	0.02267	0.0016	22.9362
Geo358	0.77	0.5201	0.02267	0.0017	22.9476

Table 5-12 Performance metrics of RG2 and the geometries with a laminar gliding ratio over 22.9

5.5.2.   Results

Table 5-13 displays the performance obtained for the best performing geometries of this work. As the results show, the turbulent flow in the laminar geometries takes a big hit in the performance. For the geometries calculated, the drag coefficient can be increased anywhere between 29 and 36 drag counts. Furthermore, as the results of Geo267 show, turbulent flow may cause that the geometry is not any more capable of achieving the design lift coefficient. Based in the results obtained, it has been decided that despite Geo267 or Geo294 have better performance than Geo358 or Geo301, Geo358 and Geo301 are a more convenient as the turbulent performance does still achieve the design lift coefficient and take less of a performance hit when turbulent.

Turbulent performance metrics

Geometry name	$\alpha \ [deg]$	C_L	C_D	E
RG2	1.25	0.5198	0.02561	20.3013
Geo267	1.95	0.4739	0.03693	12.8342
Geo294	1.34	0.5195	0.02701	19.2315
Geo301	1.27	0.5199	0.02570	20.2258
Geo356	1.32	0.5198	0.02627	19.7859
Geo357	1.29	0.5198	0.02623	19.8169
Geo358	1.27	0.5199	0.02565	20.2696

Table 5-13 Turbulent performance metrics of RG2 and the geometries with a laminar gliding ratio over 22.9 under turbulent flow

6. Results discussion and conclusion

In the following chapter an overview at the best geometry obtained will be displayed and the achieved improvements will be contrasted with the reference geometry. Later, a discussion about the future work will be presented in which the author describes which work could be considered in the future and how the actual work could be improved.

6.1. Best Geometry

In the previous chapter each of the improvements have been discussed regarding to the previous best performing Geometry. In the following section the best performing Geometries will be shown and discussed and compared to the reference geometry. As it has been previously discussed there is two geometries which have shown not only an excellent laminar performance but also an acceptable turbulent one. Those Geometries are Geo301 and Geo358, an overview of both of them is shown in Fig. 6-1.

(a) Geo301   (b) Geo358
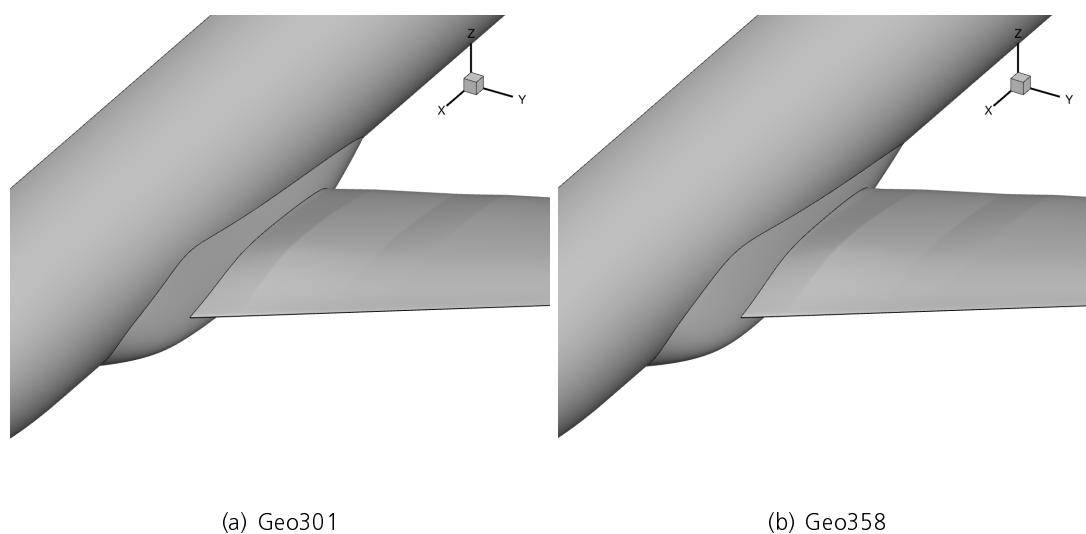
Figure 6-1 Representation of Geo301 and Geo358

Despite both geometries may look similar, Table 6-1 shows how different the values used for both geometries are, and in Fig. 6-2 can be seen how the different parameters translate to the junction line an how the junction line affects the pressure distribution under laminar flow.

Geo301 shows a stronger gradient prior to the wing with a weaker gradient along the wing than Geo358. Despite the big geometric differences between both belly fairings, a major difference can only be observed in the pressure coefficient distribution at the profile nose. RG2 shows a junction line typical of a more complex 5 cross-section belly fairing. Starts much later than the other geometries and has a much stronger first gradient, followed by a supersonic acceleration. RG2

Geo301 and Geo358 parameters					
Geometry	η_{BF2} [/]	RA_2 [deg]	YR_2 [/]	η_{BF3} [/]	RA_3 [deg]
Geo301	0.3	10	0.07	0.95	5
Geo358	0.3	4	0.0555	0.95	7.5

Table 6-1 Parameters used for the generation of Geo301 and Geo358

shows the main advantage of a 5 cross-section belly fairing, which allows a shrinking belly fairing in the supersonic region, which may lead to performance which can not be achieved with a four cross-section belly fairing.

(a) junction line   (b) C_P distribution at $\eta = 0.12331$

RG2   Geo301   Geo358
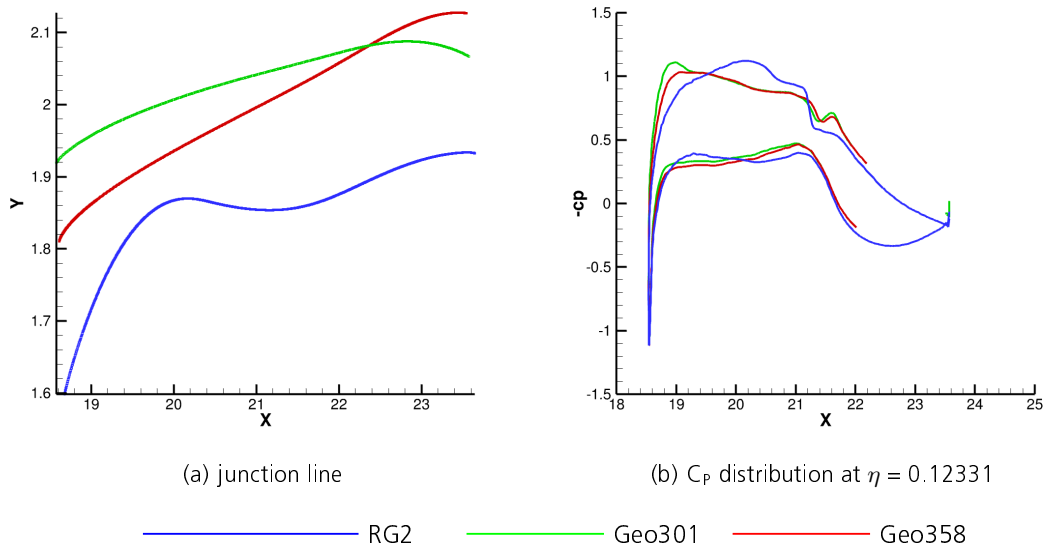
Figure 6-2 Representation of the junction line and the C_P distribution for the reference geometry, Geo301 and Geo358

6.1.1.   Laminar performance

In the following subsection the differences between Geo301 and Geo358 are displayed. Overall, there is just small diferences on the wing root leading edge, which as in Fig. 6-2 can be observed, has a higher suction peak for Geo301. This is also represented in the pressure coefficient level lines, represented in Fig. 6-3.

The shock position looks very similar between both found geometries with only little shock de-sweeping. On the other hand, both geometries show an undesired double shock, which RG2 does not have.

Although this may seem like a plus point for RG2, when looking in detail, Fig. 6-4 shows that the much stronger re-compression shock found in RG2 leads to a static pressure much lower, which can

(a) RG2   (b) Geo301   (c) Geo358
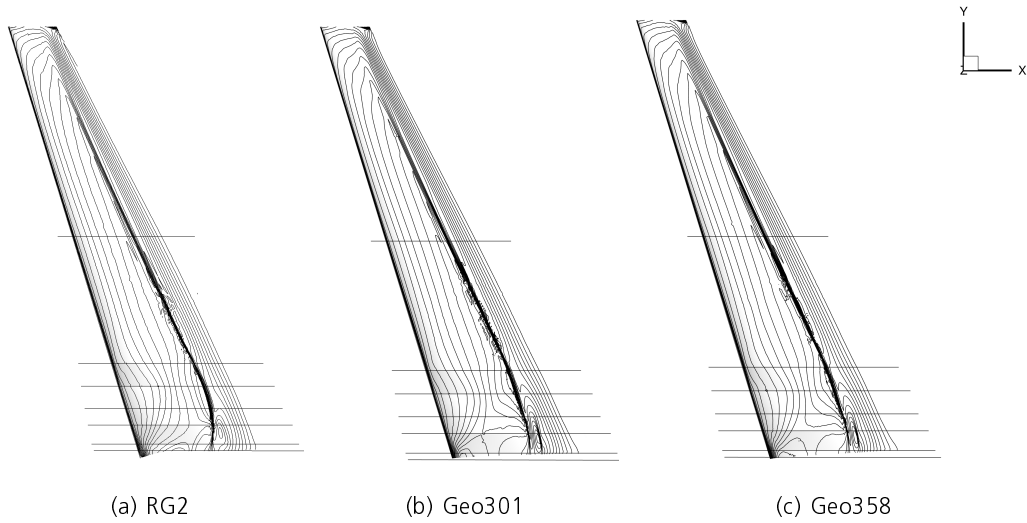
Figure 6-3 C_P Level lines of RG2, Geo301 and Geo358

(a) RG2, $\eta = 0.16332$ (b) Geo301, $\eta = 0.16332$ (c) Geo358, $\eta = 0.16332$

——— C_P ——— Geometry   ——— TS N Factors   ——— CF N Factors   ——— Transition
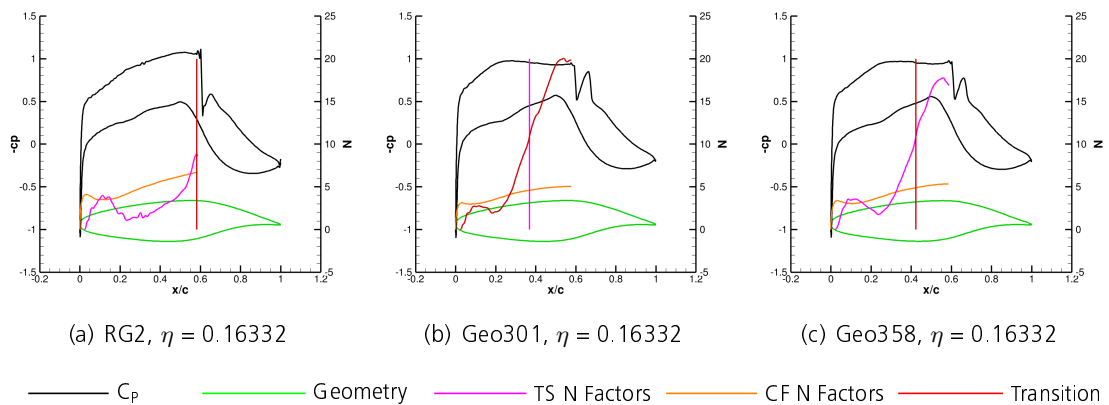
Figure 6-4 Comparison of the C_P distribution between RG2, Geo301 and Geo358 at $\eta = 0.16332$

not lead to a second shock.

When comparing Geo301 with Geo358, it can be observed that Geo358 has a slightly smaller second shock, which may explain the difference in performance.

The big differences between the initial shock position found in RG2 and the one in the found geometries, translates in a different wave drag distribution, which can be observed in Fig. 6-5. The closest region to the fuselage has been greatly improved, reducing the wave drag in the region between 2 and three meters to a very low value. The region between 3 and 5 meters has been as well improved, although there is still a big amount of wave drag. On the other hand, in the region between 5 and 8 meters the wave drag has increased. Despite on most of the inner region the sweep of the shock has been increased, there is a small region where the sweep has been reduced, which translates in a increase of the local wave drag. Overall, as the performance metrics show, the wave drag has been reduced, but this weird behaviour is worth to keep in mind for future

(a) RG2   (b) Geo301
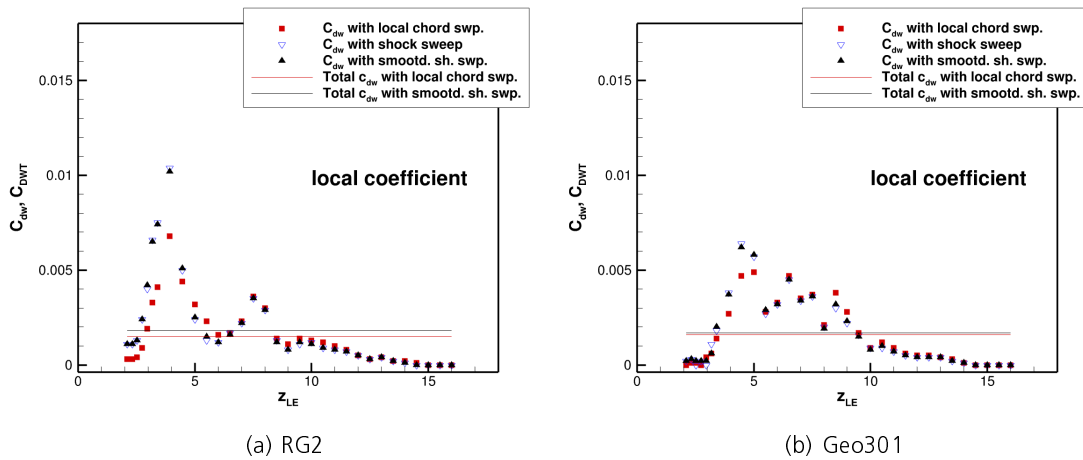
Figure 6-5 Comparison of the wave drag distribution along the wingspan between RG2 and Geo301

geometries.

Figure 6-5 shows as well that in the region between 3 and 9 meters there is a lot room for improvement, which may lead in the future to big performance improvements, but have to be tacked together with the wing profiles.

Another point which is worth to mention is the Laminar trade-off found between RG2 and the two found geometries. RG2 has for the represented profile the transition at the shock position, arround a x/c position of 0.6. For Geo301 and Geo358 the transition takes place at a position of x/c close to 0.4. Despite the found geometries have a reduced laminar region compared to RG2, the much better shock position overcompensates the losses.

Lastly, it is worth to mention the transition position difference between Geo301 and Geo358. In Geo301 the transition is around x/c = 0.38 and in Geo358 the transition is around x/c = 0.42.This and the second shock difference seem to account for the performance difference between both geometries.

6.1.2. Turbulent performance

Although in the turbulent performance between both geometries there is also only small differences, it is also worth to compare them.

Compared with the laminar flow simulations there is a strong de-sweeping. Additionally, in η = 0.12331 can be observed a much stronger re-compression shock than for the laminar case.

In the same way as for laminar flow there is not much difference between both geometries, the suction peak is slightly stronger in Geo301.

As Table 5-12 and Table 5-13 show, the de-sweeping of the shock and the ausency of laminar flow account for 30 drag counts for Geo358 and 31 for Geo301.

(a) RG2   (b) Geo301   (c) Geo358
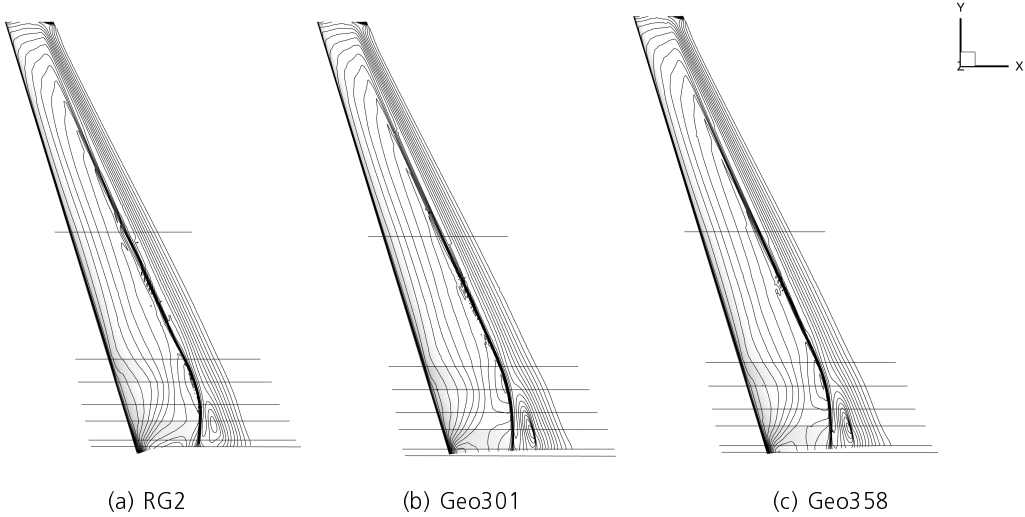
Figure 6-6 C_P Level lines of RG2, Geo301 and Geo358 under turbulent simulation

(a) RG2, $\eta = 0.12331$ (b) Geo301, $\eta = 0.12331$ (c) Geo358, $\eta = 0.12331$

—— C_P —— Geometry   —— TS N Factors   —— CF N Factors   —— Transition
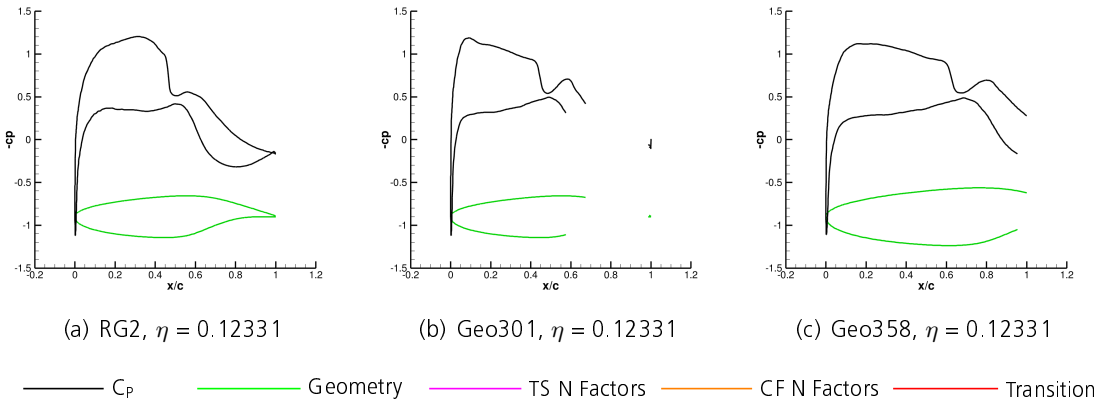
Figure 6-7 Comparision the C_P distribution between RG2, Geo301 and Geo358 at $\eta = 0.12331$ under turbulent simulation

6.1.3.   Angle of attack impact

As previously discussed, Fig. 6-5 shows a region, between 5 and 8 meters, in which the wave drag increases from RG2 to Geo301 due to a local de-sweeping. Figure 6-8 represents the problem. Although the overall wave drag has decreased from RG2 to Geo301, the local increase leads to think that something could be done better in the region, therefore, some deduction is necessary.

One could expect that this wave drag increase has been directly caused by the belly fairing, but previous experiments have shown that the belly fairing can be expected to have an influence up to 5 meters of wingspan.
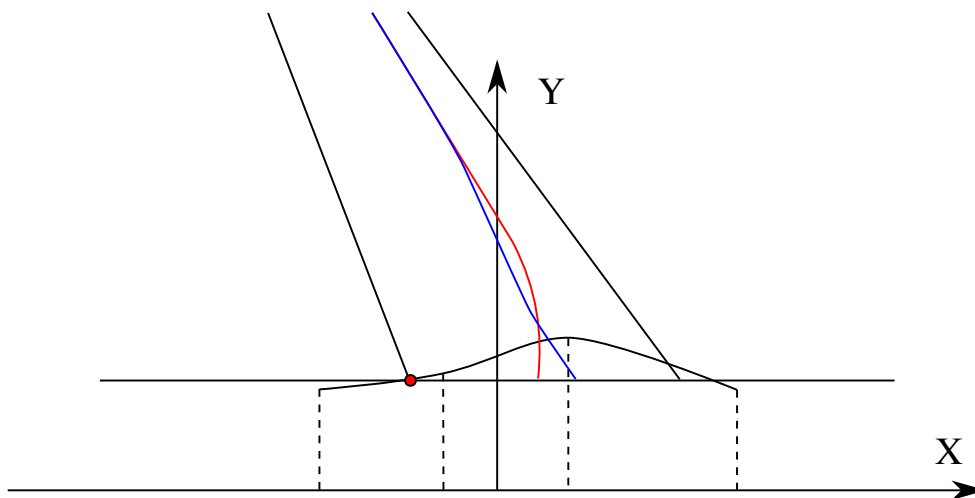
Figure 6-8 Sketch of the de-sweep found in Geo301 with respect to RG2. RG2 represented in red, Geo301 represented in blue.

It could be as well expected that the shock position in the belly fairing may lead to an influence in the shock position of the wing, but since from RG2 to Geo301 the shock has been 'pulled' backwards, it seems counter-intuitive that, at the same time, the shock has been pulled forward in a region further down the wing.

Therefore, the only open variable is the angle of attack. As Table 5-12 shows, RG2 has an angle of attack of 0.77 degrees in comparison with the 0.78 of Geo301. The difference in angle of attack is indeed very small, but it is also known that the shock position can be in some operating points very easily influenced.

On top of it, Geo267, which has an angle of attack of 0.75 does not show the increase in wave drag in the aforementioned region, as Fig. 6-9 shows.

Although Geo267 has a better local wave drag in the region between 5 and 8 meters, it is not represented in the overall wave drag coefficient because of the worse inner region.

(a) RG2   (b) Geo267
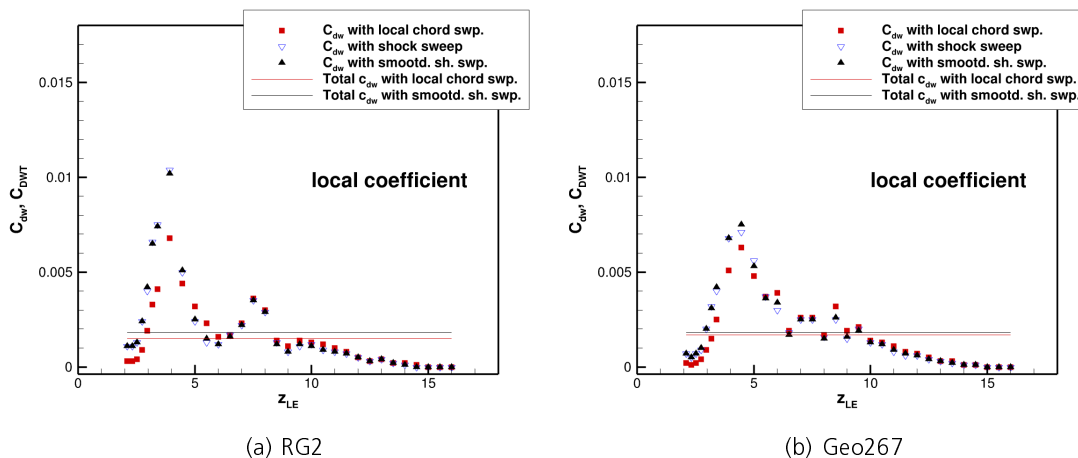
Figure 6-9 Comparison of the wave drag distribution along the wingspan between RG2 and Geo267

6.2. Methodology review

Along the work, the geometry methodology used gave some generation problems, which should be tacked for future automation. On top of it, some unexpected geometry parameters have shown very good performance. Both the new suggested geometry methodology and the unexpected geometries will be discussed in this section.

6.2.1. New geometry methodology

The methodology used for the cross-section generation has a major problem. The Y Ratio can not be any smaller than 0. That is to say the belly fairing, at the XY plane can not be any thicker than the Fuselage. Furthermore, in some cases, even choosing values higher than zero may lead to failed geometries for some combinations. If one of the cross-sections has a value close to 0, as it happened in this work for the third cross-section, the adjacent cross sections have to have a value higher than 0, otherwise, since the cross sections are connected, a region of Y ratio with negative values may appear, which lead to a non meshable, failed geometry.

Two different new methodologies are suggested to cope with this problem. The first one, repre-sented in Fig. 6-10(a), tries to tackle this problem while keeping the number of variables as low as possible. The reference angle is no longer at the Y axis but a the chord plane, which is expected to have a closer translation to the wing surface than the previous methodology. The size of each section is controlled by four ratios, and the only one which has to be smaller than one is Ratio 1, which has been strategically allocated in a position where it is not expected to need a belly fairing, therefore the value can be kept always below 1. The second suggested geometry is represented in Fig. 6-10(b) and is based in the one used in the present work, with the addition of an extra point which fulfils the same function as in the previous suggested methodology. The main advantage of the second geometry is that the already simulated data can be much easily adapted, with the cost of having a more complex methodology.

(a) New novel methodology   (b) New methodology based in the current one
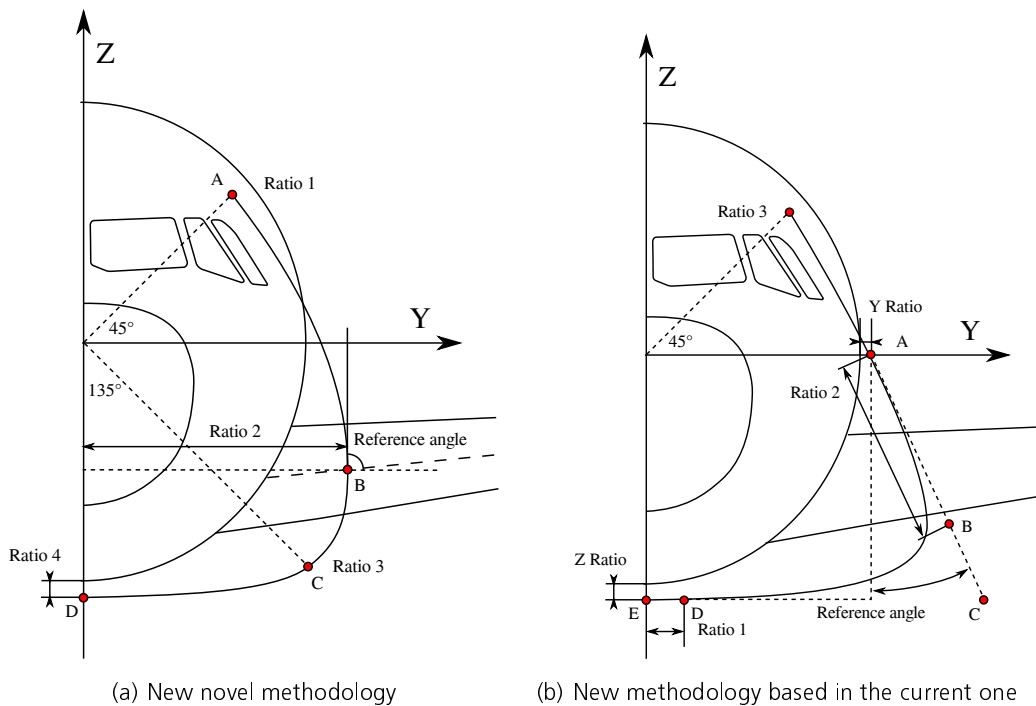
Figure 6-10 Representation of the suggested new cross-section methodologies

6.2.2.   Unexpected geometries

At the beginning of the work there was a hypothesis, which consisted in having a third cross-section being the thickest, and it was suggested that the position of the cross section may had an impact on the position of the shock. This hypothesis was derived from the TG2 geometry, which was based in the 2.75d flow at the wing. The hypothesis was proved to be false, but as in the following will be explained, the definition had an impact to the later work.

In order to ensure that the thickest cross-section in the belly fairing was indeed the third cross-section, the third cross section had a tangency imposition, and the highest values of reference angle were given to the third cross section. During the parameter study, all the parameters were explored but the tangency imposition stayed in place, which led to some combinations in which the second cross-section was thicker than the third.

Along the work, it has been discovered that this type of combination can lead to a very good performance. Geo70, Geo267 are two examples of this kind of geometry. In Fig. 6-11 can be observed how this kind of geometries look like.

In order to understand how such a geometry can be a good performing geometry, we have to take in to consideration that the transonic wing has firstly a subsonic flow field which due to the gradients in the suction surface is followed by a supersonic flow field. If we take again a look at Fig. 6-11, we can see that the belly fairing may correlate o a subsonic-supersonic flow with transition to supersonic flow slightly downstream of the second section, at the thickest point. The belly fairing grows on the first subsonic region, then, where the supersonic region may be, shrinks, causing a further acceleration. An almost constant gradient is found where the shock is supposed to take

place, and finally the belly fairing shrinks under subsonic flow causing a flow deceleration.
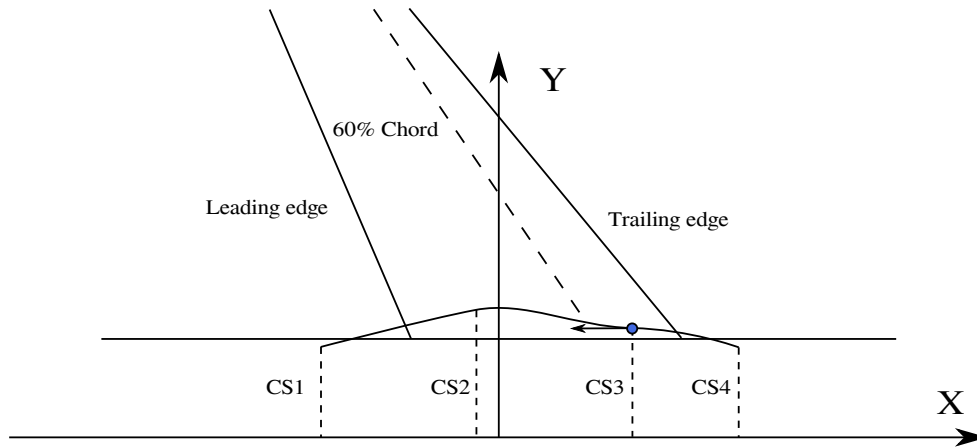
Figure 6-11 Sketch of the non expected geometries

Based in these findings, there is a new belly fairing methodology which may be worth to investigate. The main idea is based in the aforementioned phenomena, with a small difference. The basic concept is that the supersonic acceleration is slightly reduced from the original one, in this case represented by Fig. 6-11. This reduction should prevent the shock and second give some slack for off design performance. Then, a suddenly strong supersonic acceleration takes place where the shock position is desired to be, the strong acceleration may trigger the re-compression shock. A representation of this suggestion can be found in Fig. 6-12.
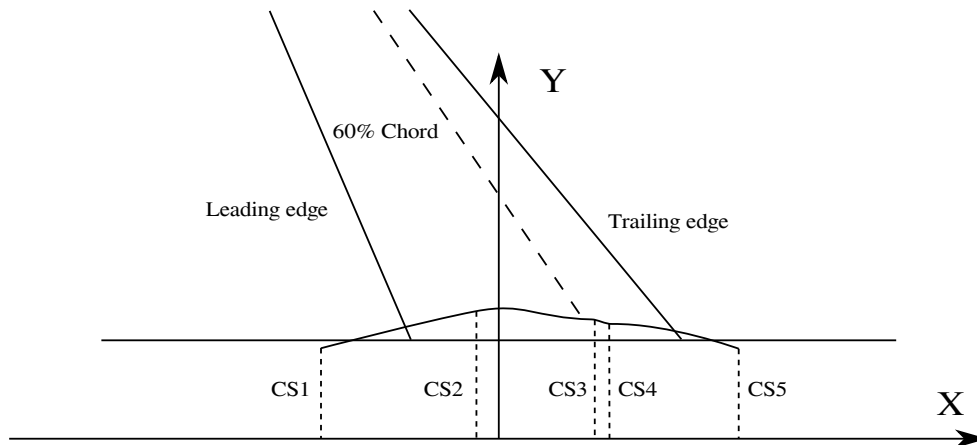
Figure 6-12 Sketch of the suggested geometry for the shock position control

The main purpose of this suggested methodology is not only to provide a method to control the shock position, but to profit of the main advantage of the belly fairing, the orientation towards the flow. Due to the normal position of the belly fairing to the angle of attack rotation axis, it can be expected that the effect of the angle of attack on the belly fairing gradients is lower than in the wings, therefore, if a shock 'onset point' is allocated in the belly fairing, it could be expected to 'lock' the shock position even for a limited off design operation.

It is worth to mention that the reduced suction gradient due to the shock onset point may affect to the lift produced.

Although this suggestion may sound attractive there has to be taken into account that the methodology is based in a five cross-section methodology. In order to properly assess the performance gains, a proper performance study of the four and five cross-section methodology has to be performed so that the suggested methodology can be properly compared.

6.3. Conclusions and future work

The main goal of the work was to assess the belly fairing impact in the aircraft's performance, generate a database of belly fairing geometries and to progress towards a best performing geometry. All these goals have been achieved and some additional ones such as the initial implementation of surrogate models or the turbulent analysis of the best geometries. Nevertheless there is still a lot of work to do towards not only the best performing geometries but towards the understanding of the real potential of a belly fairing. In this section will be discussed which tasks are still to be fulfilled towards a optimum belly fairing.

During the present work the complexity of the belly fairing generation has been constantly kept as low as possible. At this point, with the current methodology, a few surrogate model iterations are missing, in order to find the best geometry for the current simplifications. Nevertheless before further simulating the actual geometry, it should be considered to improve it, to reduce the number of failed geometries. Once the geometry has been improved, both the domain limits and the variables considered should be increased. During the first parameter study, it was found that the second cross-section had a huge impact in the performance and the third had less of an impact. This is of course because the chosen second cross-section led in combination with the chosen third cross section to a high performance plateau. A similar effect could be expected when exploring the first cross-section, as it has a direct contribution to the gradients between the first and the second cross-section.

Once the four cross-section belly fairing has been properly explored, there should be done the same with the five cross-section belly fairing, which could be expected to have performance advantages in the supersonic region. Additionally, when the performance of the five cross-section belly fairing has been assessed, both the five and the four cross section belly fairings should be compared, while considering as well the additional costs of the five cross-section belly fairing. It is important to investigate if the additional complexity pays off with an appropriate performance improvement.

Then, as the results have shown, there is still some work to do in the wing root of the actual configuration. Once it has been decided which belly fairing configuration is the best, the belly fairing should be explored all together with the profiles of the wing root. This would enable to achieve the very optimum performance.

Finally, the off-design performance should be assessed. At this point the available knowledge of the belly fairing should be good enough to design a multi-objective belly fairing, with not only good on-design performance but also off-design.

Bibliography

[1] G-EZBR easyJet Airbus A319-111. `https://commons.wikimedia.org/wiki/File:` `G-EZBR_easyJet_Airbus_A319-111_-_cn_3088_taxiing_14july2013.JPG,.` – Accessed: 2020-07-30

[2] ANTONY, J. : Design of experiments for engineers and scientists. Elsevier, 2014

[3] BEKEMEYER, P. : Internal report. (2019)

[4] BRASLOW, A. L.: A history of suction-type laminar-flow control with emphasis on flight research. NASA History Division, Office of Policy and Plans, NASA Headquarters, 1999 (13)

[5] CUMPSTY, N. ; HEAD, M. : The Calculation of Three-Dimensional Turbulent Boundary Layers: Part II: Attachment-Line Flow on an Infinite Swept Wing. In: The Aeronautical Quarterly 18 (1967), Nr. 2, S. 150–164

[6] FISCHER, M. C.: Spreading of a turbulent disturbance. In: AIAA journal 10 (1972), Nr. 7, S. 957–959

[7] HORSTMANN, K. ; REDEKER, G. ; QUAST, A. ; DRESSLER, U. ; BIELER, H. : Flight tests with a natural laminar flow glove on a transport aircraft. In: Flight Simulation Technologies Conference and Exhibit, 1990, S. 3044

[8] M. KRUSE, L. H. T. Wunderlich W. T. Wunderlich: A conceptual study of a transonic NLF transport aircraft with forward swept wings. In: 30th AAIA Applied Aerodynamics Conference, New Orleans, USA, 2012

[9] MCKAY, M. D. ; BECKMAN, R. J. ; CONOVER, W. J.: A comparison of three methods for selecting values of input variables in the analysis of output from a computer code. In: Technometrics 42 (2000), Nr. 1, S. 55–61

[10] MONNER, H. ; KINTSCHER, M. ; LORKOWSKI, T. ; STORM, S. : Design of a smart droop nose as leading edge high lift system for transportation aircrafts. In: 50th AIAA/ASME/ASCE/AHS/ASC Structures, Structural Dynamics, and Materials Conference 17th AIAA/ASME/AHS Adaptive Structures Conference 11th AIAA No, 2009, S. 2128

[11] OPERATIONS, A. : A320 Dimensions and Key Data. 2016

[12] PFENNINGER, W. : Some results from the x-21 program. part 1- flow phenomena at the leading edge of swept wings(X-21 aircraft program results- laminar and turbulent boundary layer flow phenomena at leading edge of swept wings). In: 1965. 47 P (1965)

[13] POLL, D. : Transition in the infinite swept attachment line boundary layer. In: The Aeronautical Quarterly 30 (1979), Nr. 4, S. 607–629

[14] REDEKER, G. ; HORSTMANN, K. ; KOESTER, H. ; THIEDE, P. ; SZODRUCH, J. : Design for a natural laminar flow glove for a transport aircraft. In: Flight Simulation Technologies Conference and Exhibit, 1990, S. 3043

[15] ROHNZHEIMER, A. : Internal report. (2017)

[16] RUNYAN, L. J. ; NAVRAN, B. H. ; ROZENDAAL, R. A.: F-111 natural laminar flow glove flight test data analysis and boundary layer stability analysis. (1984)

[17] RUNYAN, L. J. ; BIELAK, G. ; BEHBEHANI, R. ; CHEN, A. ; ROZENDAAL, R. A.: The 757 NLF glove flight test results. (1987)

[18] SEITZ, A. ; KRUSE, M. ; WUNDERLICH, T. ; BOLD, J. ; HEINRICH, L. : The DLR project LamAiR: design of a NLF forward swept wing for short and medium range transport application. In: 29th AIAA applied aerodynamics conference, 2011, S. 3526

[19] SEITZ, K. A. H. A. Hübner: The DLR TuLam Project-Design of a short and medium range transport aircraft with forward swept NLF wing. In: Journal of Turbomachinery 137 (2015), Nr. 2, S. 021001

[20] SONG, W. ; LV, P. : Two-level wing-body-fairing optimization of a civil transport aircraft. In: Journal of aircraft 48 (2011), Nr. 6, S. 2114–2121

[21] STREIT, T. ; HOFFROGGE, C. : DLR transonic inverse design code, extensions and modifications to increase versatility and robustness. In: The Aeronautical Journal 121 (2017), Nr. 1245, S. 1733–1757

[22] STRÜBER, H. ; WILD, J. : Aerodynamic design of a high-lift system compatible with a natural laminar flow wing within the DeSiReH project. In: 29th Congress of the International Council of the Aeronautical Sciences, St. Petersburg, 2014

[23] TORENBEEK, E. : Synthesis of subsonic airplane design: an introduction to the preliminary design of subsonic general aviation and transport aircraft, with emphasis on layout, aerodynamic design, propulsion and performance. Springer Science & Business Media, 2013

[24] WAGNER, R. D. ; MADDALON, D. V. ; BARTLETT, D. ; COLLIER JR, F. ; BRASLOW, A. : Laminar-flow flight experiments. (1989)

Register of illustrations

71

List of tables

A. Appendix

A.1. RG2 Aerodynamic postprocessing

RG2, $\alpha = 0.77$ deg, Ma = 0.78, $C_L = 0.5200$, $C_D = 0.02277$, $C_{DW} = 0.0018$, E = 22.8370, Reynolds number = 23.83 Millionen, Iterations Runed = 10000

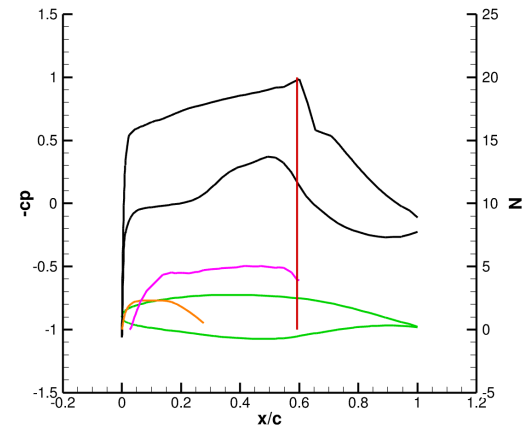(a) Schnitt 1, $\eta = 0{,}10988$

(b) Schnitt 2, $\eta = 0{,}12331$

(c) Schnitt 3, $\eta = 0{,}16332$

(d) Schnitt 4, $\eta = 0{,}2$
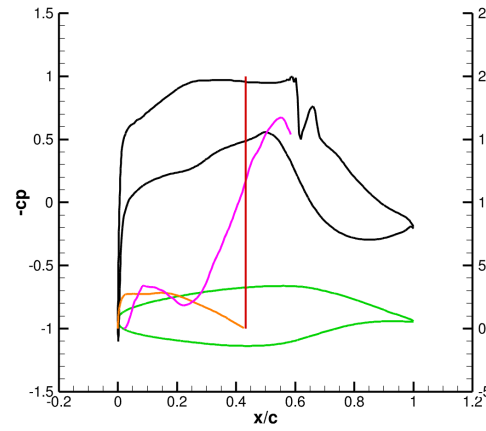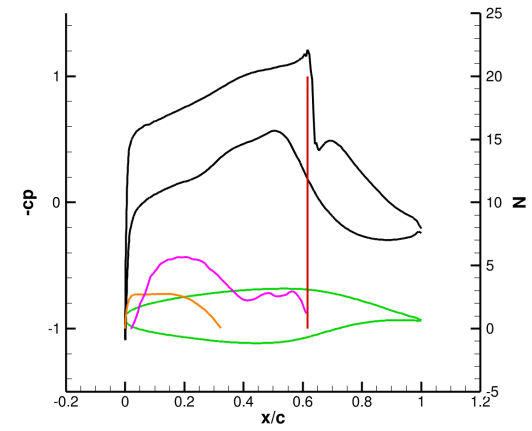
(e) Schnitt 5, $\eta = 0{,}24565$

(f) Schnitt 6, $\eta = 0{,}294$

(g) Schnitt 7, $\eta = 0{,}56$

Cp

Geometry

TS N Factors

CF N Factors

Transition

Strömung

(a) Isobar contours

(b) Laminar contour

(c) Cp verteilung

(a) C_{DW} distribution

(b) Local sweep

(c) f_{dw} distribution

(d) Shock position

(a) Residuals

A.2. Geo70 Aerodynamic postprocessing

Geo, $\alpha = 0.81$ deg, Ma = , $C_L = 0.5200$, $C_D = 0.02288$, $C_{DW} = 0.0023$, E = 22.7272, Reynolds number = Millionen, Iterations Runed = 10000
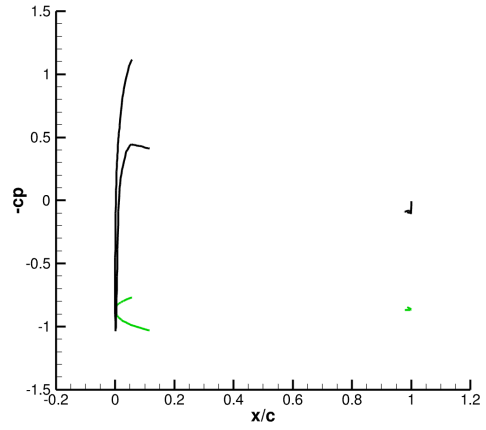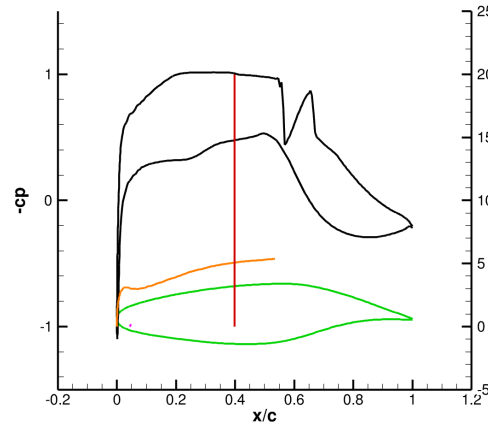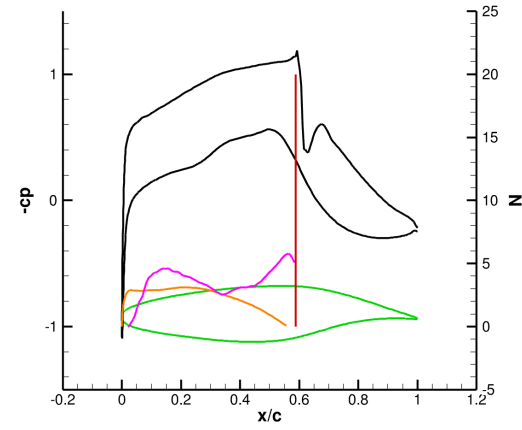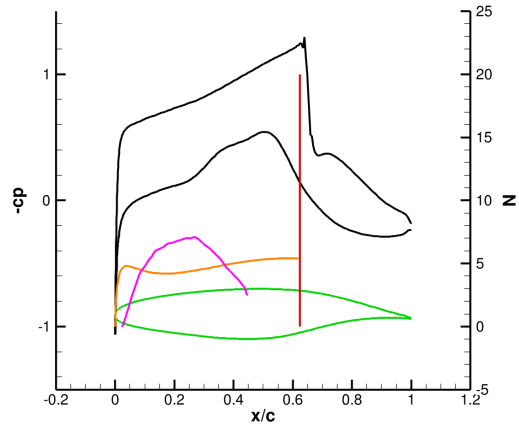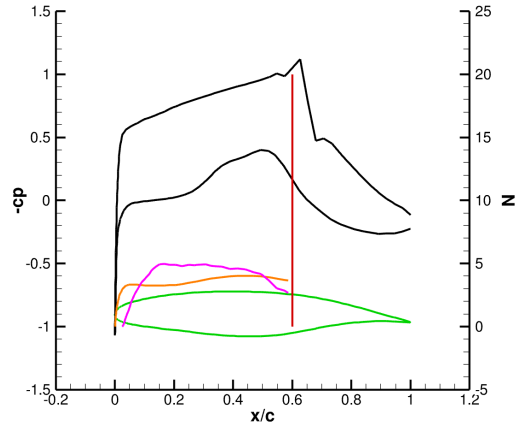

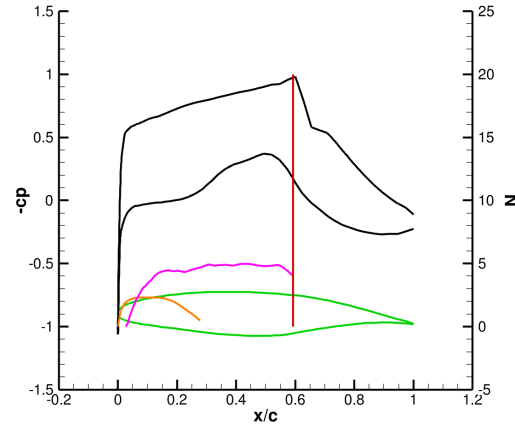(a) Schnitt 2, $\eta = 0{,}12331$

(b) Schnitt 3, $\eta = 0{,}16332$

(c) Schnitt 4, $\eta = 0{,}2$

(d) Schnitt 5, $\eta = 0{,}24565$

(e) Schnitt 6, $\eta = 0{,}294$

(f) Schnitt 7, $\eta = 0{,}56$

Cp

Geometry

TS N Factors

CF N Factors

Transition

Strömung →

(a) Isobar contours

(b) Laminar contour

(c) Cp verteilung

Y

X

cp

0
-0.06
-0.12
-0.18
-0.24
-0.3
-0.36
-0.42
-0.48
-0.54
-0.6
-0.66
-0.72
-0.78
-0.84
-0.9
-0.96
-1.02
-1.08
-1.14
-1.2
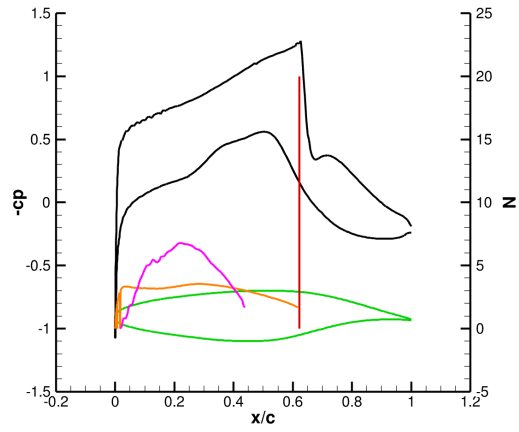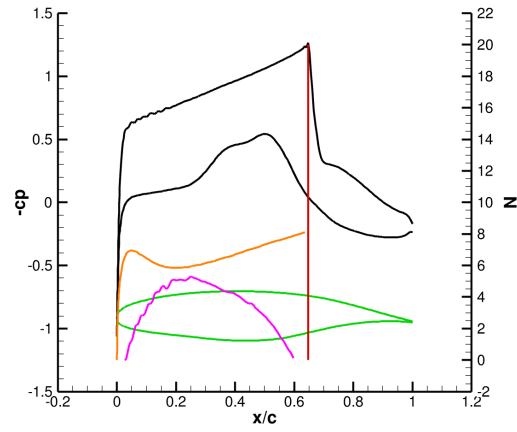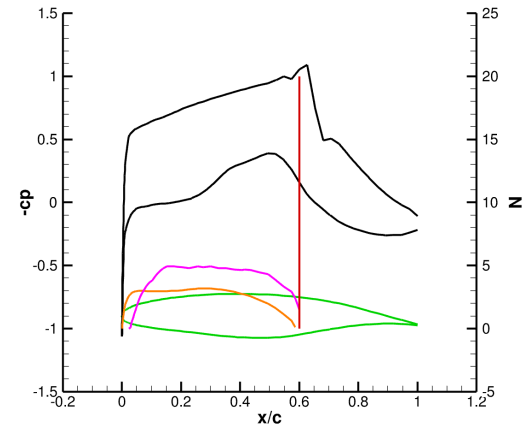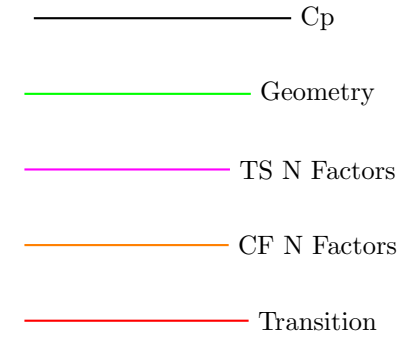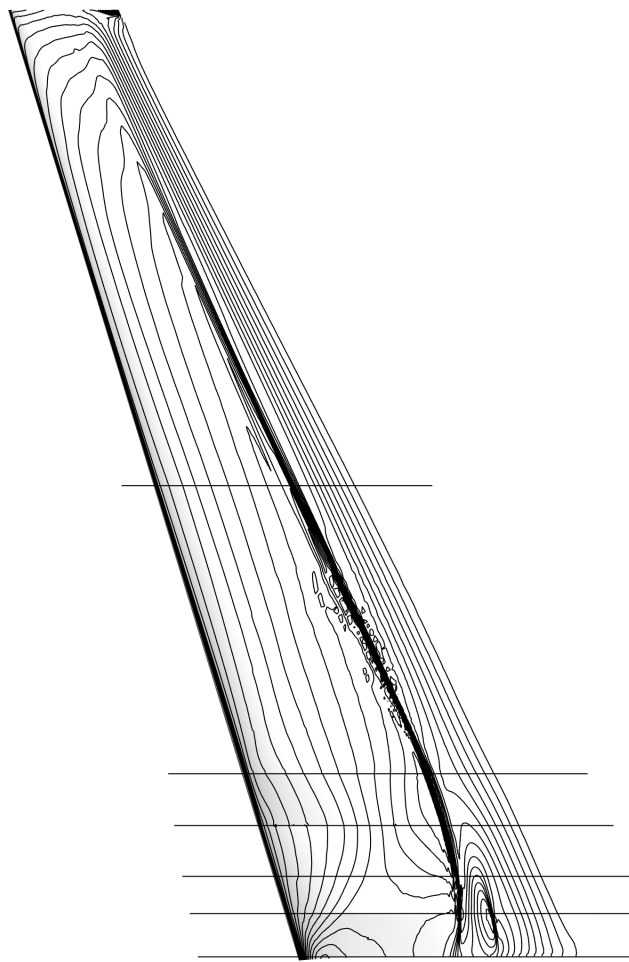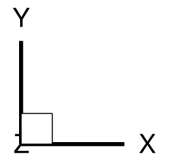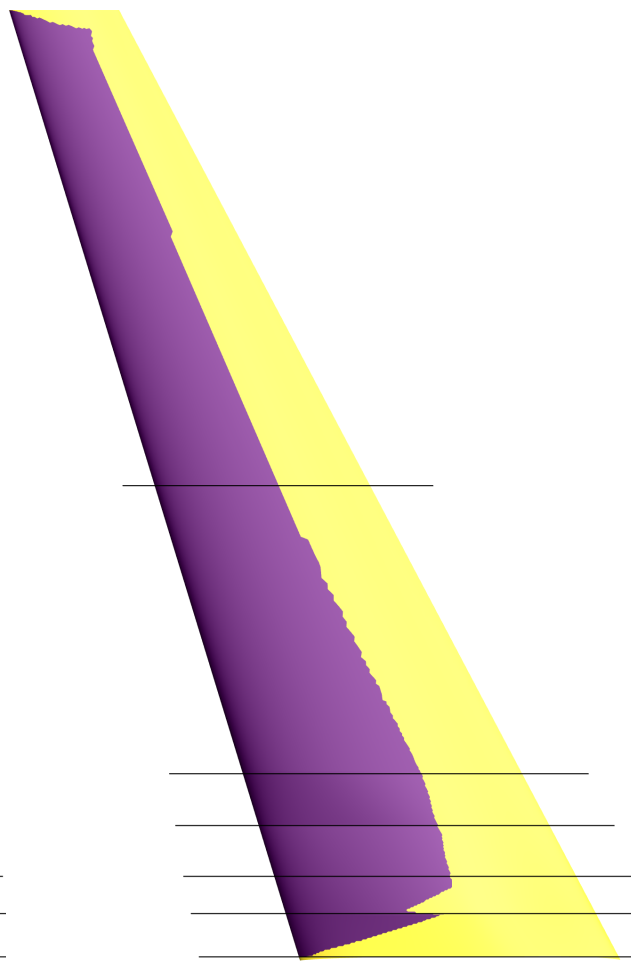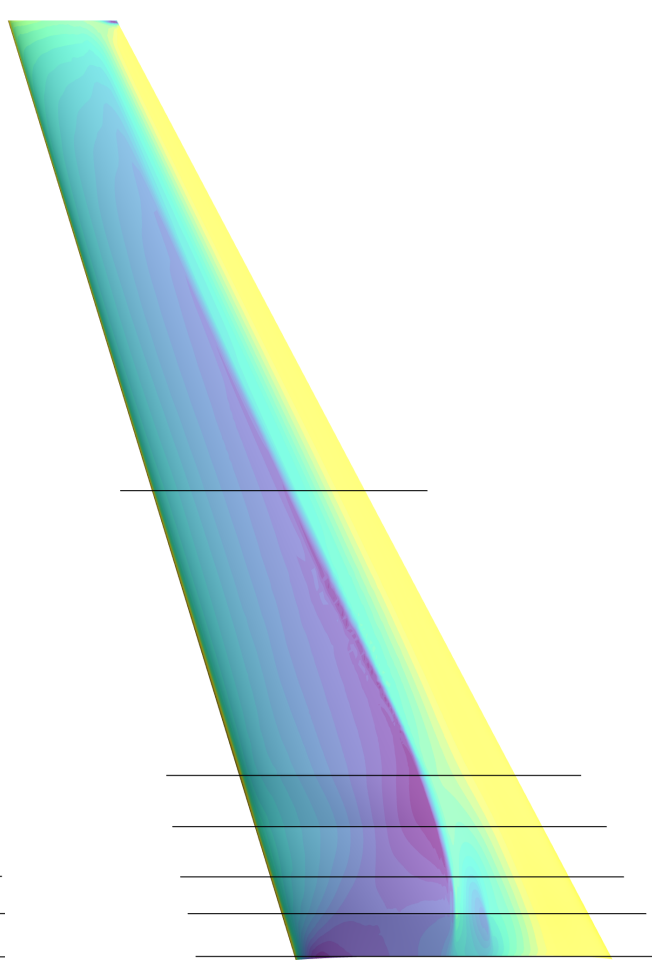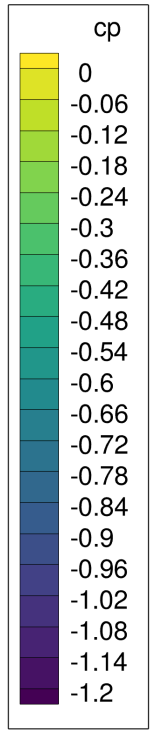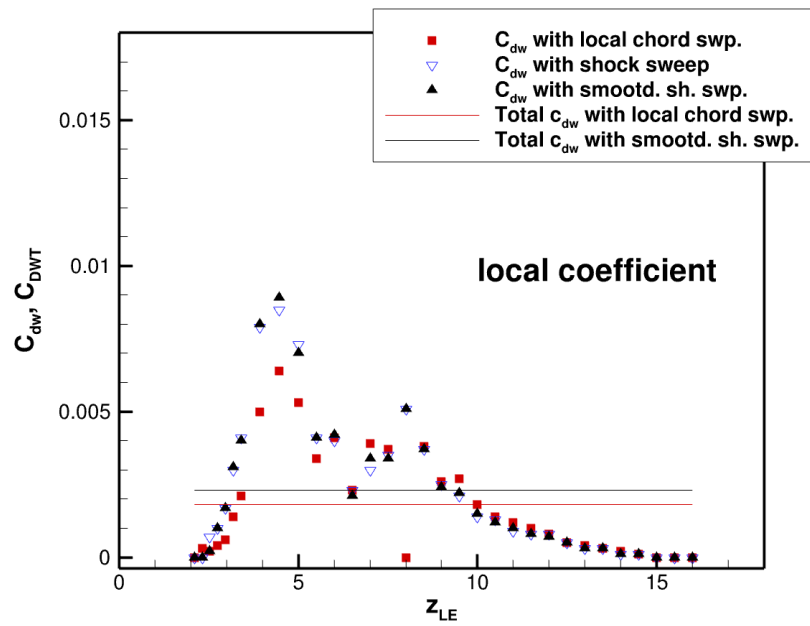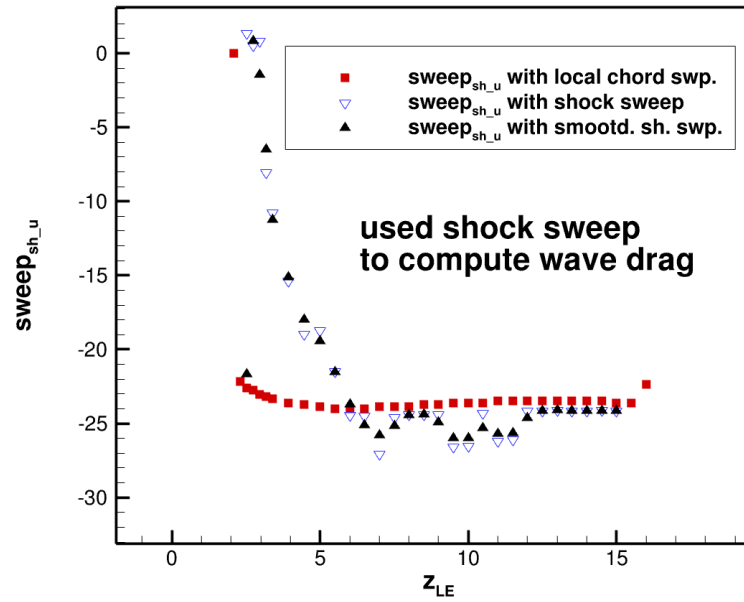
(a) C_{DW} distribution

(b) Local sweep
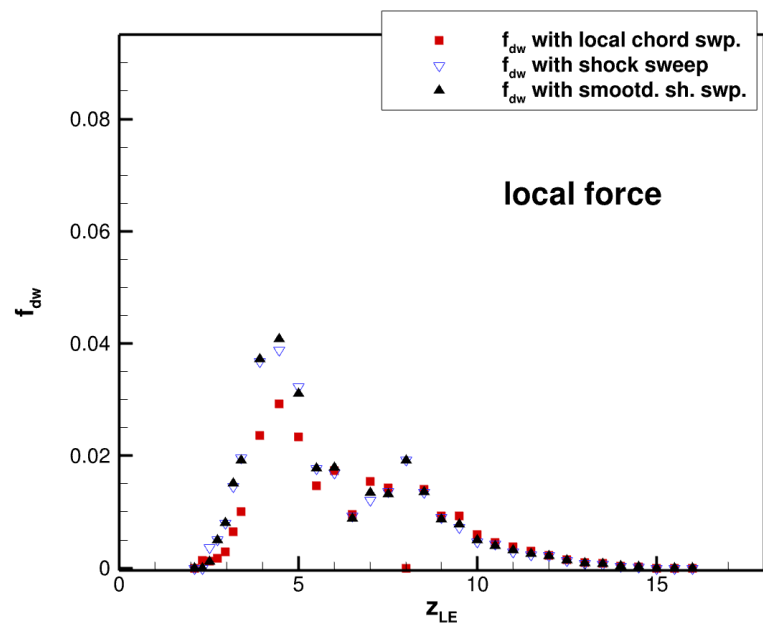
(c) f_{dw} distribution
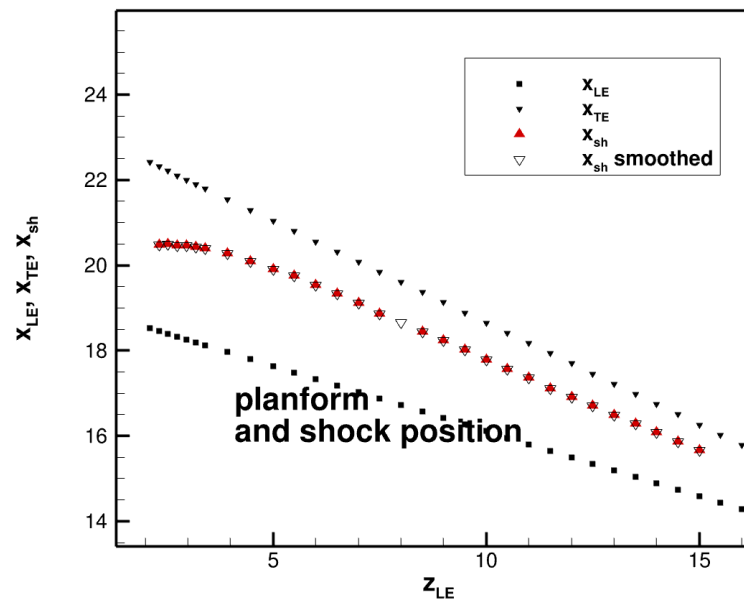
(d) Shock position
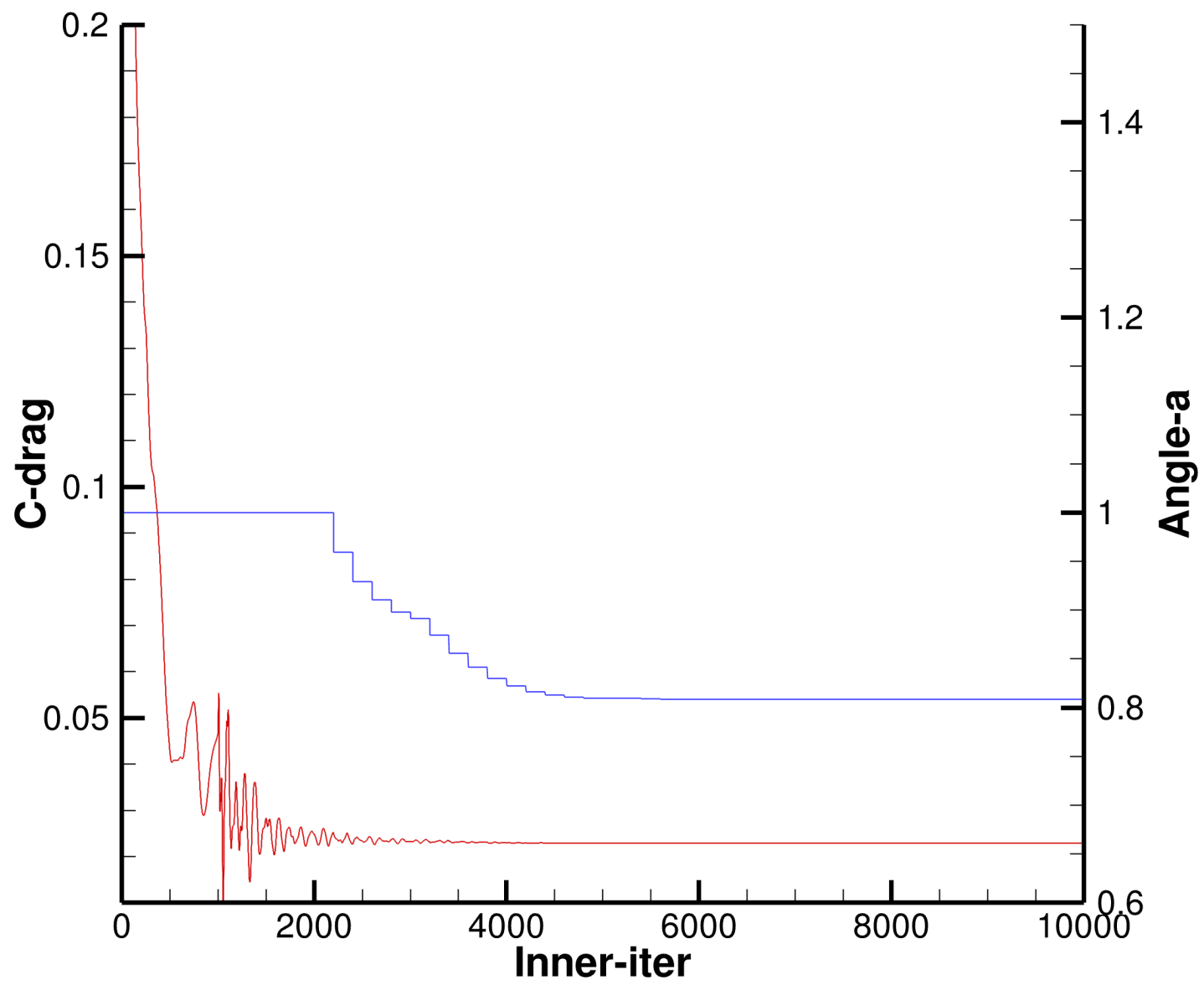
(a) Residuals

A.3. Geo267 Aerodynamic postprocessing

Geo, $\alpha = 0.75$ deg, Ma = , $C_L = 0.5201$, $C_D = 0.02260$, $C_{DW} = 0.0018$, E = 23.0132, Reynolds number = Millionen, Iterations Runed = 10000
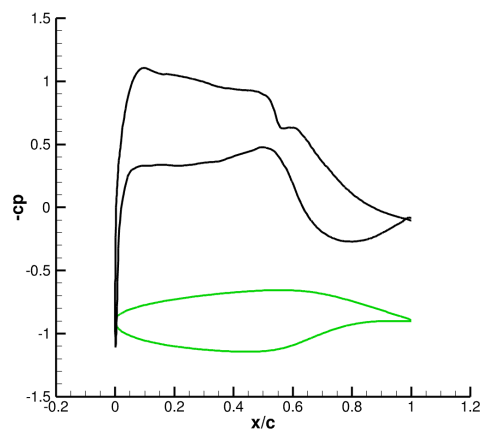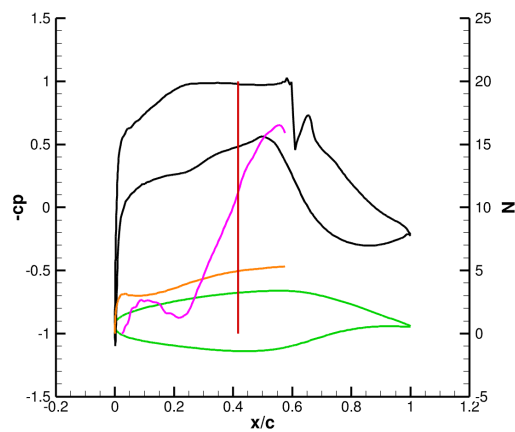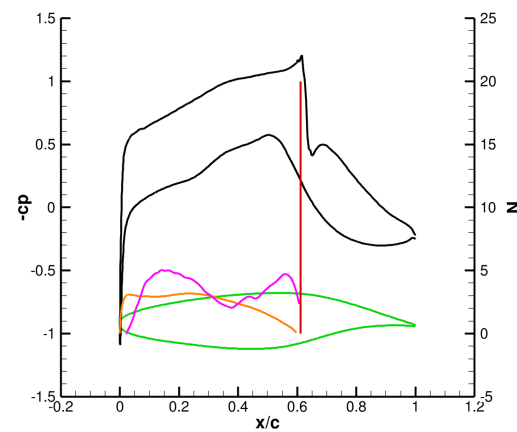
(a) Schnitt 2, $\eta = 0{,}12331$

(b) Schnitt 3, $\eta = 0{,}16332$

(c) Schnitt 4, $\eta = 0{,}2$

(d) Schnitt 5, $\eta = 0{,}24565$

(e) Schnitt 6, $\eta = 0{,}294$

(f) Schnitt 7, $\eta = 0{,}56$

Cp

Geometry

TS N Factors

CF N Factors

Transition

Strömung →

(a) Isobar contours

(b) Laminar contour

(c) Cp verteilung

cp

| 0 |
| -0.06 |
| -0.12 |
| -0.18 |
| -0.24 |
| -0.3 |
| -0.36 |
| -0.42 |
| -0.48 |
| -0.54 |
| -0.6 |
| -0.66 |
| -0.72 |
| -0.78 |
| -0.84 |
| -0.9 |
| -0.96 |
| -1.02 |
| -1.08 |
| -1.14 |
| -1.2 |
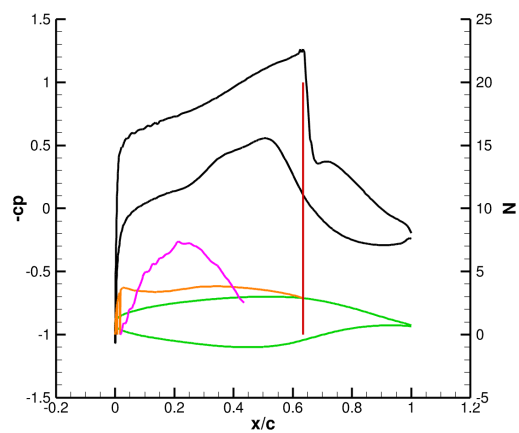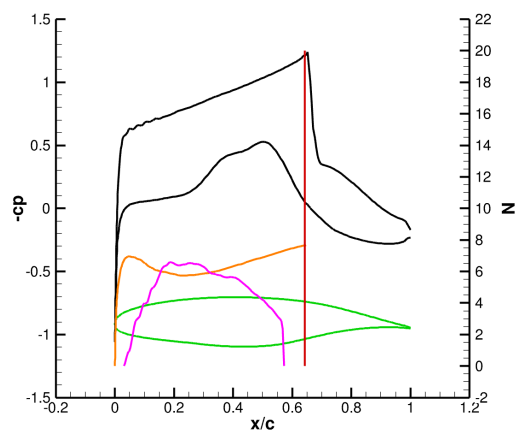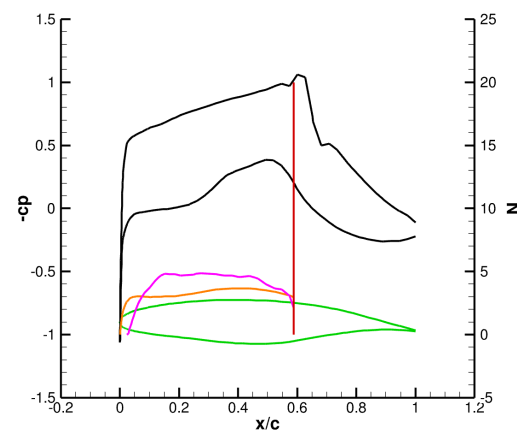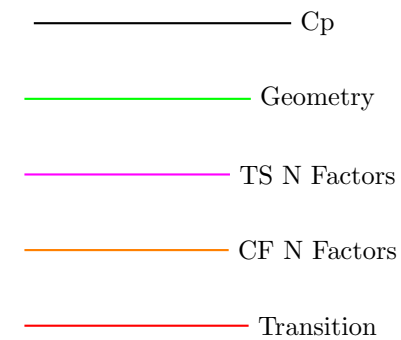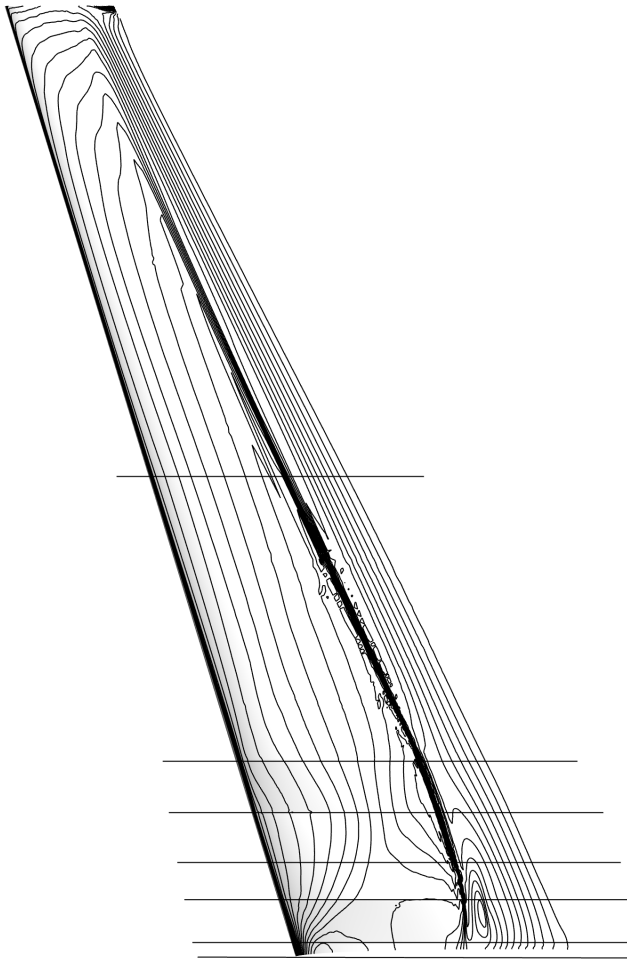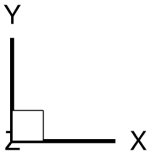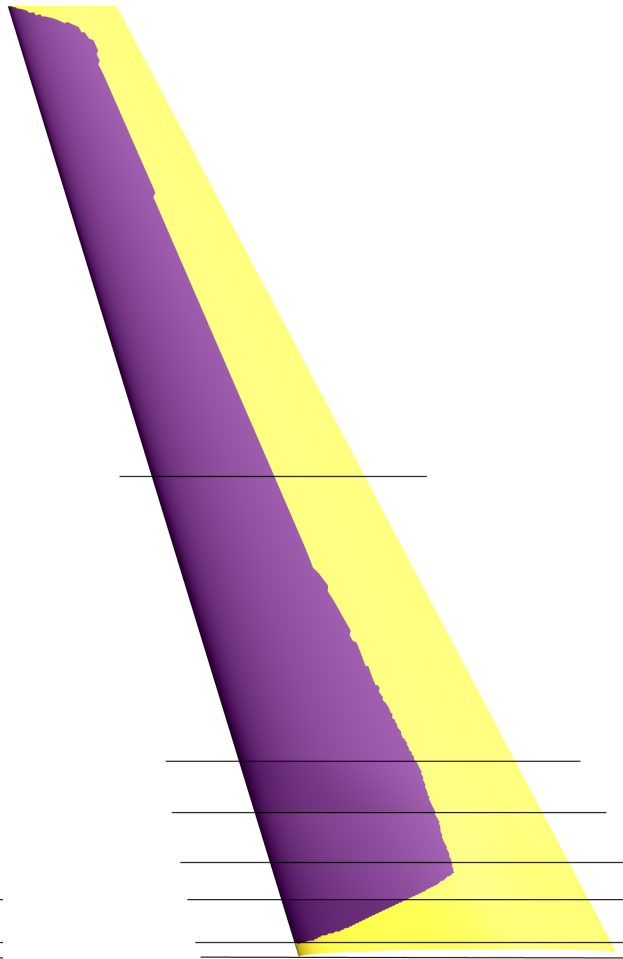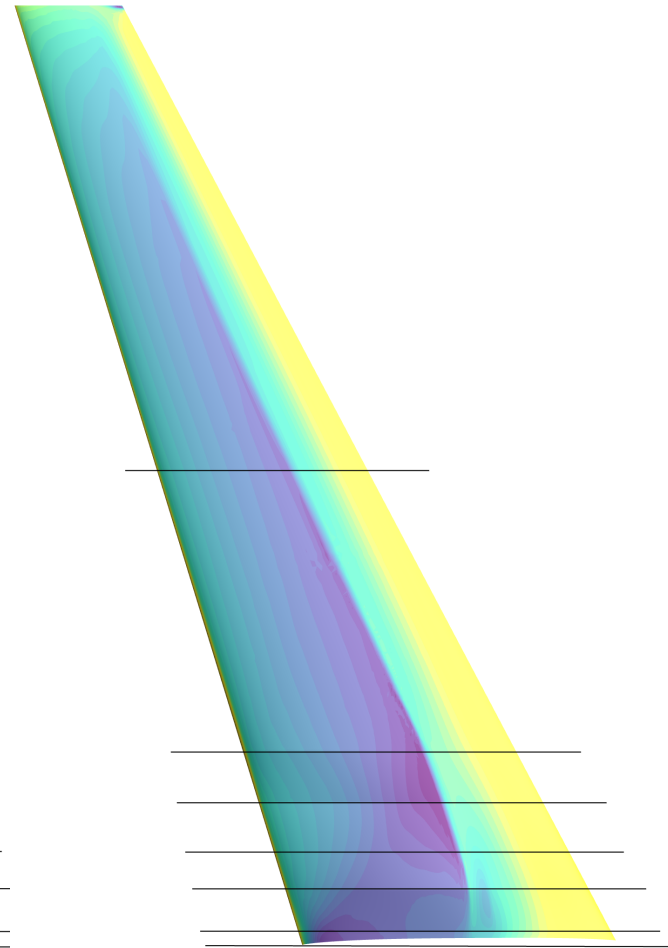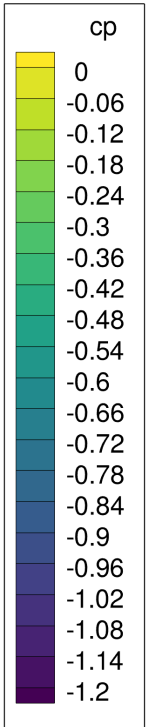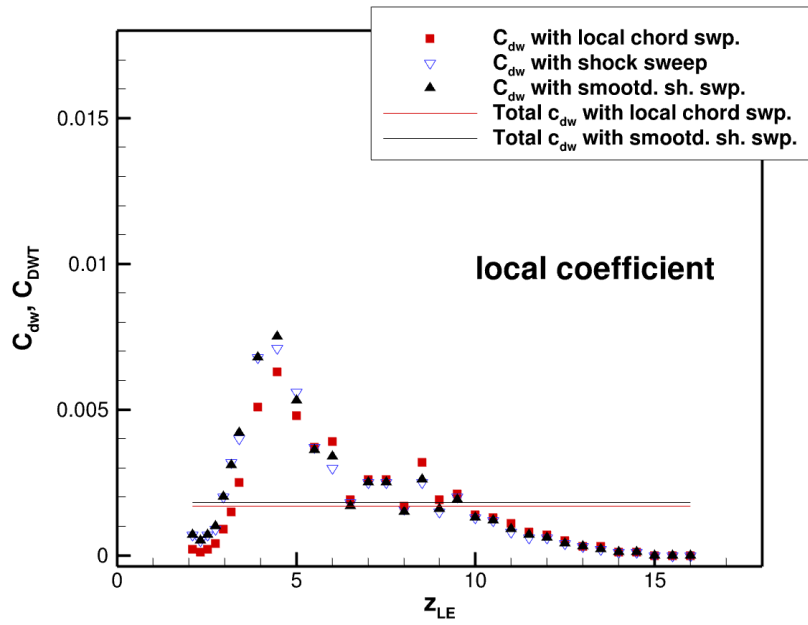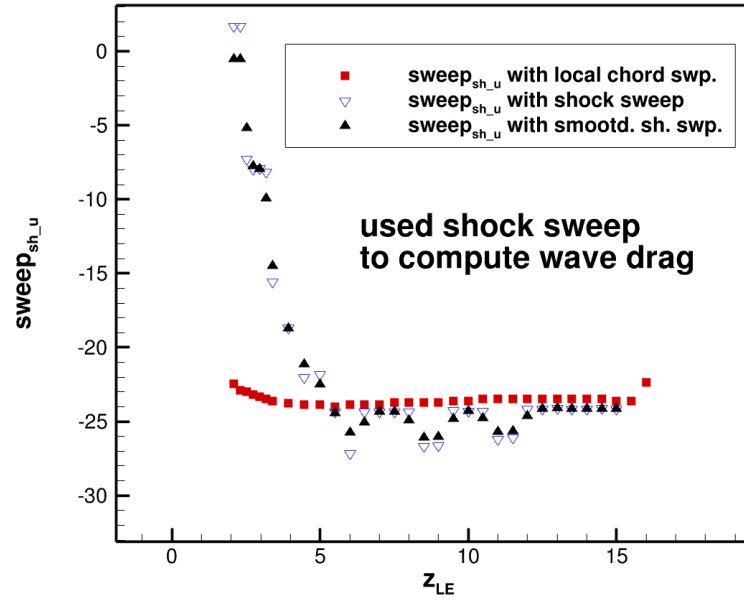
(a) C_{DW} distribution

(b) Local sweep
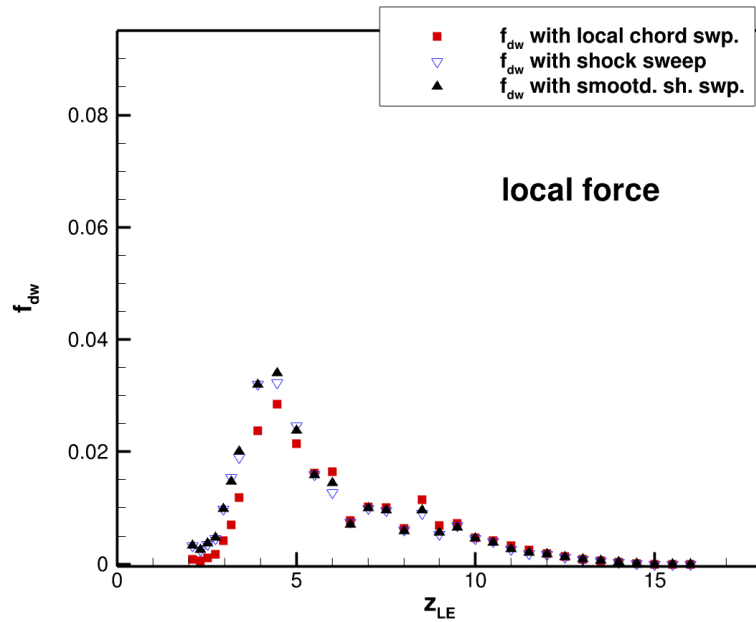
(c) f_{dw} distribution
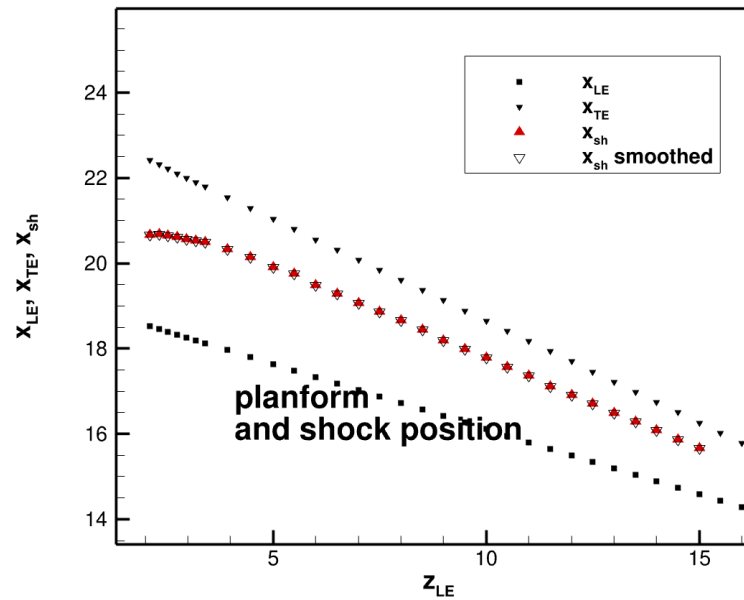
(d) Shock position
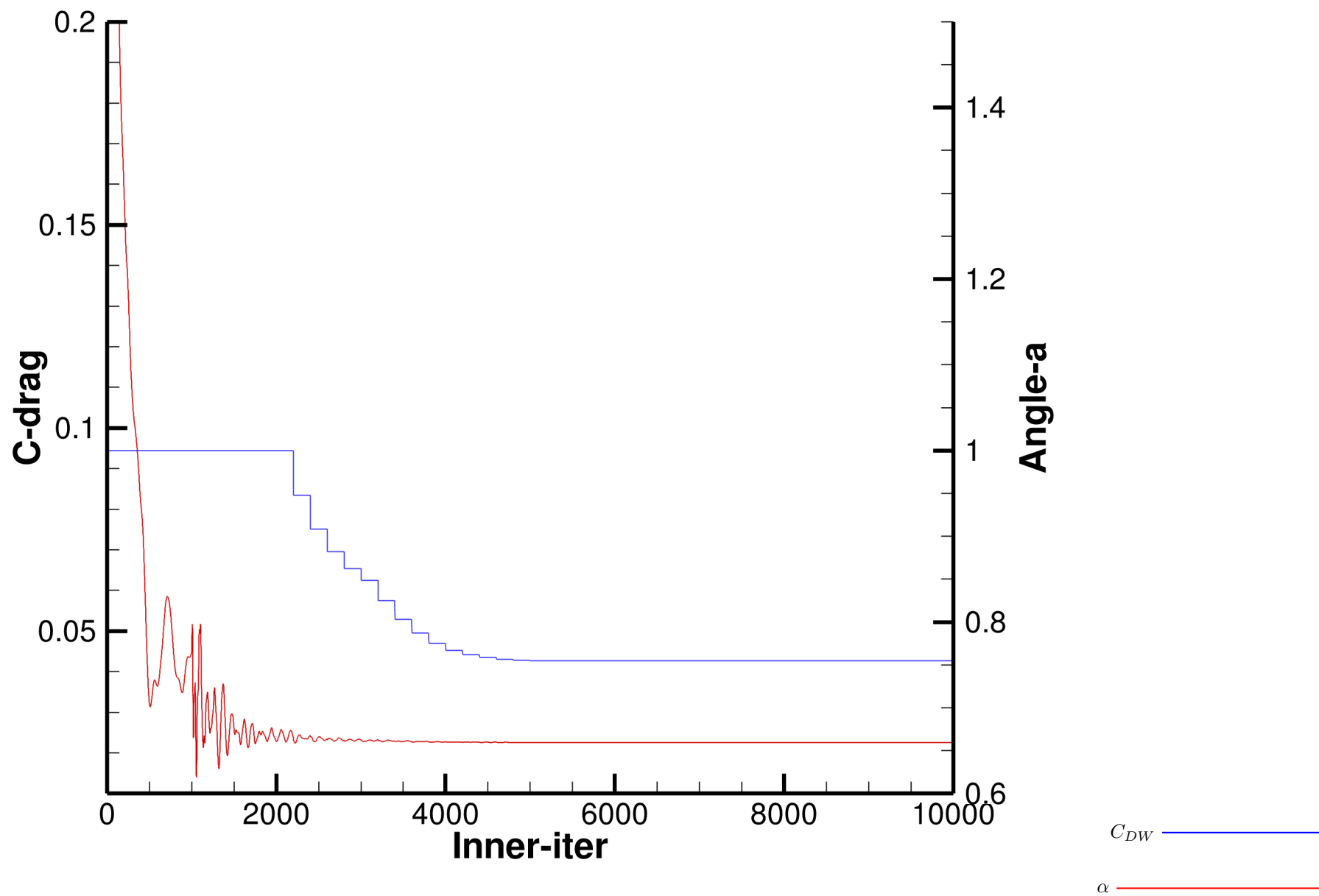
(a) Residuals

A.4. Geo294 Aerodynamic postprocessing

Geo, $\alpha = 0.76$ deg, Ma = , $C_L = 0.5199$, $C_D = 0.02264$, $C_{DW} = 0.0026$, E = 22.9637, Reynolds number = Millionen, Iterations Runed = 10000
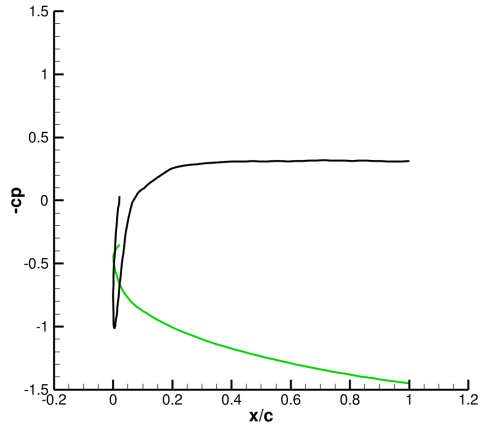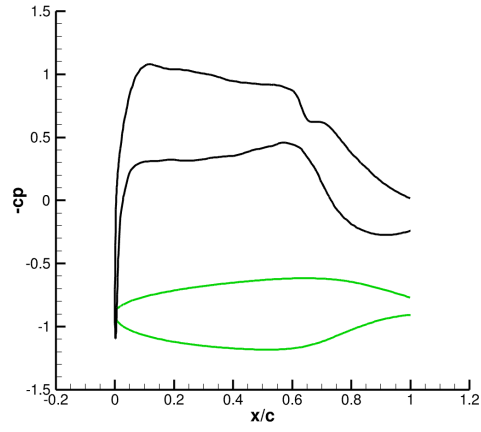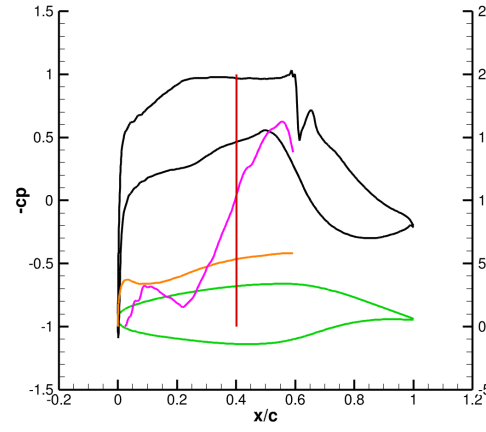
(a) Schnitt 1, $\eta = 0{,}10988$

(b) Schnitt 2, $\eta = 0{,}12331$

(c) Schnitt 3, $\eta = 0{,}16332$

(d) Schnitt 4, $\eta = 0{,}2$

(e) Schnitt 5, $\eta = 0{,}24565$

(f) Schnitt 6, $\eta = 0{,}294$

(g) Schnitt 7, $\eta = 0{,}56$

Cp

Geometry

TS N Factors

CF N Factors

Transition

**Strömung** →

(a) Isobar contours

(b) Laminar contour

(c) Cp verteilung

cp
0
-0.06
-0.12
-0.18
-0.24
-0.3
-0.36
-0.42
-0.48
-0.54
-0.6
-0.66
-0.72
-0.78
-0.84
-0.9
-0.96
-1.02
-1.08
-1.14
-1.2
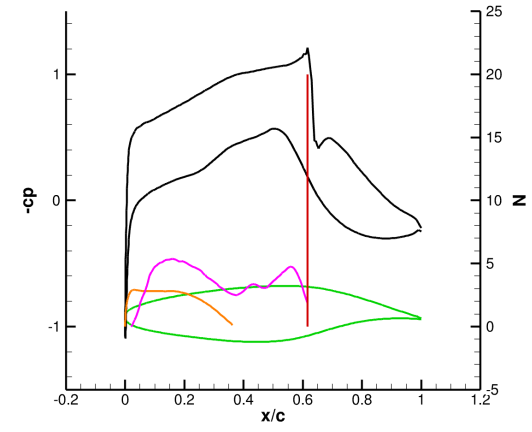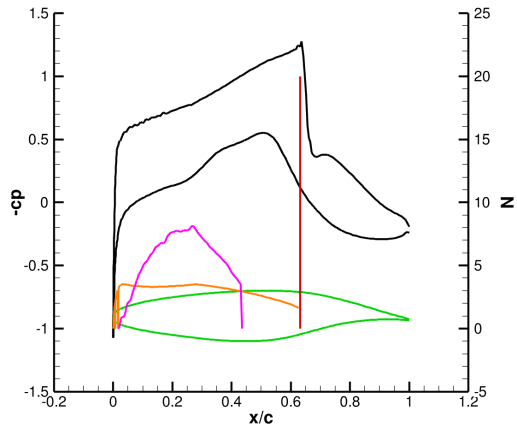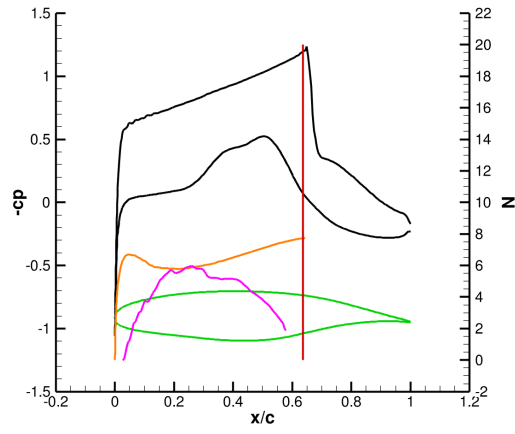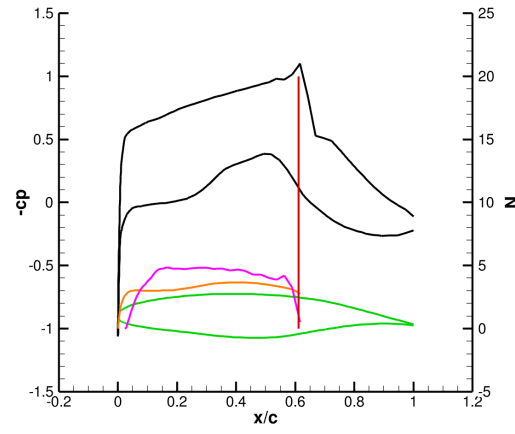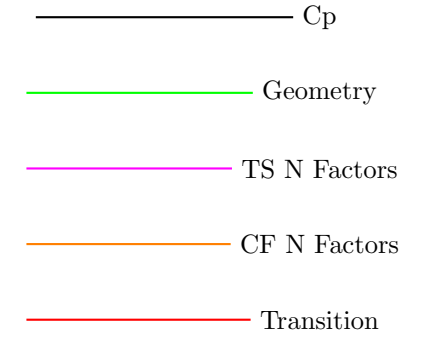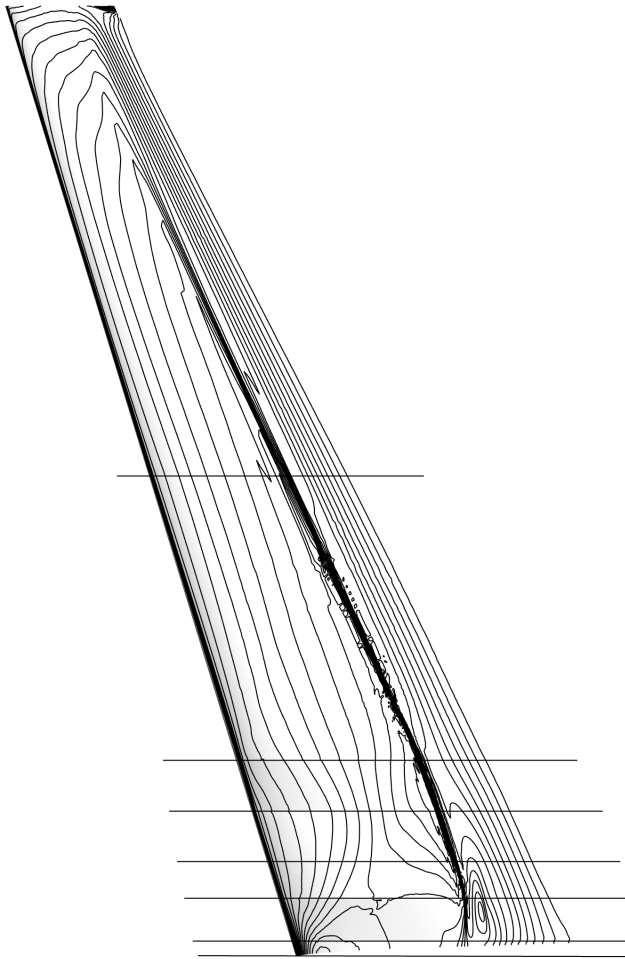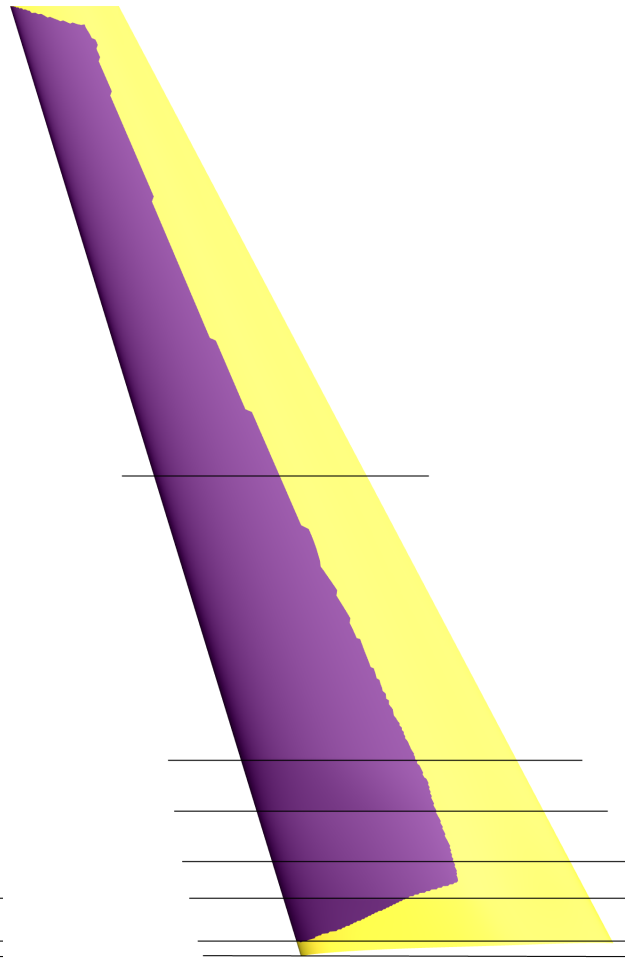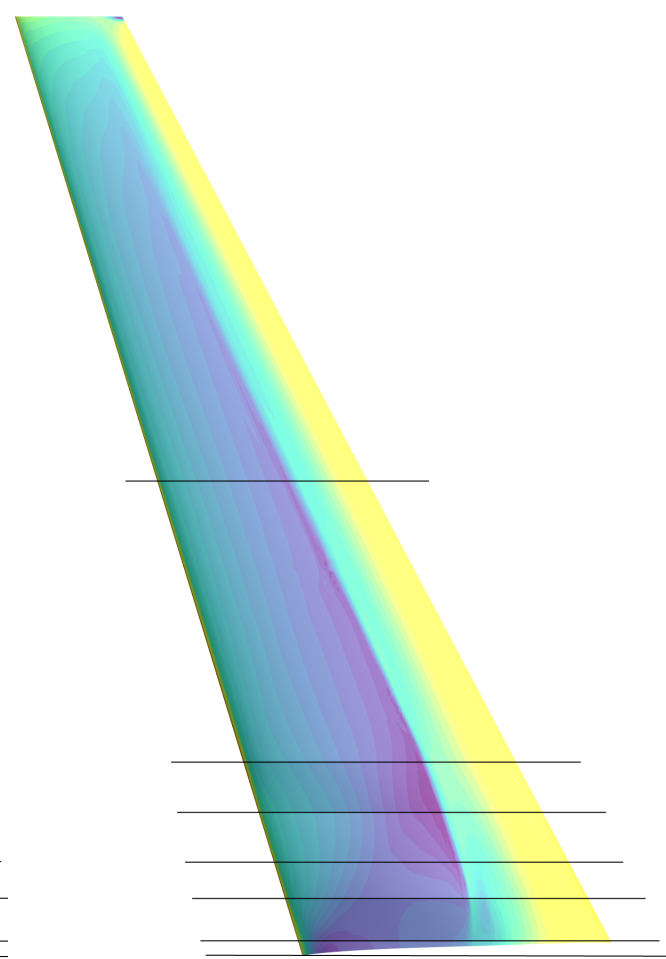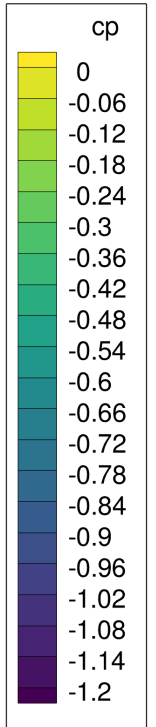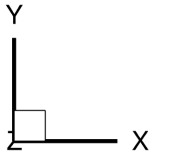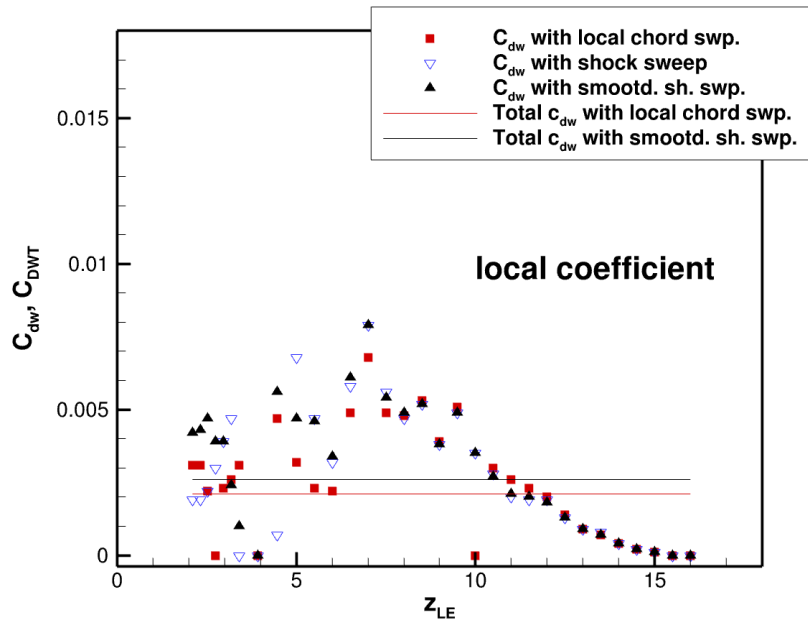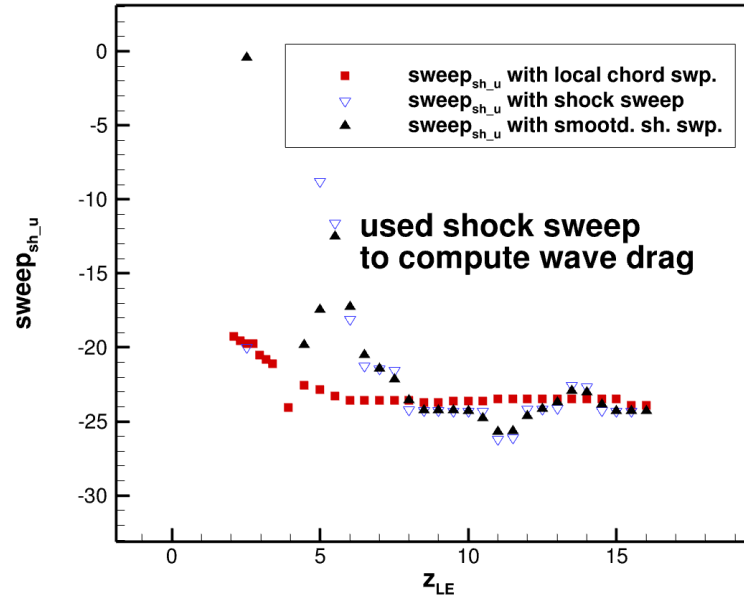
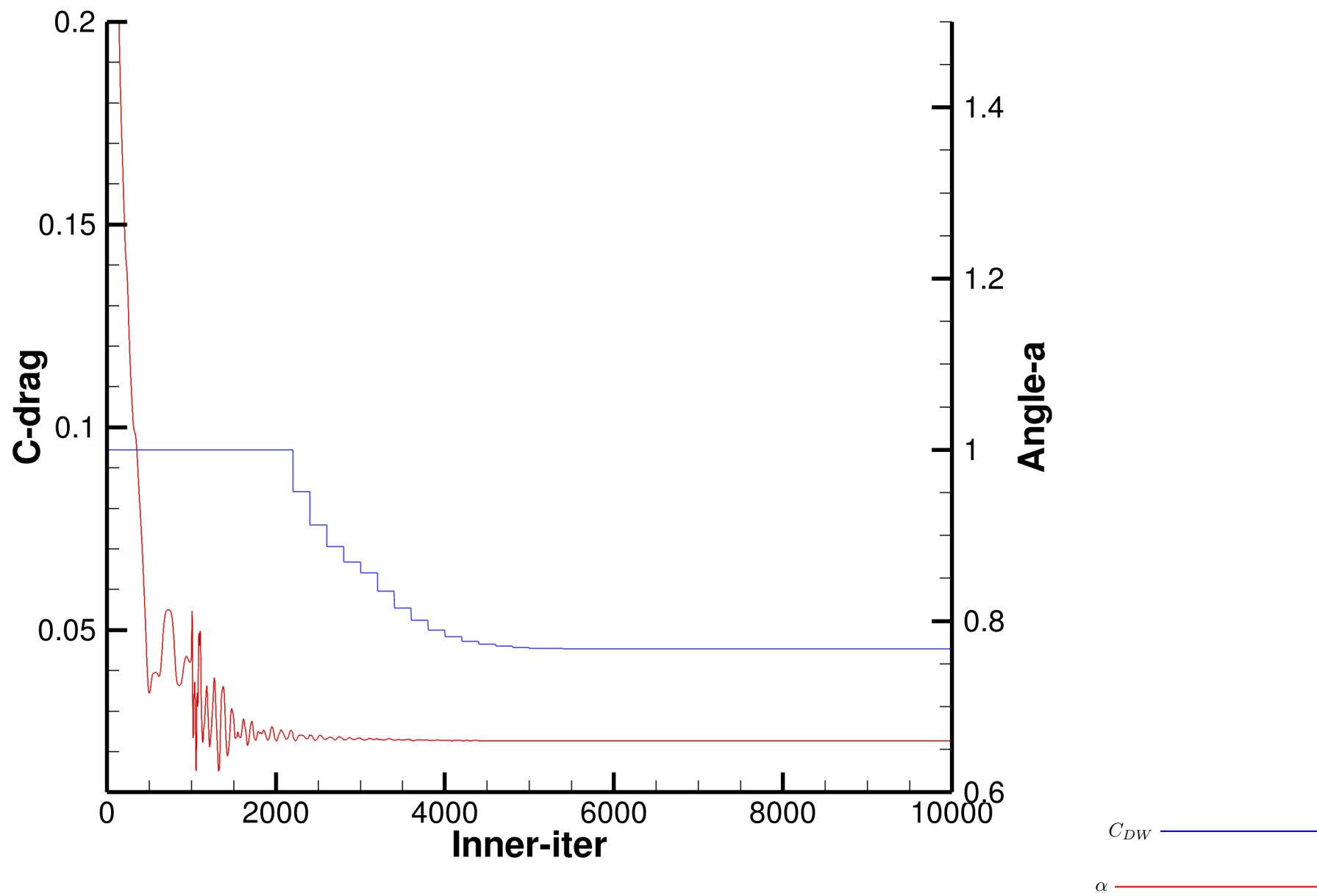(a) C_{DW} distribution

(b) Local sweep
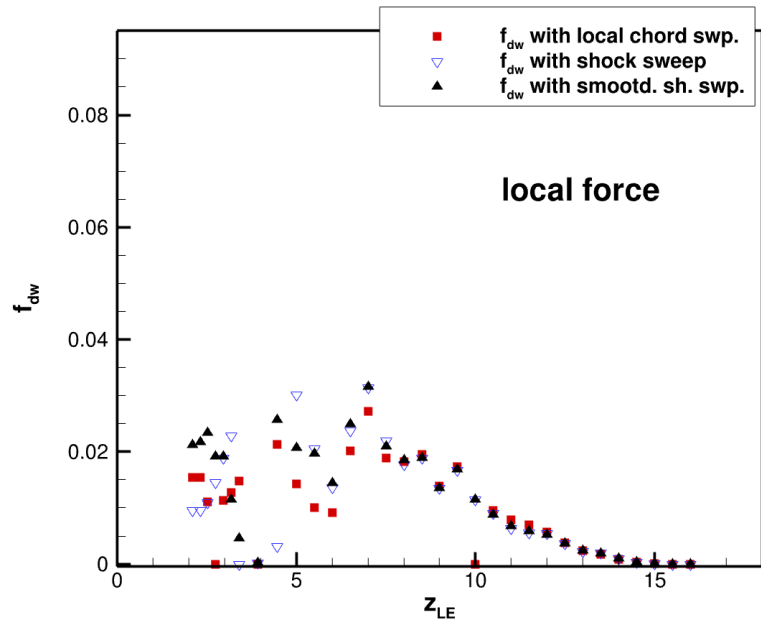
(c) f_{dw} distribution
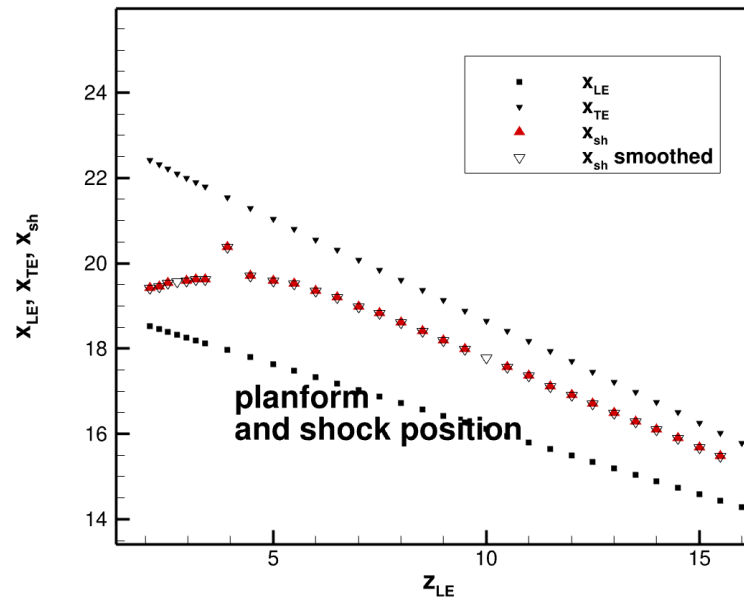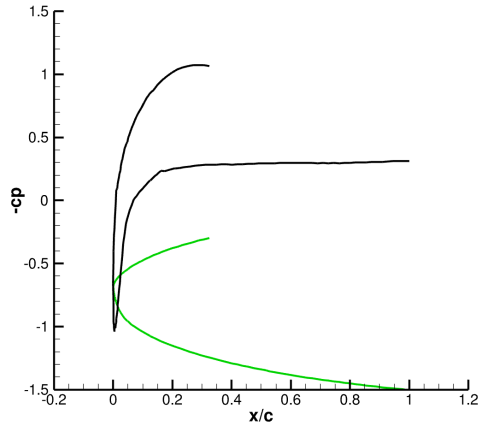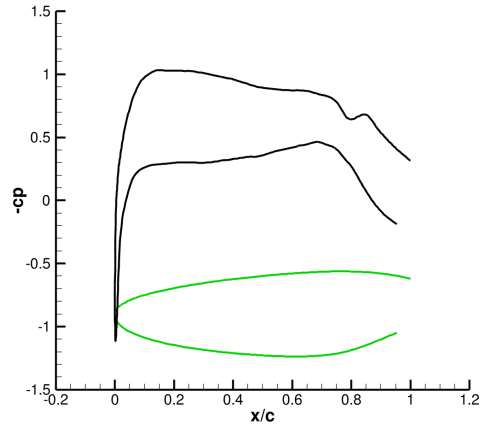
(d) Shock position
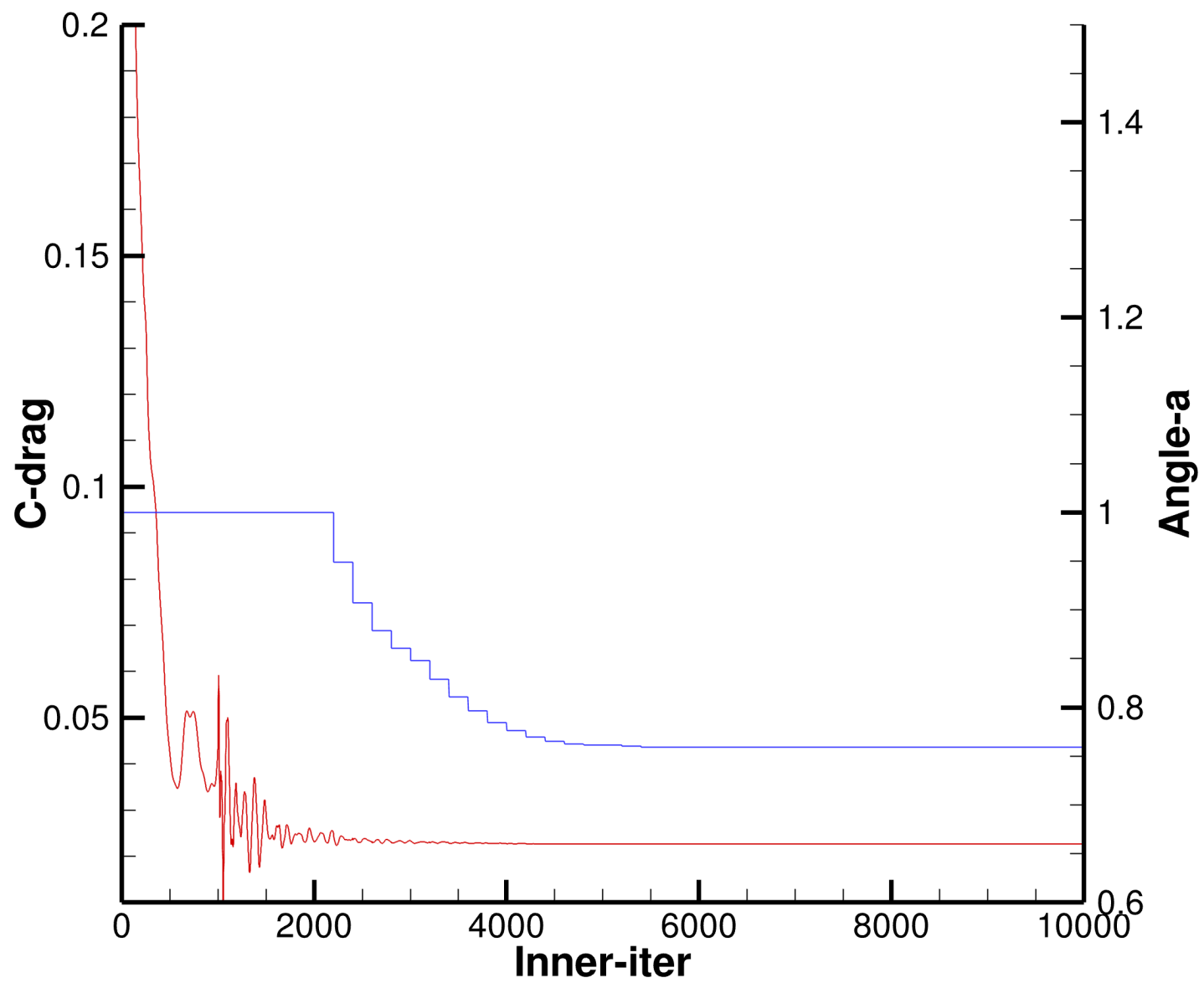
(a) Residuals

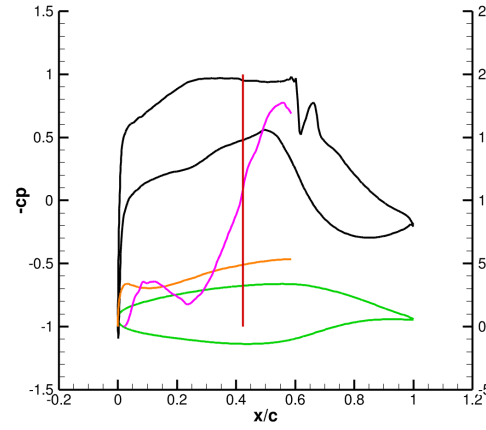## A.5. Geo301 Aerodynamic postprocessing

Geo, $\alpha = 0.78$ deg, Ma $=$, $C_L = 0.5199$, $C_D = 0.02269$, $C_{DW} = 0.0017$, E $= 22.9131$, Reynolds number $=$ Millionen, Iterations Runed $= 10000$
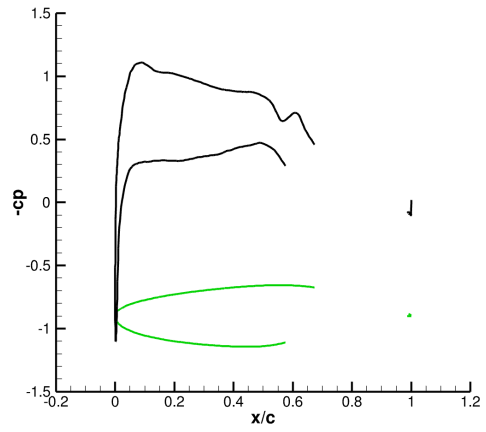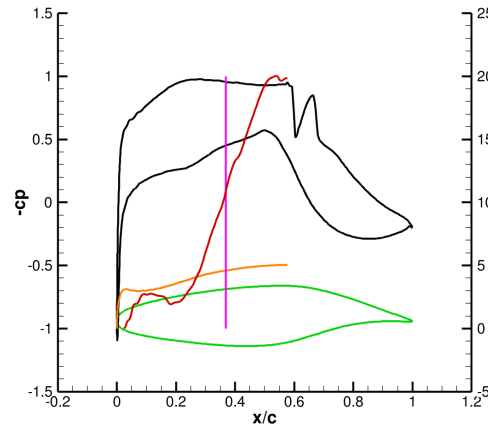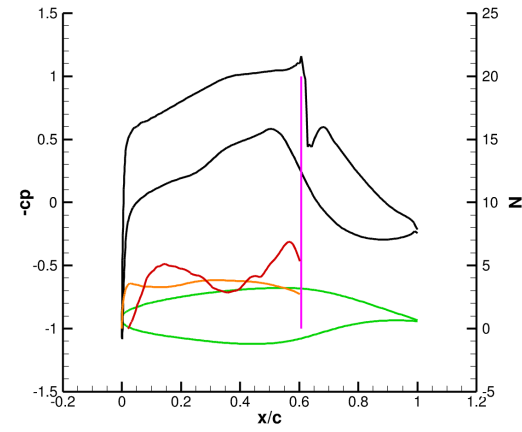
(a) Schnitt 2, $\eta = 0{,}12331$

(b) Schnitt 3, $\eta = 0{,}16332$

(c) Schnitt 4, $\eta = 0{,}2$

(d) Schnitt 5, $\eta = 0{,}24565$

(e) Schnitt 6, $\eta = 0{,}294$

(f) Schnitt 7, $\eta = 0{,}56$

Cp

Geometry

TS N Factors

CF N Factors

Transition
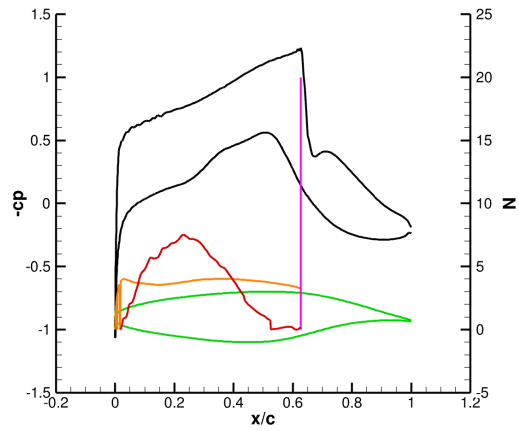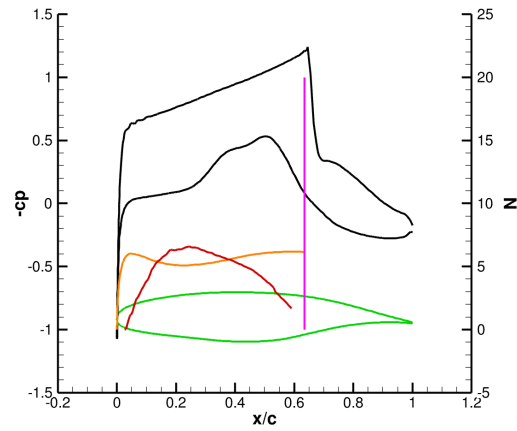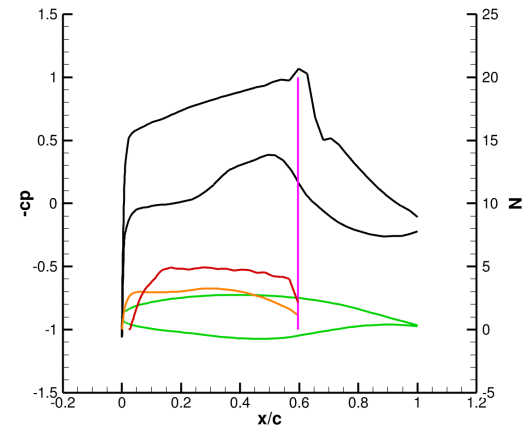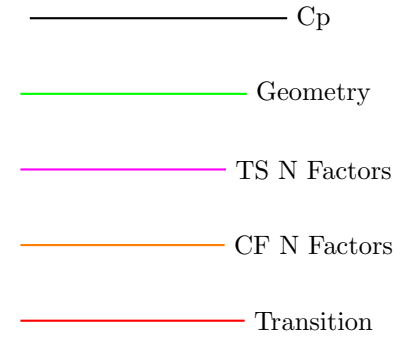
Strömung
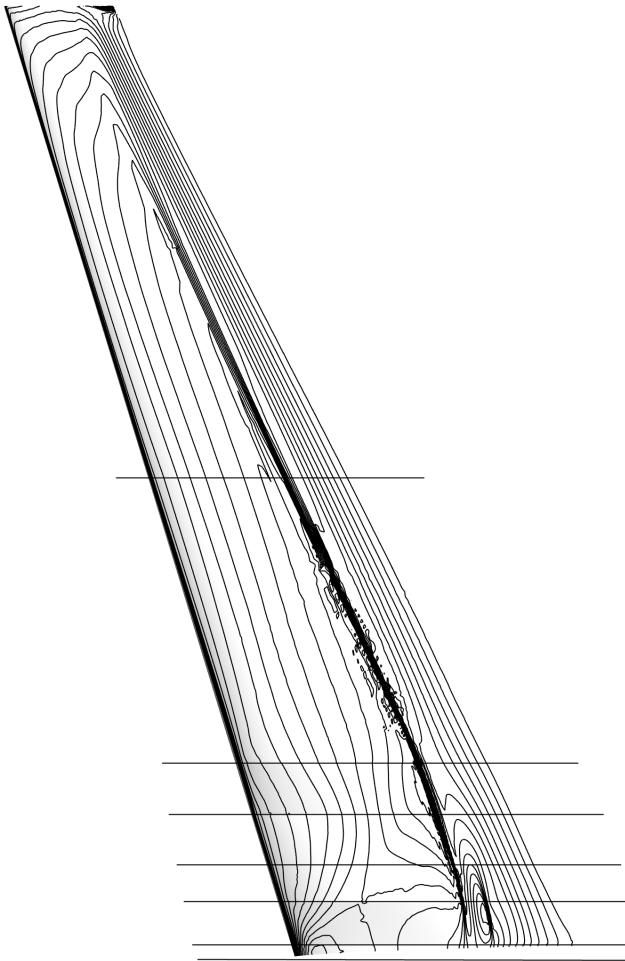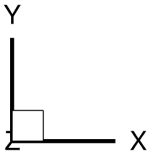
(a) Isobar contours
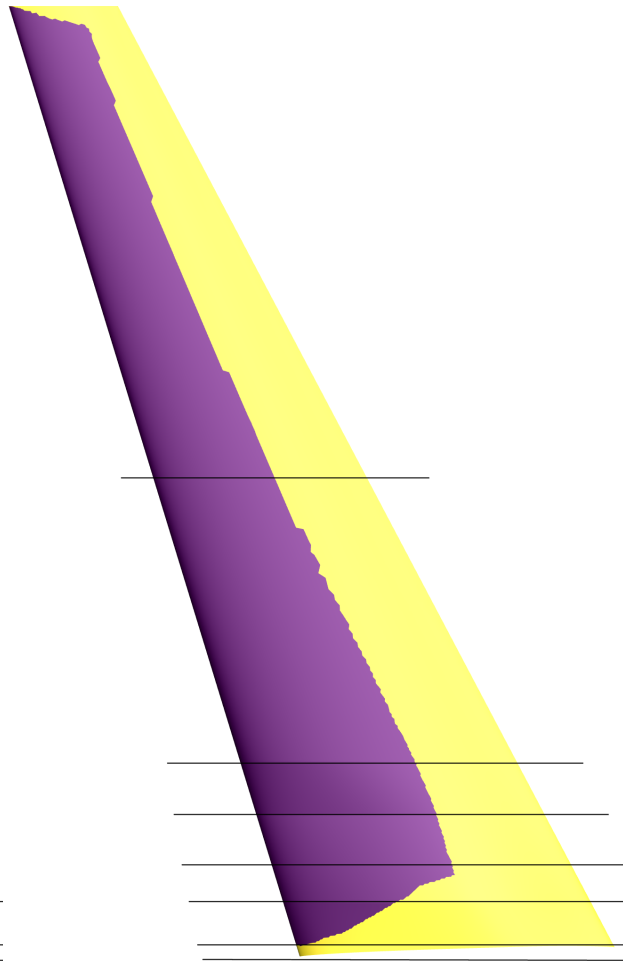
(b) Laminar contour
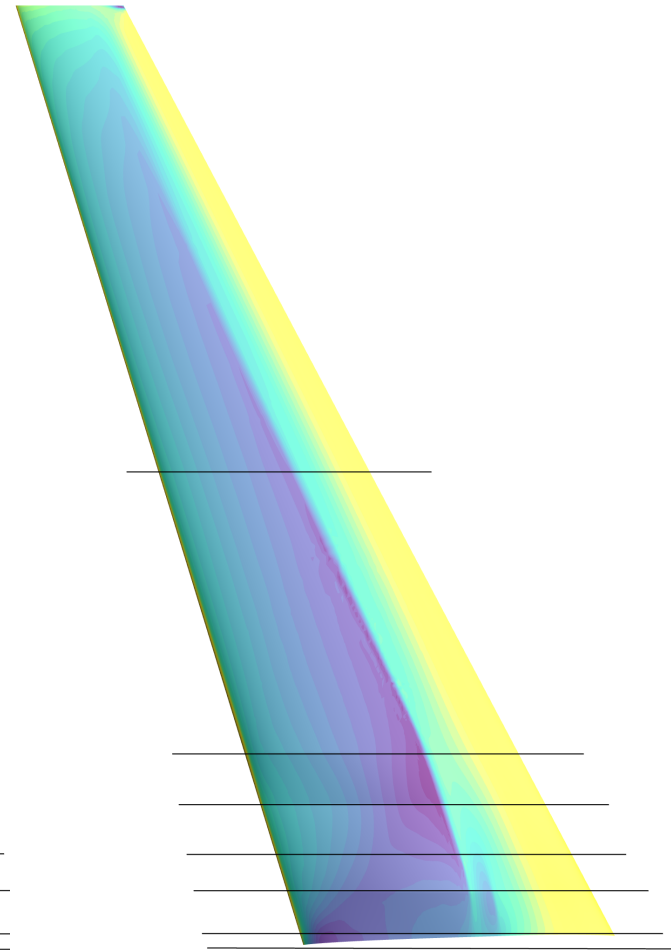
(c) Cp verteilung
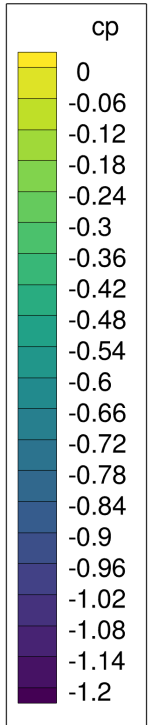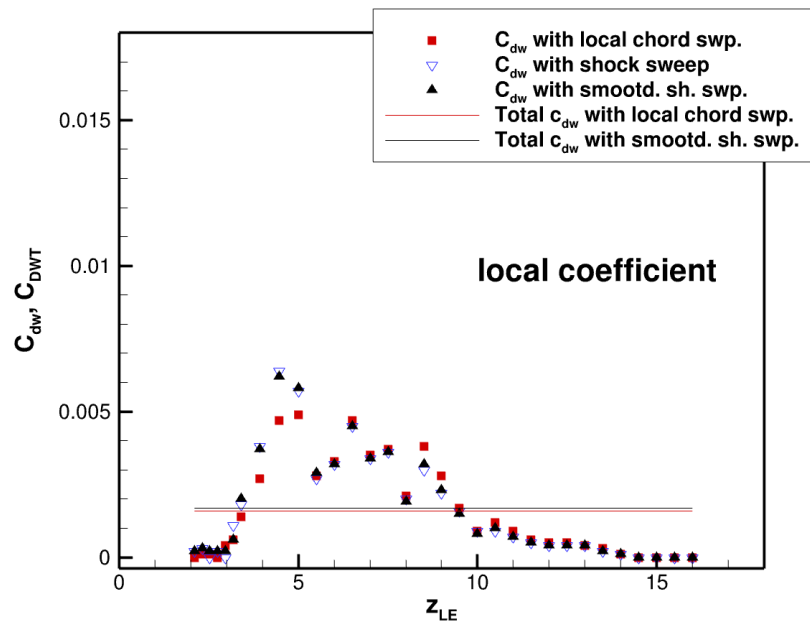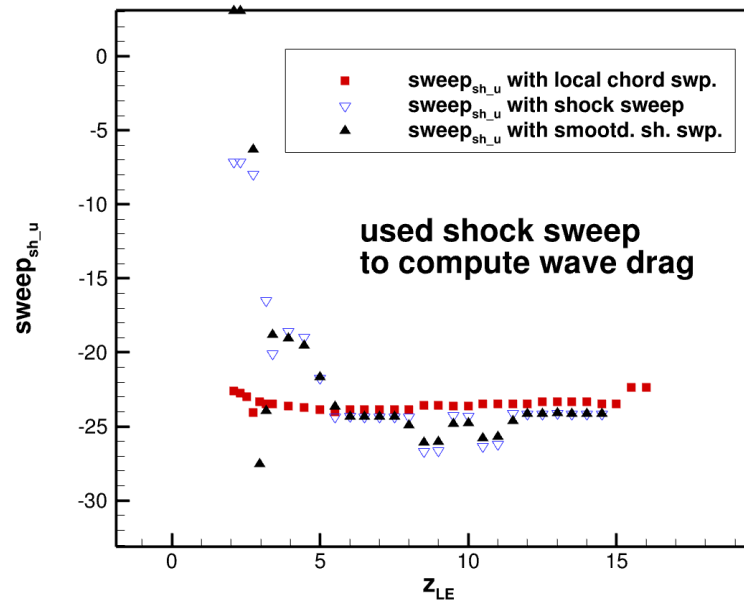
(a) C_{DW} distribution

(b) Local sweep
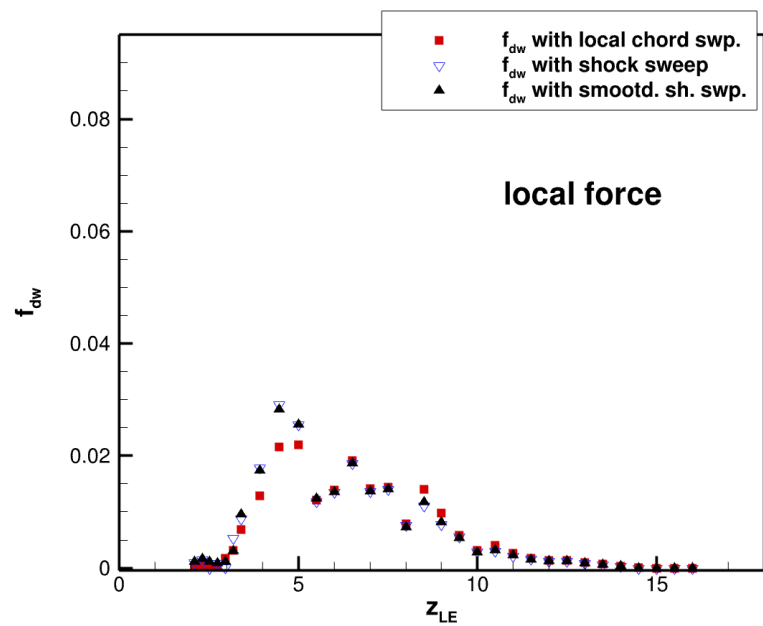
(c) f_{dw} distribution
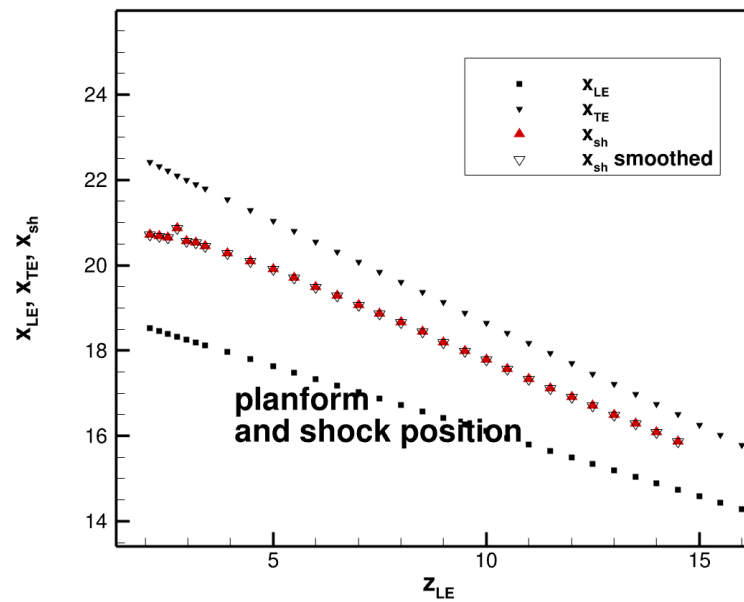
(d) Shock position
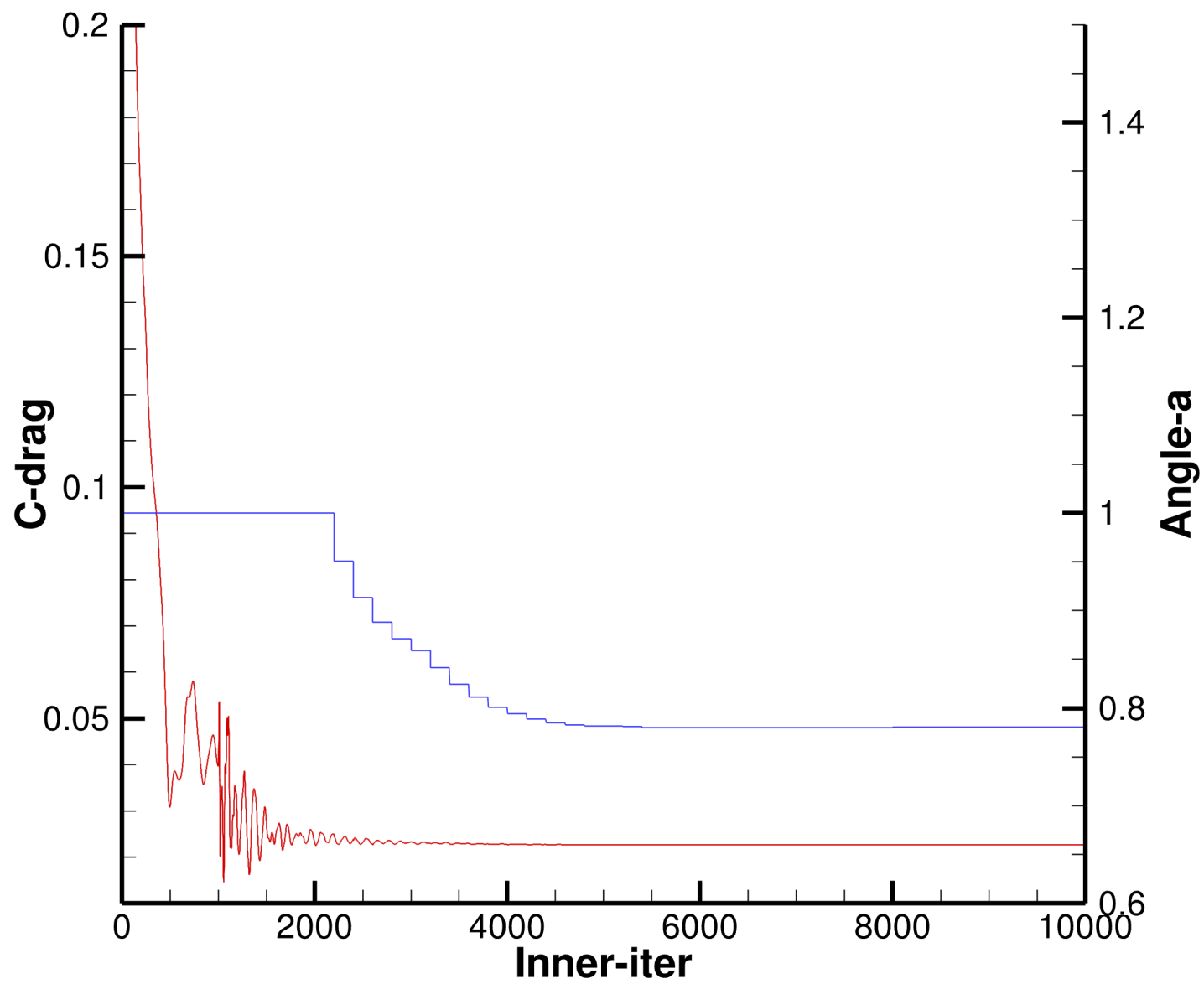
(a) Residuals

A.6. Geo356 Aerodynamic postprocessing

Geo, $\alpha = 0.79$ deg, Ma $=$, $C_L = 0.5201$, $C_D = 0.02268$, $C_{DW} = 0.0016$, E $= 22.9320$, Reynolds number $=$ Millionen, Iterations Runed $= 10000$
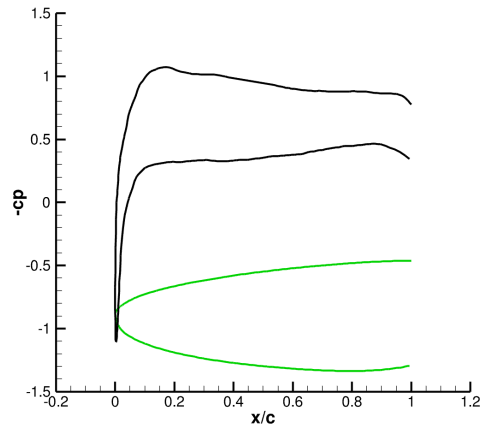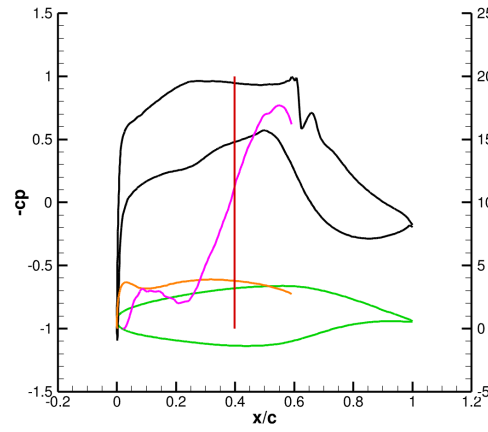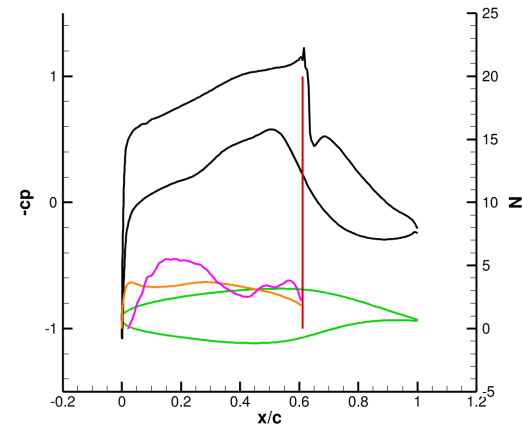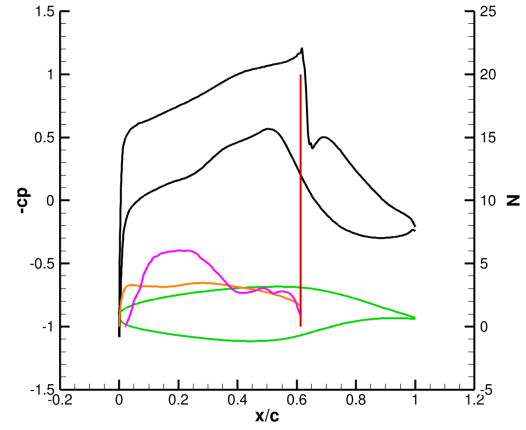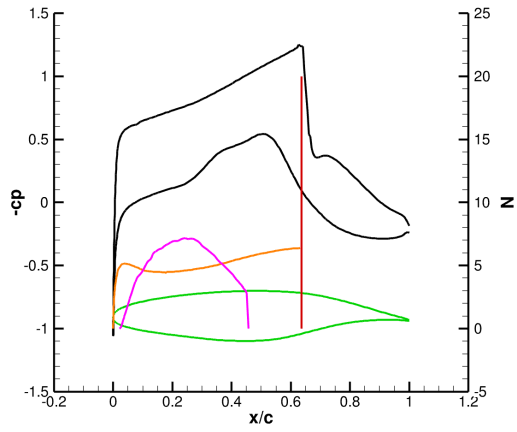

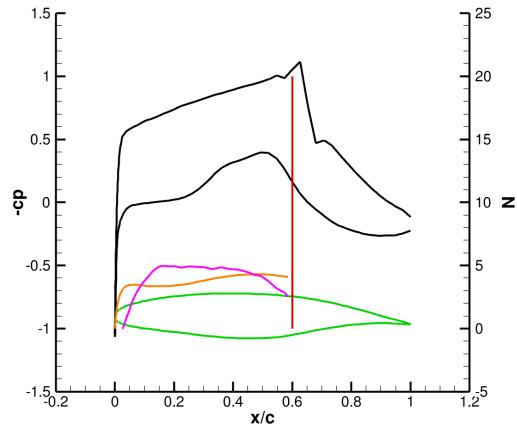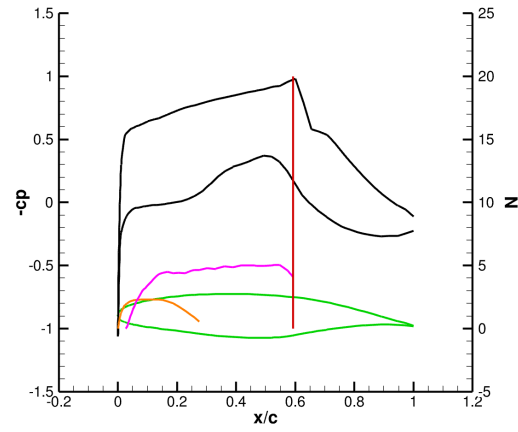(a) Schnitt 2, $\eta = 0{,}12331$

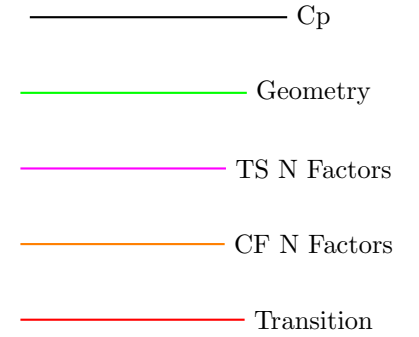(b) Schnitt 3, $\eta = 0{,}16332$
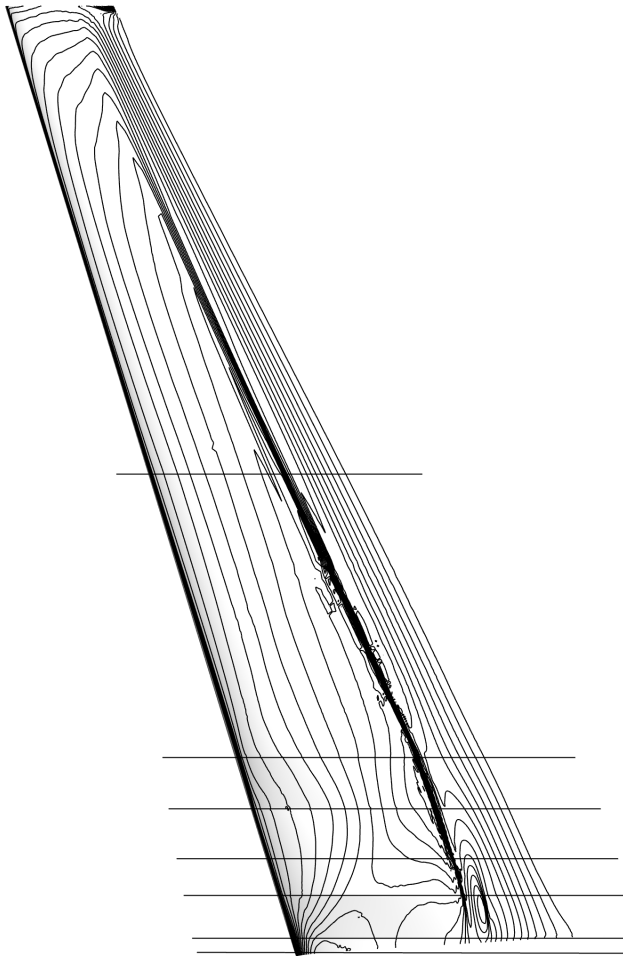
(c) Schnitt 4, $\eta = 0{,}2$

(d) Schnitt 5, $\eta = 0{,}24565$

(e) Schnitt 6, $\eta = 0{,}294$

(f) Schnitt 7, $\eta = 0{,}56$

Cp

Geometry

TS N Factors

CF N Factors

Transition

Strömung →

(a) Isobar contours

(b) Laminar contour

(c) Cp verteilung

cp

0
-0.06
-0.12
-0.18
-0.24
-0.3
-0.36
-0.42
-0.48
-0.54
-0.6
-0.66
-0.72
-0.78
-0.84
-0.9
-0.96
-1.02
-1.08
-1.14
-1.2
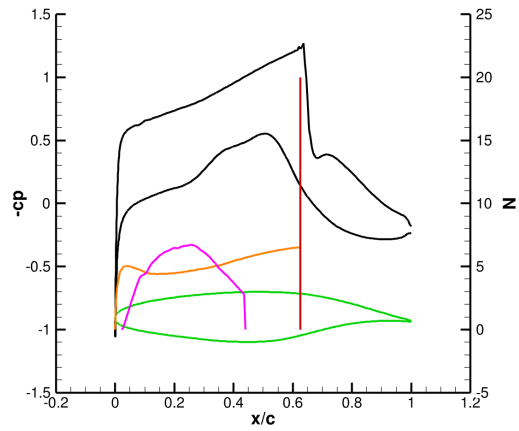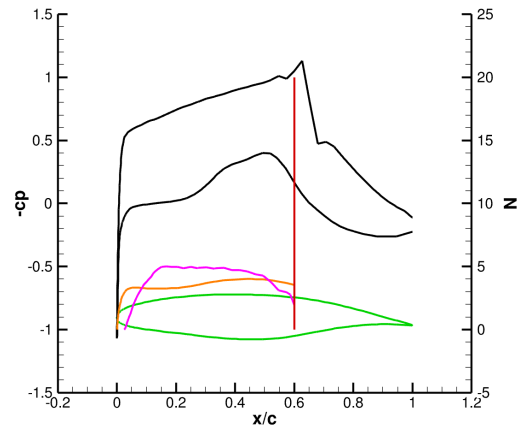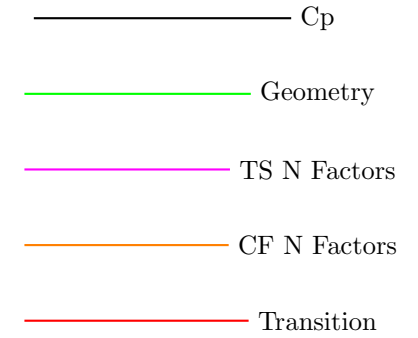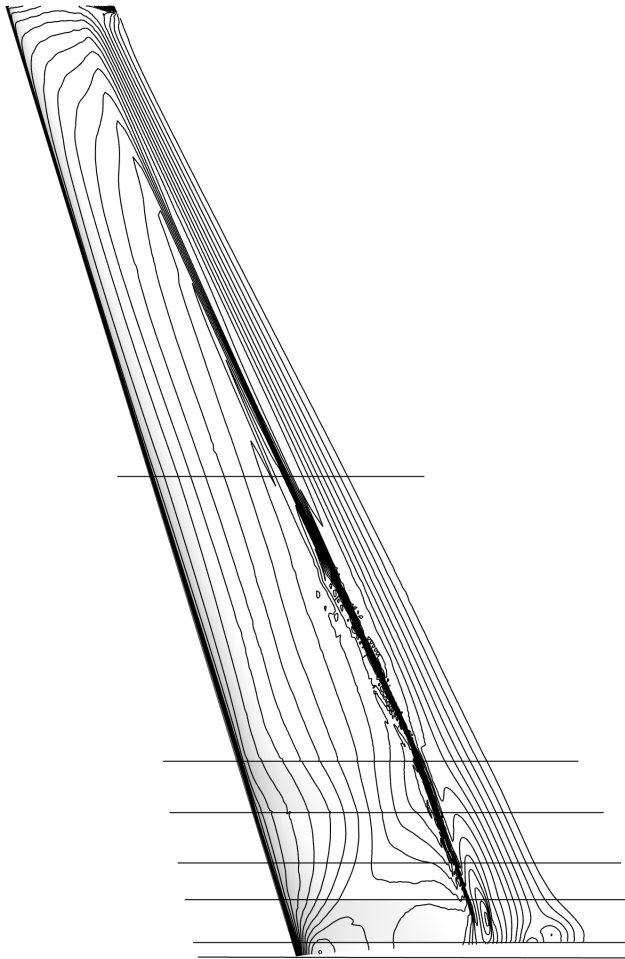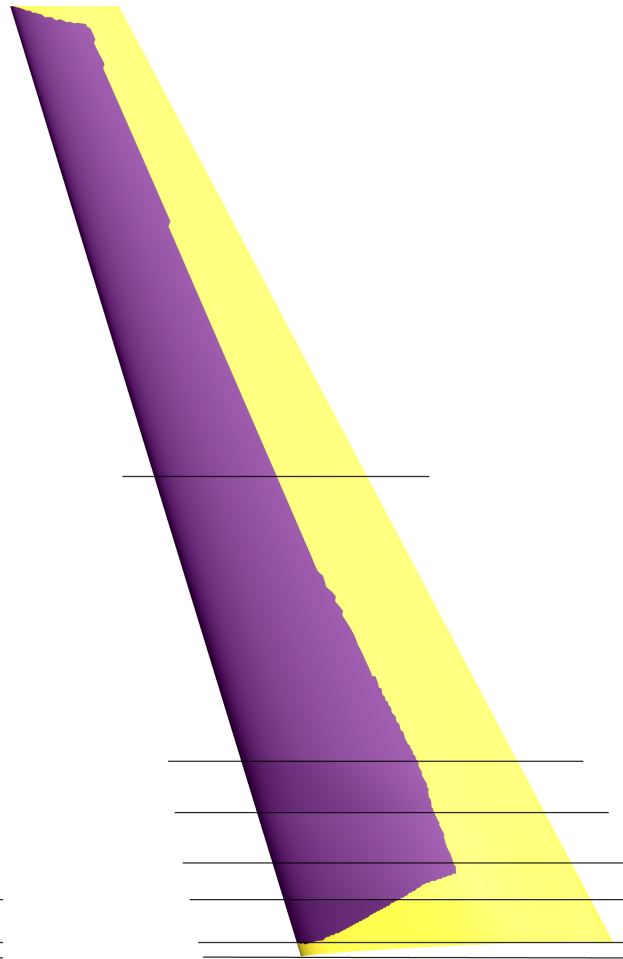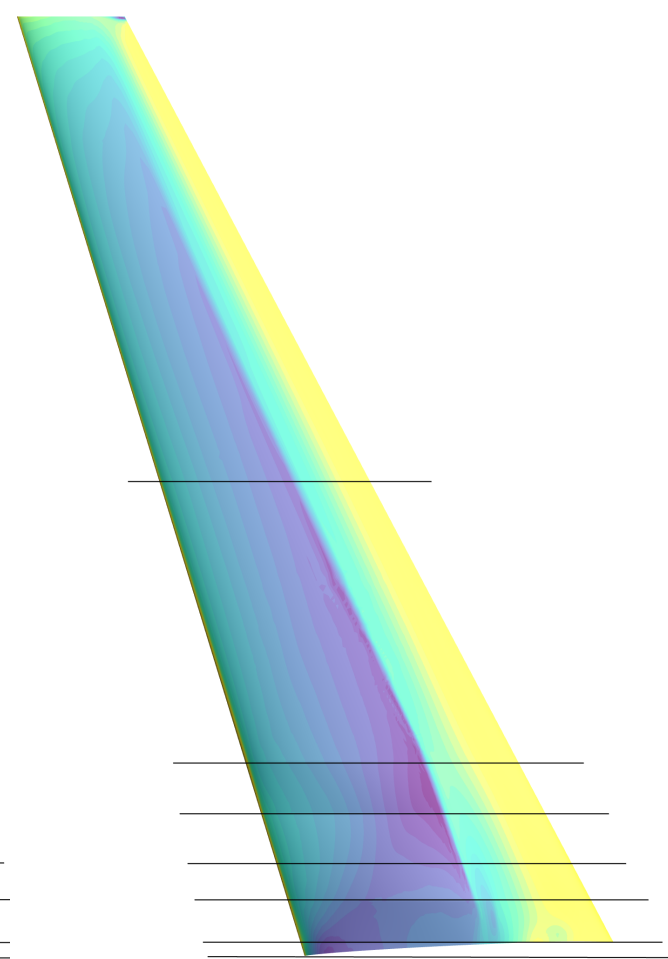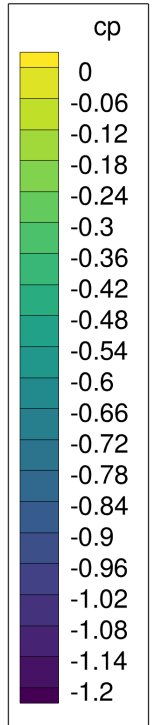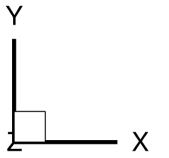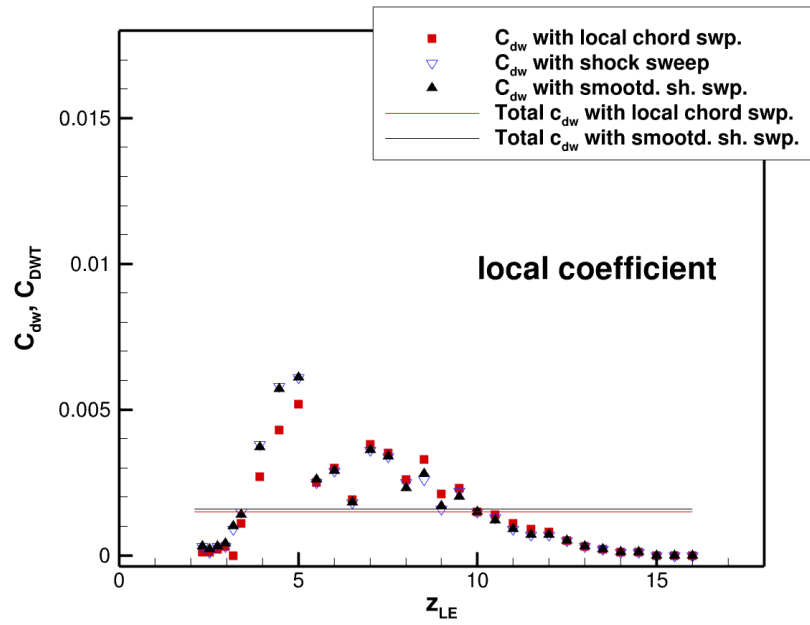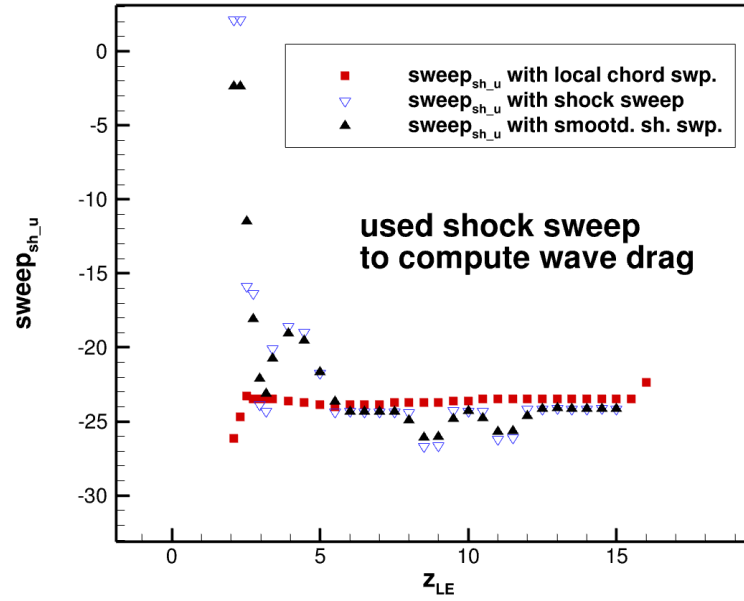
(a) C_{DW} distribution

(b) Local sweep
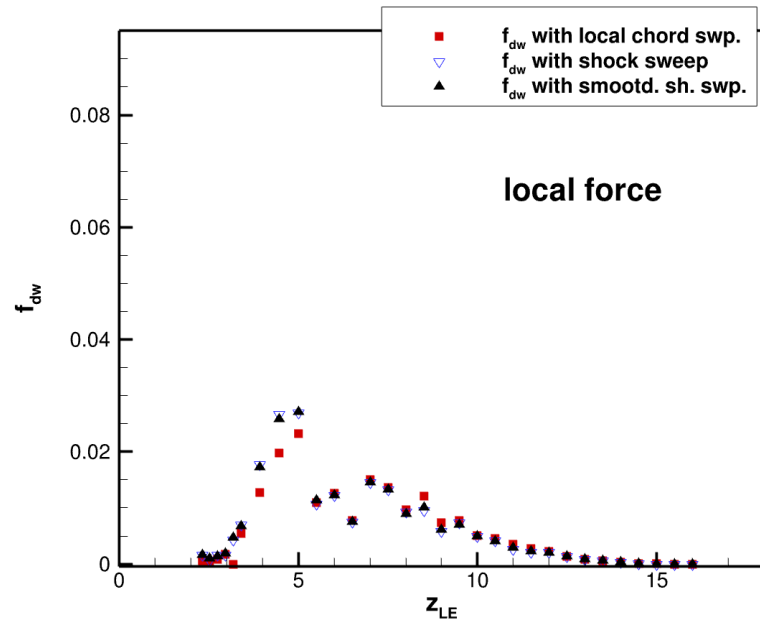
(c) f_{dw} distribution
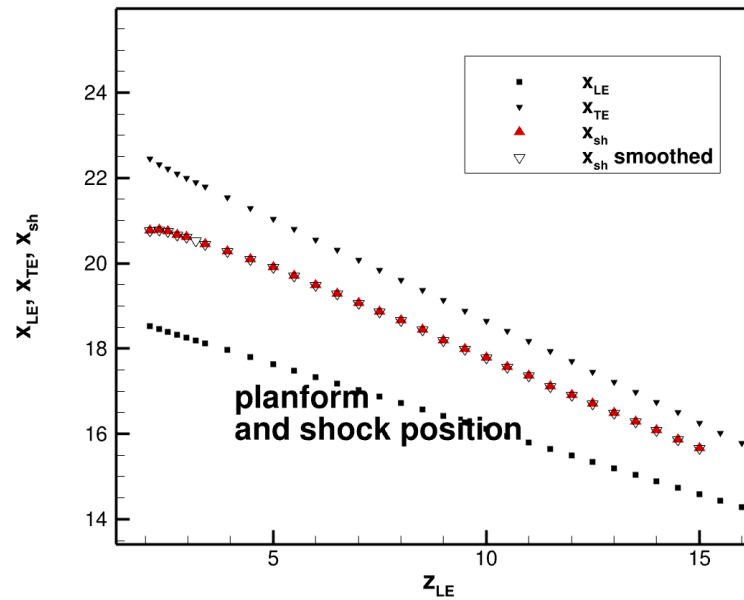
(d) Shock position
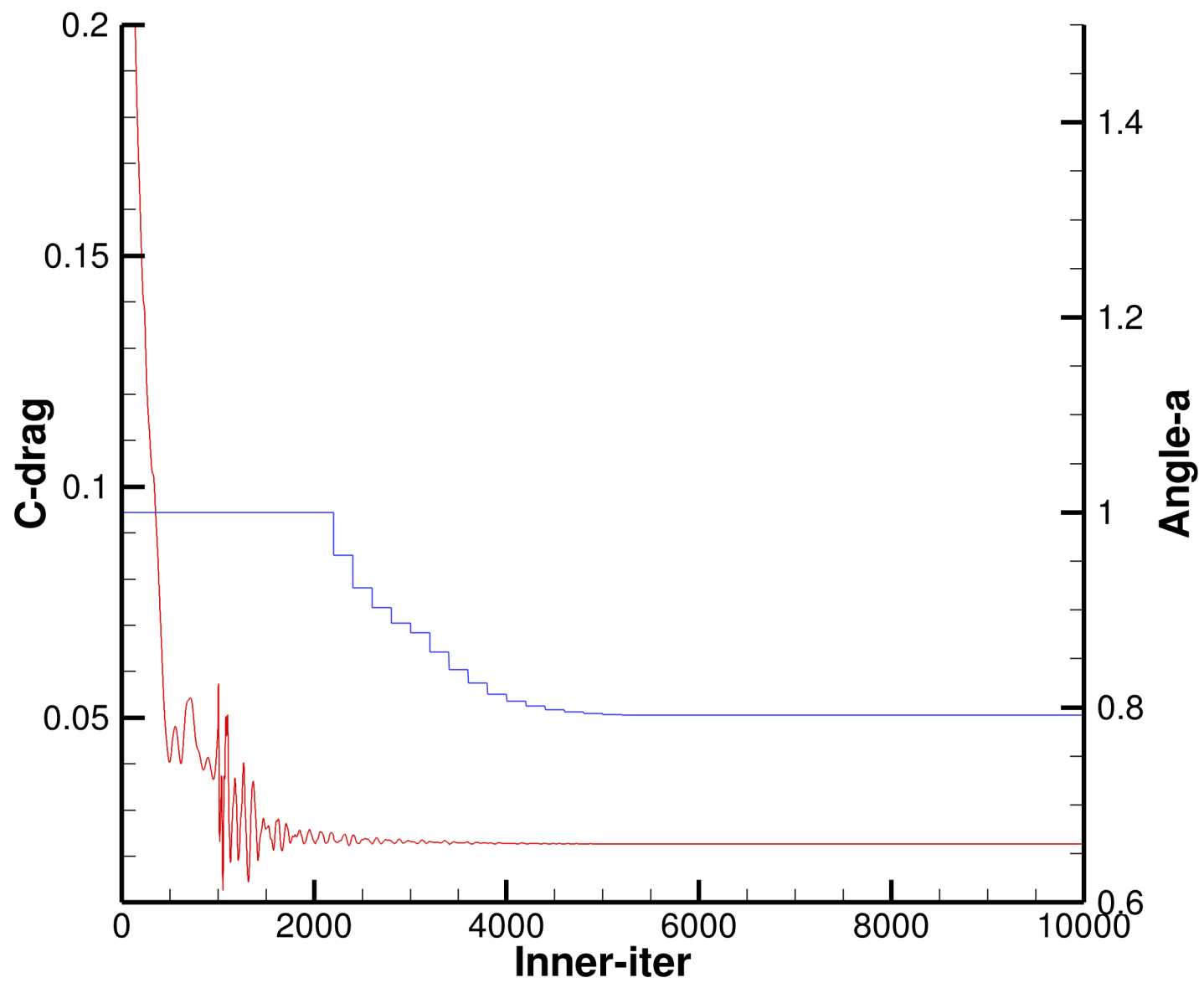
(a) Residuals

A.7. Geo357 Aerodynamic postprocessing

Geo, $\alpha = 0.77$ deg, Ma = , $C_L = 0.5201$, $C_D = 0.02267$, $C_{DW} = 0.0016$, E = 22.9422, Reynolds number = Millionen, Iterations Runed = 10000
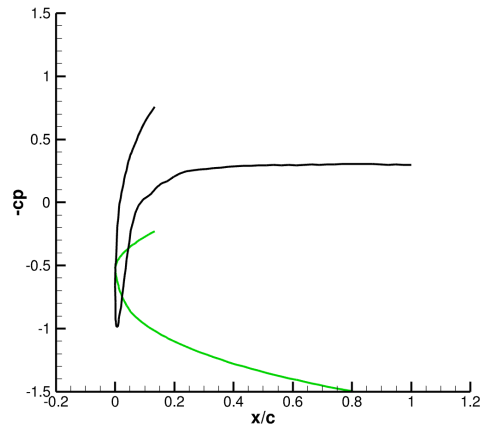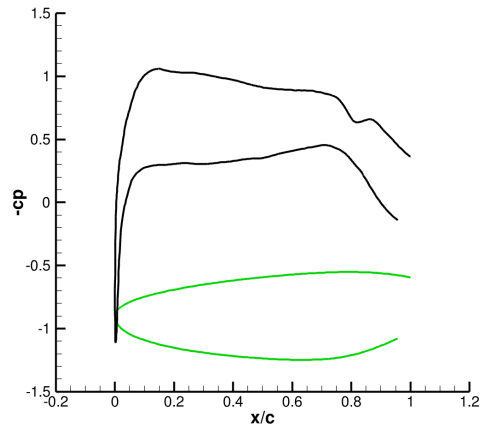
(a) Schnitt 1, $\eta = 0{,}10988$

(b) Schnitt 2, $\eta = 0{,}12331$

(c) Schnitt 3, $\eta = 0{,}16332$

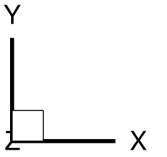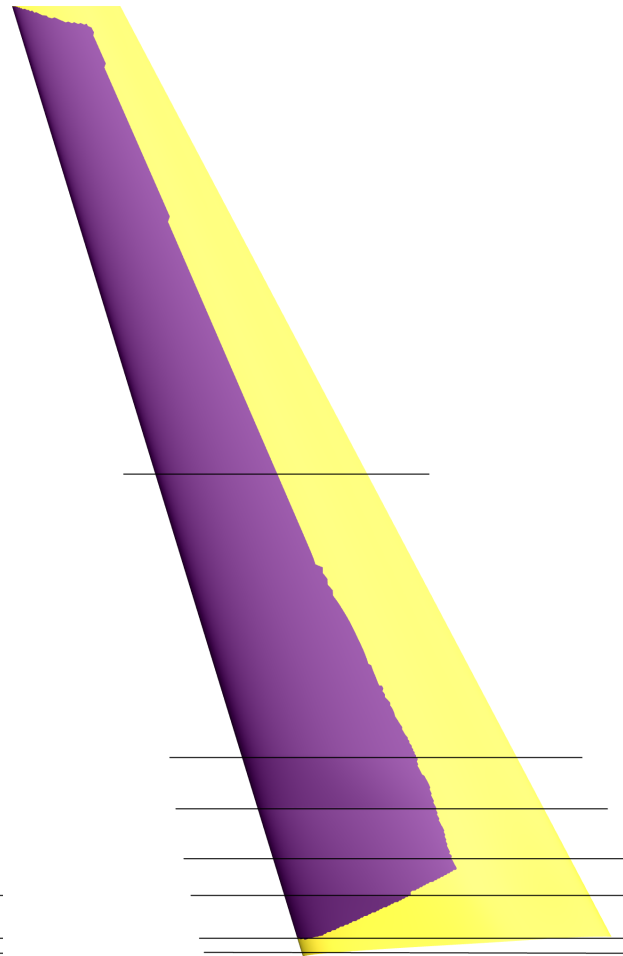(d) Schnitt 4, $\eta = 0{,}2$

(e) Schnitt 5, $\eta = 0{,}24565$

(f) Schnitt 6, $\eta = 0{,}294$

(g) Schnitt 7, $\eta = 0{,}56$
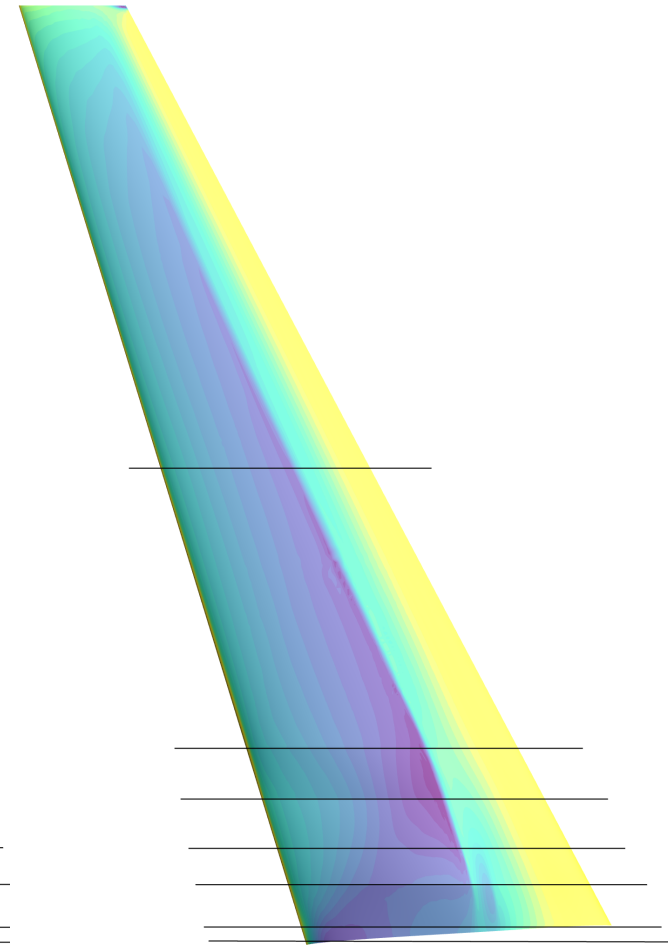
Cp

Geometry

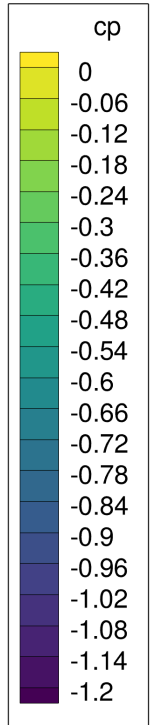TS N Factors

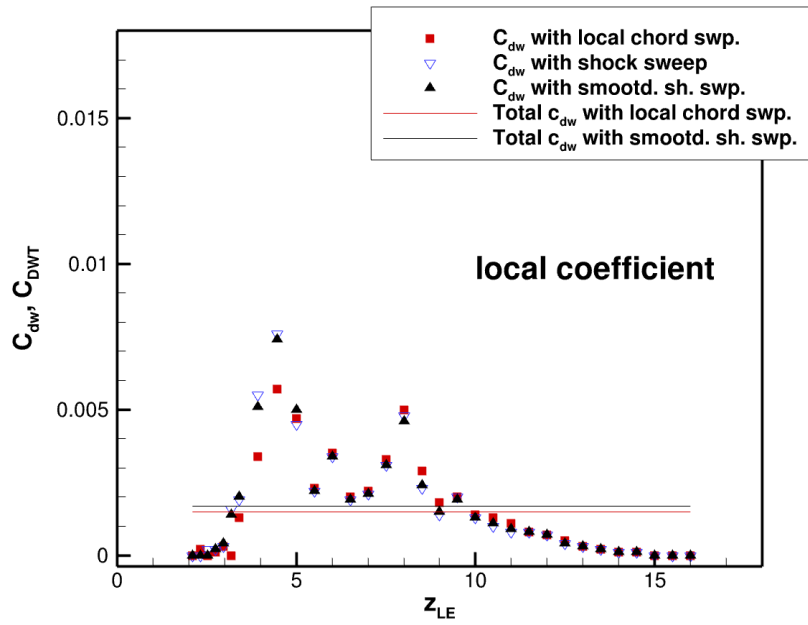CF N Factors

Transition
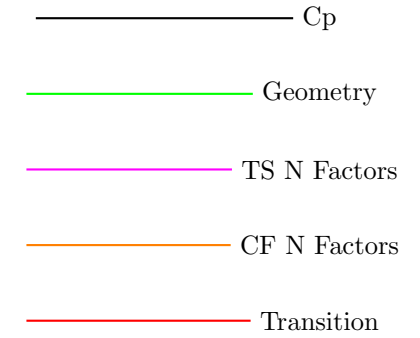
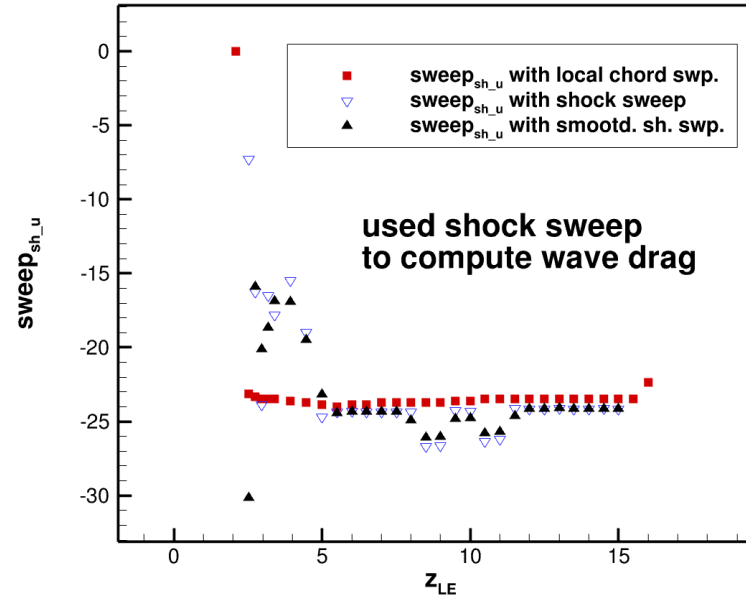**Strömung**
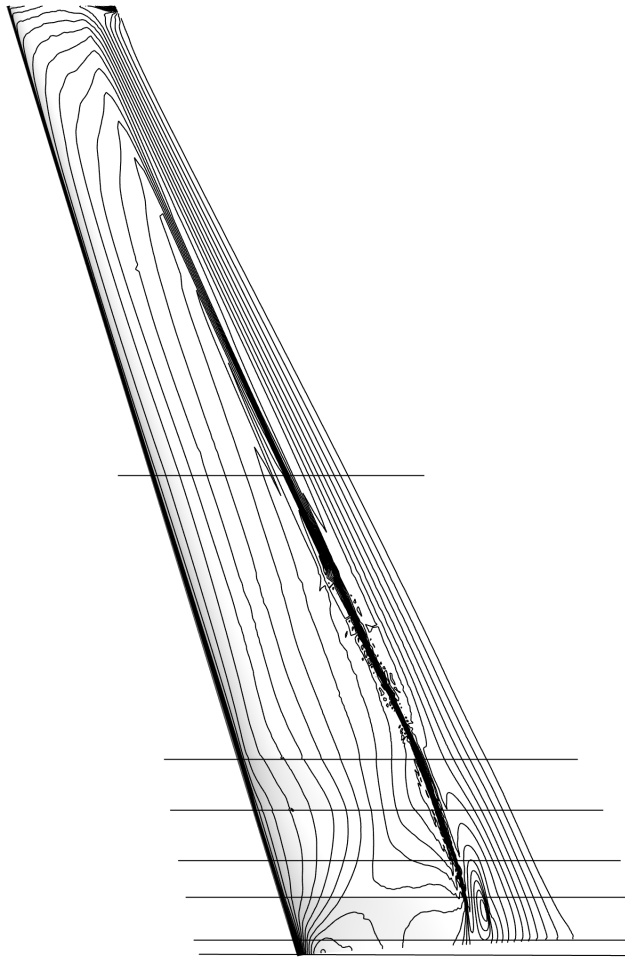
(a) Isobar contours
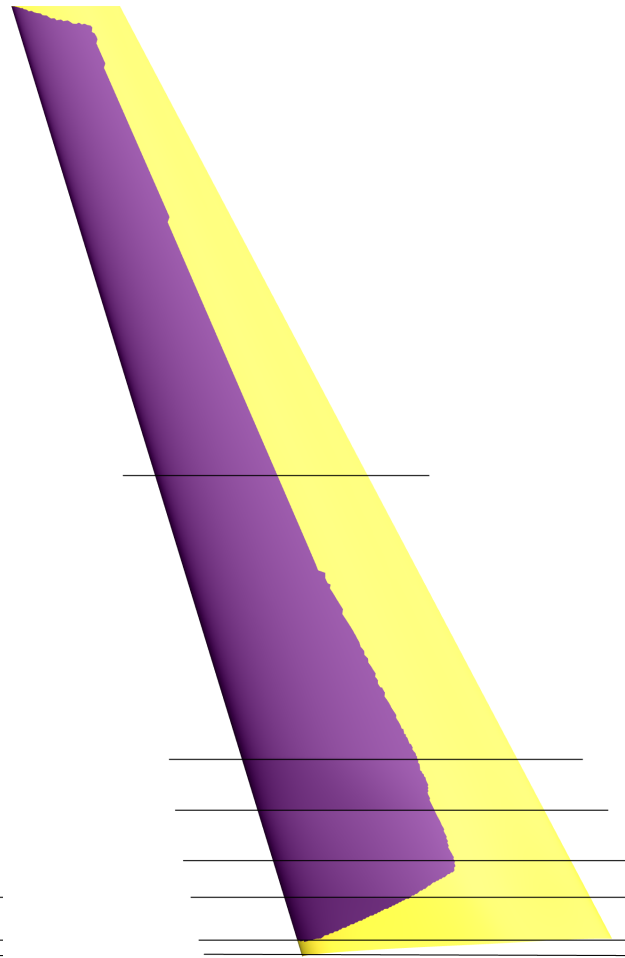
(b) Laminar contour
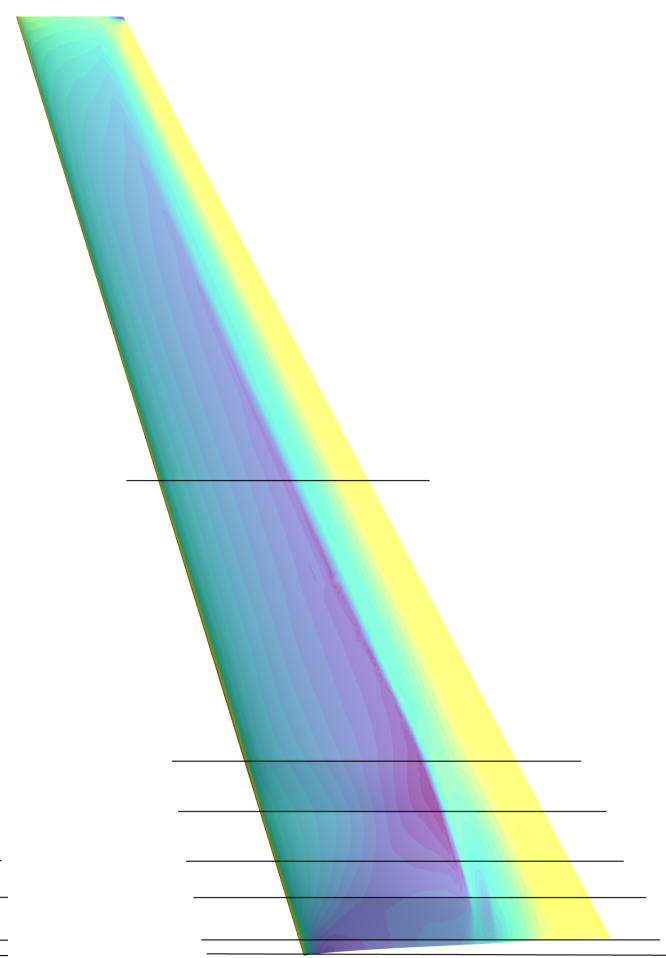
(c) Cp verteilung
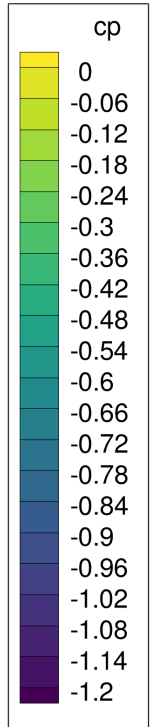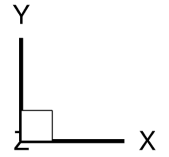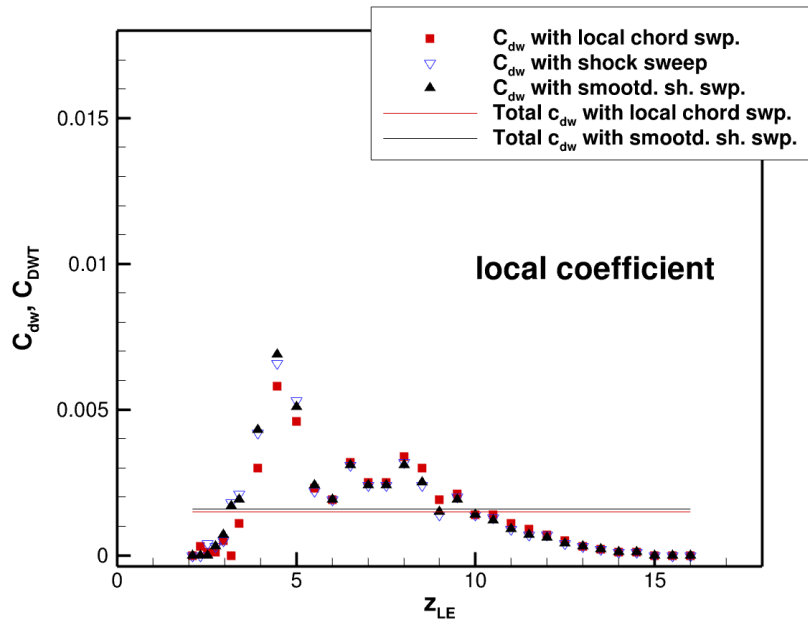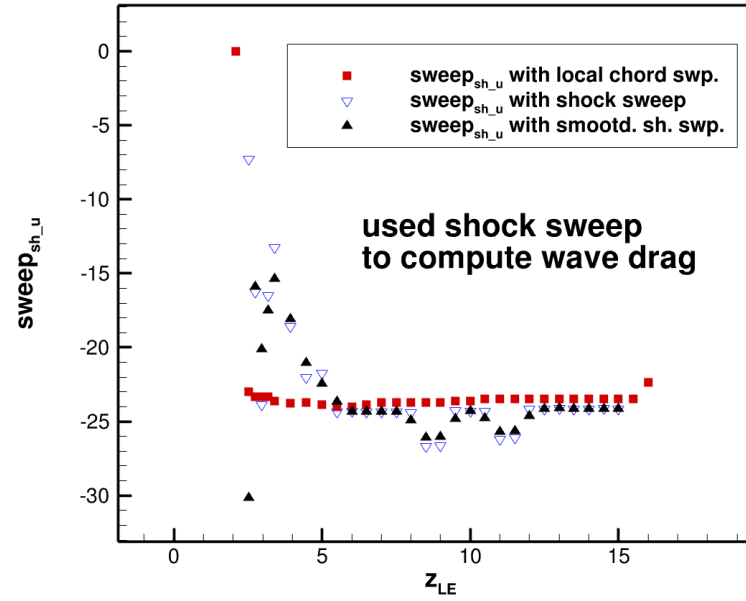
(a) C_{DW} distribution

(b) Local sweep
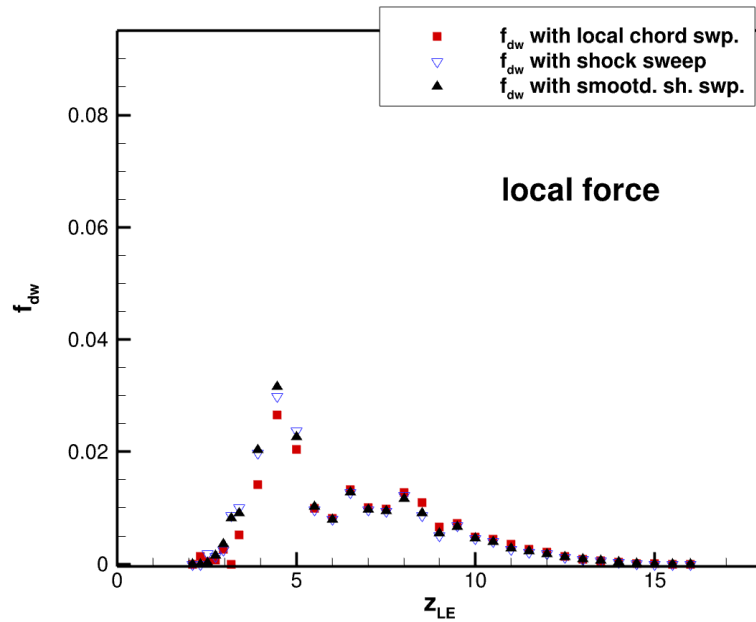
(c) f_{dw} distribution
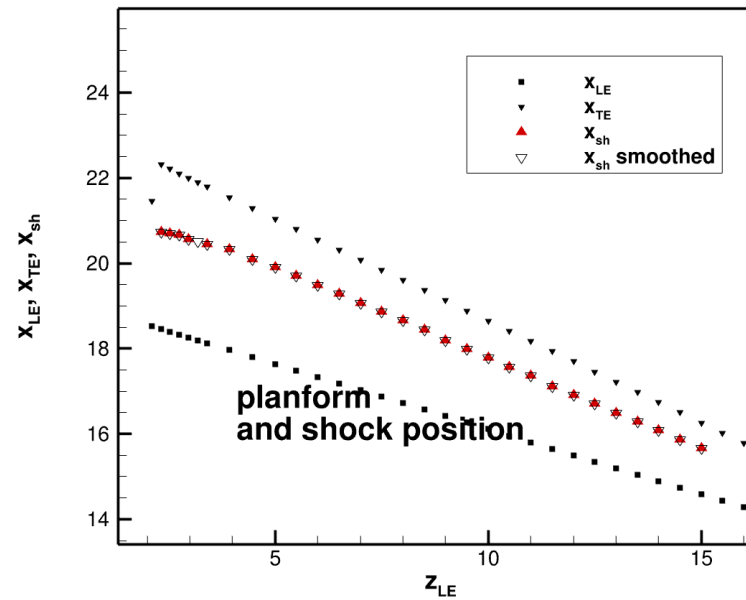
(d) Shock position

(a) Residuals

A.8. Geo358 Aerodynamic postprocessing

Geo, $\alpha = 0.77$ deg, Ma = , $C_L = 0.5201$, $C_D = 0.02267$, $C_{DW} = 0.0017$, E = 22.9422, Reynolds number = Millionen, Iterations Runed = 10000

(a) Schnitt 1, $\eta = 0{,}10988$

(b) Schnitt 2, $\eta = 0{,}12331$

(c) Schnitt 3, $\eta = 0{,}16332$

(d) Schnitt 4, $\eta = 0{,}2$

(e) Schnitt 5, $\eta = 0{,}24565$

(f) Schnitt 6, $\eta = 0{,}294$

(g) Schnitt 7, $\eta = 0{,}56$

Cp

Geometry

TS N Factors

CF N Factors

Transition
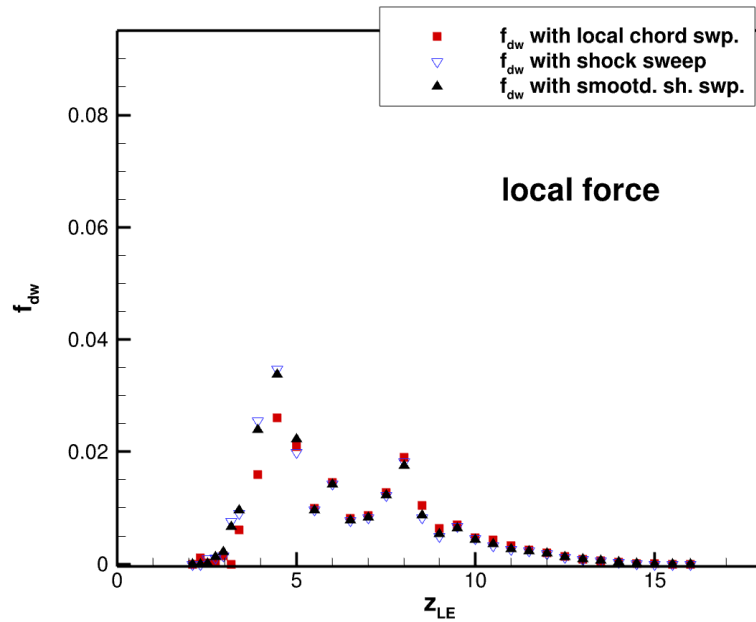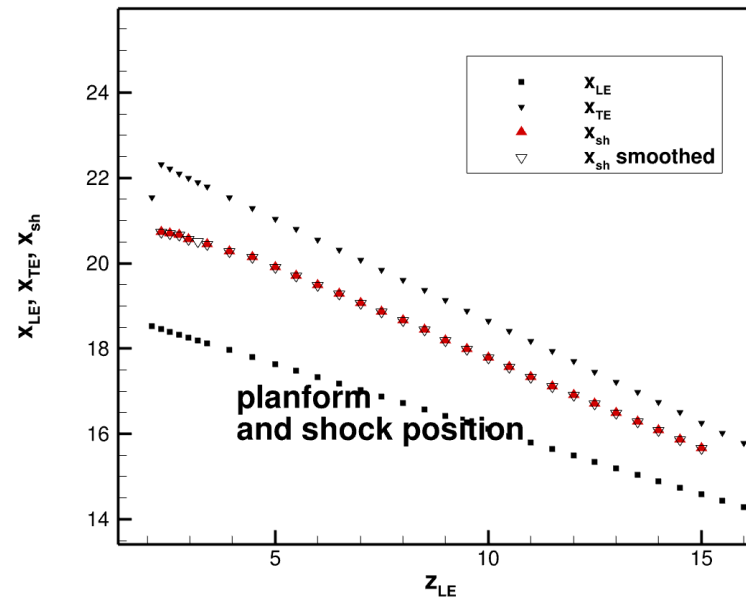
Strömung

(a) Isobar contours

(b) Laminar contour

(c) Cp verteilung

cp
0
-0.06
-0.12
-0.18
-0.24
-0.3
-0.36
-0.42
-0.48
-0.54
-0.6
-0.66
-0.72
-0.78
-0.84
-0.9
-0.96
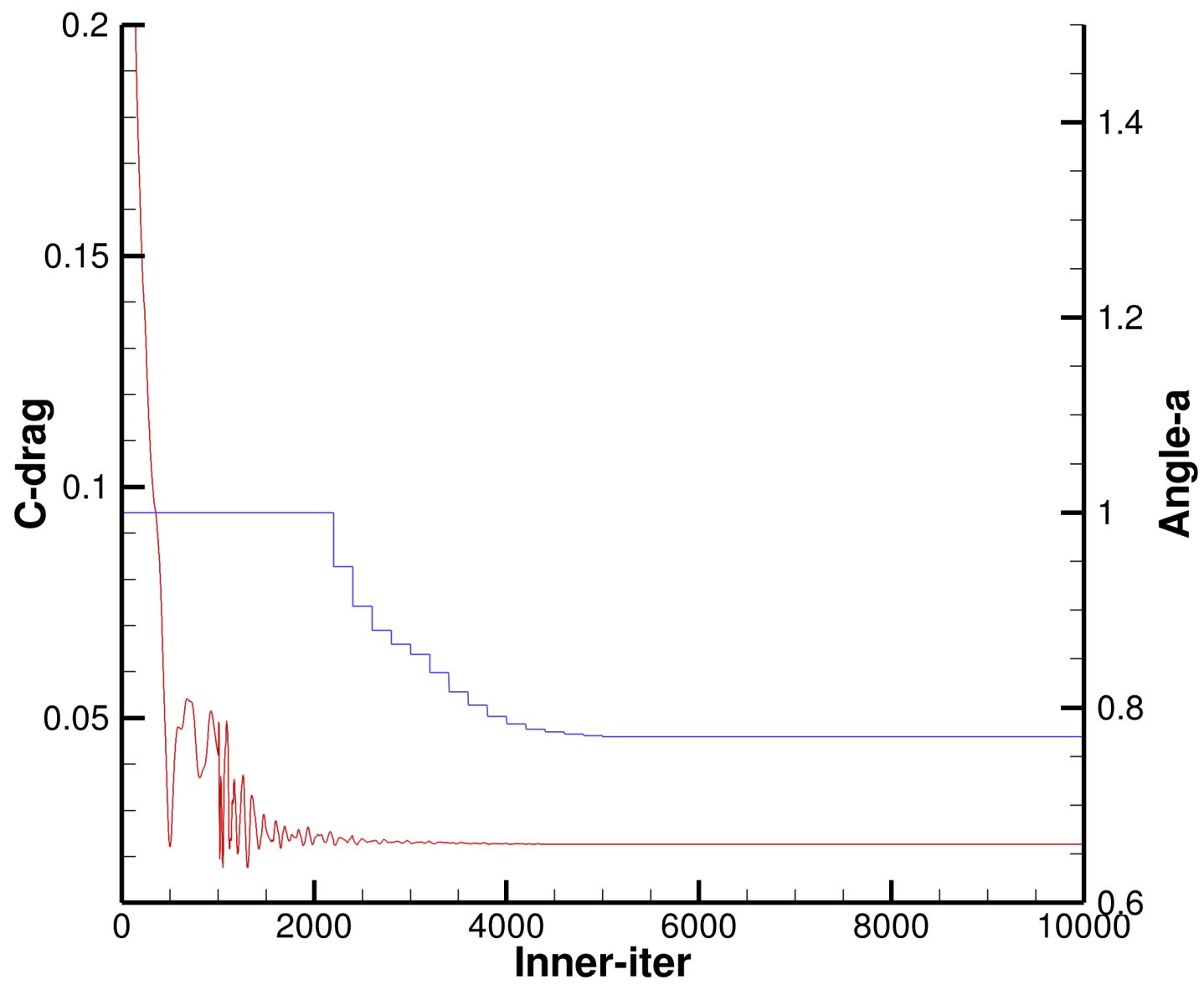-1.02
-1.08
-1.14
-1.2

(a) C_{DW} distribution

(b) Local sweep

(c) f_{dw} distribution

(d) Shock position

(a) Residuals